



Biochemical and functional characterization of DHX30, an RNA helicase linked to neurodevelopmental disorder

Biochemische und funktionelle Charakterisierung von DHX30, einer RNA Helikase assoziiert mit neurologischen Entwicklungsstörungen

Doctoral thesis for a doctoral degree
at the Graduate School of Life Sciences,
Julius-Maximilians-Universität Würzburg,

Section: Biomedicine
submitted by

Hannes Huber

from Rockville, USA

Würzburg, 2022



Submitted on:

Chairperson: Prof. Dr. Christoph Sotriffer

Members of the Thesis committee:

Primary Supervisor:

Professor Dr. Utz Fischer
Department of Biochemistry
Biocenter, University of Würzburg
Am Hubland
97074 Würzburg
e-mail: utz.fischer@biozentrum.uni-wuerzburg.de

Supervisor (Second):

PD Dr. Sibylle Jablonka
University hospital Würzburg
Institute for Clinical Neurobiology
Versbacher Straße 5
97078 Würzburg
e-mail: Jablonka_S@ukw.de

Supervisor (Third):

Professor Dr. Alexander Buchberger
Department of Biochemistry
Biocenter, University of Würzburg
Am Hubland
97074 Würzburg
e-mail: alexander.buchberger@uni-wuerzburg.de

Date of Public Defence:

Date of Receipt of Certificates:

Affidavit

I hereby confirm that my thesis entitled “**Biochemical and functional characterization of DHX30, an RNA helicase linked to neurodevelopmental disorder**” is the result of my own work. I did not receive any help or support from commercial consultants. All sources and/or materials applied are listed and specified in the thesis.

Furthermore, I confirm that this thesis has not yet been submitted as part of another examination process neither in identical nor in similar form.

Place, Date:

Signature:

Eidesstattliche Erklärung

Hiermit erkläre ich an Eides statt, die Dissertation „**Biochemische und funktionelle Charakterisierung von DHX30, einer RNA Helikase assoziiert mit neurologischen Entwicklungsstörungen**“ eigenständig, d.h. insbesondere selbständig und ohne Hilfe eines kommerziellen Promotionsberaters, angefertigt und keine anderen als die von mir angegebenen Quellen und Hilfsmittel verwendet zu haben.

Ich erkläre außerdem, dass die Dissertation weder in gleicher noch in ähnlicher Form bereits in einem anderen Prüfungsverfahren vorgelegen hat.

Ort, Datum:

Unterschrift:

Table of Contents

1. Summary	11
2. Zusammenfassung	12
3. Introduction	15
3.1 mRNA binding proteins, mRNPs and RNA helicases	15
3.2 Helicase families and their mechanism of action	19
3.3 RNA helicases in translation	23
3.4 Signaling pathways associated to translation	24
3.5 The RNA helicase DHX30	26
3.5.2 Putative cellular functions of DHX30	27
3.5.3 DHX30 is linked to neurodevelopmental disorder NEDMIAL	28
3.6 Aim of this study	30
4. Results	31
4.1 Purification and biochemical characterization of DHX30, a putative member of the Helicase Superfamily 2	31
4.1.1 Expression and Purification of recombinant full-length DHX30	31
4.1.2 RNA unwinding activity of recombinant DHX30	33
4.2 Cellular localization of DHX30 via immunofluorescence microscopy	35
4.3 DHX30 co-migrates with ribosomes	36
4.4 DHX30 directly interacts with ribosomes via its N-terminal dsRNA-binding domain	39
4.5 Determination of the DHX30 interactome - purification of DHX30 protein complexes	41
4.6 Studies on the cellular function of DHX30 upon amino acid and serum starvation	46
4.6.1 DHX30 shifts from polysomes into monosomes upon amino acid starvation and serum starvation	46
4.6.2 DHX30 shifts from polysomes into monosomes upon starvation independently of LARP1	49
4.7 The depletion of DHX30 results in the accumulation of RNAs in the 80S peak and changes in the polysome profile	53
4.7.1 DHX30 depletion results in the deregulation of mRNAs involved in neurogenesis and nervous system development.	55
4.7.2 DHX30 KO affects the abundance of 5'TOP mRNAs in the 80S peak and in the polysomes	59
4.8 Biochemical characterization of pathogenic missense mutations of DHX30	61
4.8.1 Pathogenic missense mutations in the helicase core of DHX30 interfere with its ATPase activity and helicase activity	61
4.8.2 Co-migration of DHX30 with ribosomes is independent from its catalytic activity	64
4.8.3 Comparative analysis between the interactome of DHX30 wild-type and disease-causing mutants	65

4.8.4 Unwinding activity of DHX30 on RNA:DNA and DNA:DNA duplexes.	67
5. Discussion.....	70
5.1 Enzymatic properties of DHX30.....	70
5.2 DHX30 interactome and direct interaction with the ribosome	72
5.3 DHX30 depletion results in the deregulation of mRNAs involved in neurogenesis and nervous system development.	74
5.4 Depletion of DHX30 results in the reduced abundance of 5'TOP mRNAs in 80S and polysomes	76
5.5 Pathogenic variants of DHX30 lose their enzymatic activities <i>in vitro</i> , but are still associated with ribosomes	78
5.6 A potential function of DHX30 in the nucleus - enzymatic activity of DHX30 on R-loop and D-loop substrates	79
5.7 The Pathomechanism of NEDMIAL: a Hypothesis.....	80
6. Material & Methods	83
6.1 Material.....	83
6.1.1 Nucleotide and Protein Ladders.....	83
6.1.2 Buffers and Solution.....	83
6.1.3 Cell Culture.....	85
6.1.4 Cell Culture Media.....	86
6.1.5 Antibodies.....	87
6.1.6 Plasmids	87
6.1.7 DNA and RNA Oligonucleotides	88
6.2 Methods.....	90
6.2.1 Molecular Methods.....	90
6.2.2 Eukaryotic Cell Culture.....	95
6.2.3 Biochemical Methods	96
6.2.4 Immunobiological Methods	100
6.2.5 RNA Methods	102
6.2.6 Bioinformatics Methods.....	110
7. Abbreviations	111
8. Appendix	112
9. References.....	131
10. Publications.....	138
11. Acknowledgments.....	139
12. Curriculum vitae	140

Table of figures

Figure 1: RNA helicases unwind RNA duplexes and remodel RNA-protein complexes.....	16
Figure 2: Overview of cellular processes eukaryotic RNA helicases are involved.	18
Figure 3: Overview of members of the SF1 and SF2 helicase families.	21
Figure 4: Overview of the helicase core of DEAH-box helicases.....	22
Figure 5: Domain organization of DHX30.....	26
Figure 6: Overview of identified mutations of DHX30 in NEDMIAL patients.....	29
Figure 7: Strategy for expression and purification of DHX30 in <i>E. coli</i>	32
Figure 8: ATP-dependent RNA unwinding activity of recombinant DHX30.	34
Figure 9: Cellular localization of DHX30 via immunofluorescence microscopy.	35
Figure 10: Polysome sucrose gradient distribution of DHX30 after ultracentrifugation.	37
Figure 11: DHX30 forms a complex with ribosomal particles in vitro.	38
Figure 12: Cross-linking/mass spectrometry of DHX30/Ribosome complexes.....	41
Figure 13: Purification of DHX30 protein complexes using Flp-In T-REx 293 cells.....	43
Figure 14: Quantitative mass spectrometry of the DHX30 interactome.	44
Figure 15: Gene ontology enrichment analysis of the DHX30 interactome.	45
Figure 16: Grad-seq experiment in HEK293 cells upon starvation conditions.....	48
Figure 17: LARP1 and 5'TOP mRNA shift from polysomes to 80s upon starvation as a result of the TOP-response.....	50
Figure 18: Polysome sucrose gradient distribution of DHX30 in dependence of LARP1.	52
Figure 19: Polysome sucrose gradients of DHX30 KO cells and HEK29T control cells.....	55
Figure 20: RNA sequencing of total RNAs upon DHX30 KO.	57
Figure 21: Gene ontology enrichment analysis of candidate mRNAs upon DHX30 KO from total RNAs identified by RNAseq.	58
Figure 22: DHX30 KO affects the abundance of 5'TOP mRNAs in the 80S peak and in the polysomes.	60
Figure 23: ATPase activity and unwinding assays of pathogenic DHX30 variants.....	63
Figure 24: Sucrose gradient distribution of pathogenic DHX30 variants after ultracentrifugation.	64
Figure 25: Comparative Analysis of mass spectrometry data of the protein interactome of pathogenic DHX30 variants.	66
Figure 26: Unwinding assays of recombinant DHX30 with different R-loop and D-loop substrates...68	
Figure 27: Unwinding assays of recombinant DHX30 (WT and inactive mutant) with 3'-R-loop substrate.....	69
Figure 28: Model of the potential function of DHX30 in the RNA metabolism of human cells.....	82

1. Summary

RNA helicases are key players in the regulation of gene expression. They act by remodeling local RNA secondary structures as well as RNA-protein interactions to enable the dynamic association of RNA binding proteins to their targets. The putative RNA helicase DHX30 is a member of the family of DEAH-box helicases with a putative role in the ATP-dependent unwinding of RNA secondary structures. Mutations in the *DHX30* gene causes the autosomal dominant neuronal disease “Neurodevelopmental Disorder with severe Motor Impairment and Absent Language” (NEDMIAL;OMIM#617804). In this thesis, a strategy was established that enabled the large-scale purification of enzymatically active DHX30. Through enzymatic studies performed *in vitro*, DHX30 was shown to act as an ATP-dependent 3' → 5' RNA helicase that catalyzes the unwinding of RNA:RNA and RNA:DNA substrates. Using recombinant DHX30, it could be shown that disease-causing missense mutations in the conserved helicase core caused the disruption of its ATPase and helicase activity. The protein interactome of DHX30 however, was unchanged indicating that the pathogenic missense-mutations do not cause misfolding of DHX30, but rather specifically affect its catalytic activity. DHX30 localizes predominantly in the cytoplasm where it forms a complex with ribosomes and polysomes. Using a cross-linking mass spectrometry approach, a direct interaction of the N-terminal double strand RNA binding domain of DHX30 with sites next to the ribosome's mRNA entry channel and the subunit interface was uncovered. RNA sequencing of DHX30 knockout cells revealed a strong de-regulation of mRNAs involved in neurogenesis and nervous system development, which is in line with the NEDMIAL disease phenotype. The knockdown of DHX30 results in a decreased 80S peak in polysome gradients, indicating that DHX30 has an effect on the translation machinery. Sequencing of the pool of active translating mRNAs revealed that upon DHX30 knockout mainly 5'TOP mRNAs are downregulated. These mRNAs are coding for proteins of the translational machinery and translation initiation factors. This study identified DHX30 as a factor of the translation machinery that selectively impacts the expression of a subset of proteins and provides insight on the etiology of NEDMIAL.

2. Zusammenfassung

RNA-Helikasen sind Schlüsselfaktoren bei der Regulierung der Genexpression. Sie remodellieren RNA-Sekundärstrukturen und RNA-Protein Interaktionen und dadurch die dynamische Interaktion von RNA-bindenden Proteinen mit deren Substraten. Die putative RNA-Helikase DHX30 ist Mitglied der DEAH-box Helikasen, welche in Abhängigkeit von ATP in der Lage sind, RNA-Sekundärstrukturen aufzulösen. Mutationen im *DHX30* Gen verursachen die autosomal-dominante neuronale Krankheit "Neurodevelopmental Disorder with Severe Motor Impairment and Absent Language" (NEDMIAL; OMIM#617804). In dieser Arbeit wurde eine Aufreinigungs-Strategie etabliert, um im präparativen Maßstab enzymatisch-aktives DHX30 Protein zu gewinnen. Mit dem aufgereinigten Protein wurden enzymatische Experimente durchgeführt, wodurch DHX30 als ATP abhängige RNA-Helikase charakterisiert wurde. Es konnte gezeigt werden, dass es in der Lage ist RNA:RNA sowie RNA:DNA Substrate in einer 3' → 5' Richtung zu entwinden. Mithilfe des rekombinanten Proteins konnte weiter gezeigt werden, dass krankheitsverursachende Mutationen im hoch-konservierten Helikase-Kern von DHX30 zur Beeinträchtigung der ATPase und Helikase-Aktivität des Proteins führen. Des Weiteren ergab sich, dass das Protein-Interaktom der DHX30 Mutanten sich im Vergleich zum Wildtyp nicht verändert, was impliziert, dass die Mutationen nicht zu einer Missfaltung des Proteins, sondern dessen katalytische Aktivität inhibieren. DHX30 lokalisiert hauptsächlich im Cytoplasma und bildet dort einen Proteinkomplex mit Ribosomen und Polysomen. Mittels eines *cross-linking mass spectrometry*-Experiments konnte eine direkte Interaktion von DHX30 mit Stellen der ribosomalen mRNA Eintrittsstelle und dem Interface der ribosomalen Untereinheiten identifiziert werden. Die RNA Sequenzierung von DHX30-deletierten Zellen zeigte eine starke Deregulierung von mRNAs welche für die Entwicklung des Nervensystems und in der Neurogenese eine Rolle spielen, was mit dem Krankheits-Phänotyp von NEDMIAL korreliert. Weiter konnte gezeigt werden, dass es in DHX30-deletierten Zellen zur Abnahme von 80S Ribosomen in Polysomen-Gradienten kommt, was auf eine Funktion von DHX30 während der Translation schließen lässt. Durch das Sequenzieren aktiv translatierender mRNAs zeigte sich, dass der KO von DHX30 zur Abnahme von 5'TOP mRNAs führt. Diese

mRNAs kodieren für Proteine der Translations-Maschinerie und für Translations-Initiations Faktoren. Diese Studie identifiziert DHX30 als Faktor der Translations-Maschinerie, der selektiv die Expression einer mRNA-Untergruppe beeinflusst und Einblicke in die Ätiologie von NEDMIAL liefert.

3. Introduction

3.1 mRNA binding proteins, mRNPs and RNA helicases

From the process of transcription, over mRNA processing to translation and finally decay, cellular mRNAs are always associated with many mRNA binding proteins (mRBPs). The unit of a given mRNA bound to a specific subset of proteins is called a messenger ribonucleoprotein (mRNP). The interplay between mRBPs and the bound mRNA is important for the correct gene expression and its regulation on the post-transcriptional level. mRBPs are involved in the regulation of RNA stability, RNA splicing, translation, RNA modification or RNA localization (Gehring et al., 2017). Most mRBPs contain canonical RNA-binding domains including the RNA recognition motif (RRM), hnRNP K homology (KH), DEAD (aspartic acid-glutamic acid-alanine-aspartic acid) box helicase domains, the double-stranded RNA-binding domain (dsRBD), RNA-binding zinc-finger domains (ZnF), but also Arginine-Glycine-motifs (RGG/RG motifs), the oligonucleotide and oligosaccharide-binding fold (OB-fold) and numerous others (Castello et al., 2012), (Theobald et al., 2003), (Lunde et al., 2007), (Thandapani et al., 2013). Every RNA interacting domain provides different modes of RNA recognition. This is determined in *cis* by a defined sequence motif, local RNA structural elements, RNA modifications or a combination of events. It can be further complemented and/or regulated by accessory domains involved in protein-protein interactions (Corley et al., 2020). The repertoire of mRNA-associated proteins at a single message is constantly changing and all these proteins shift between a target bound and target unbound state. On one hand we understand the functions of some mRNA-binding proteins in mRNP regulation, on the other hand little is known about how mRNP dynamics is facilitated and which factors are involved (Mitchell & Parker, 2014). One of the key players in the mRNP transitions are mRNA associated proteins belonging to the class of RNA helicases.

These enzymes are a family of ubiquitously expressed nucleotide triphosphate (NTP)-dependent motor proteins, that have the capability to remodel RNA-RNA, RNA-DNA structures (RNA unwinding activity), and RNA-protein complexes (RNase activity) (see figure 1) (Fairman et al., 2004), (Jankowsky et al., 2001), (Pyle, 2008).

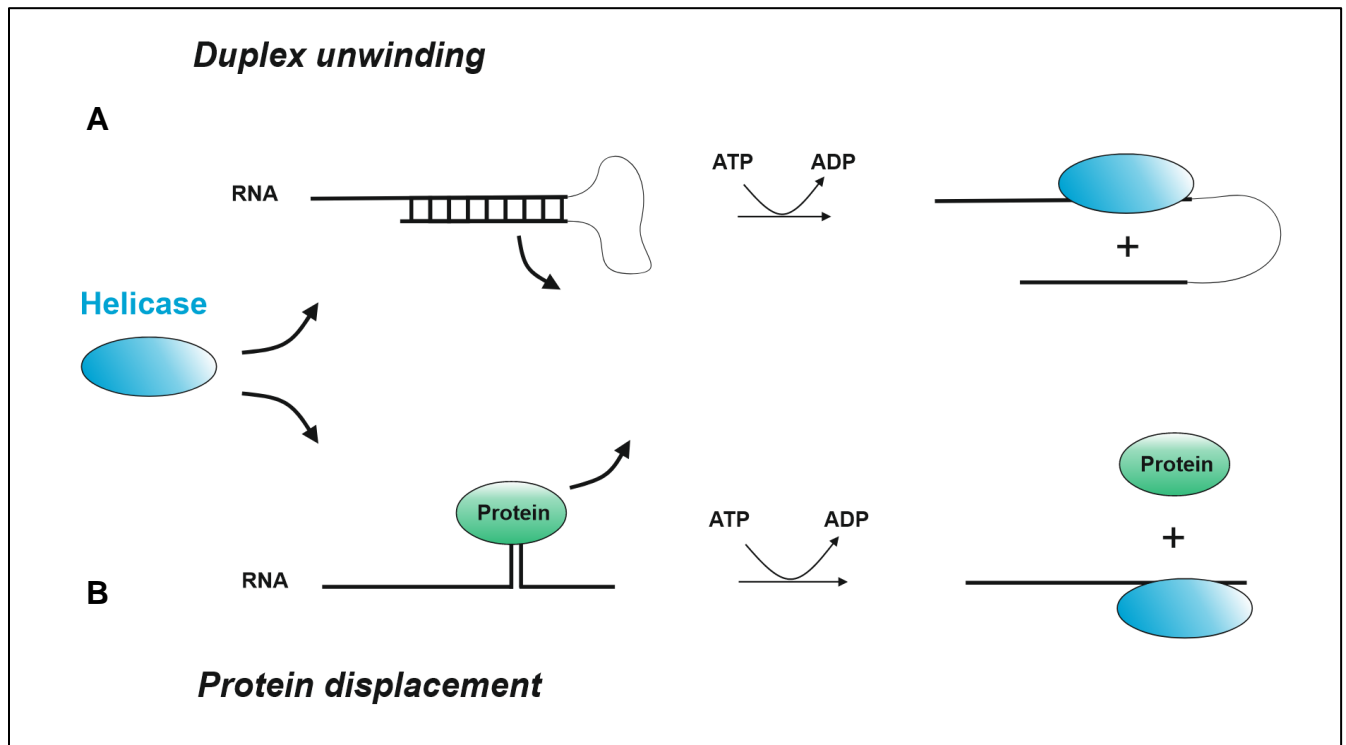


Figure 1: RNA helicases unwind RNA duplexes and remodel RNA-protein complexes. (A) During the duplex unwinding process, the helicase binds in a ATP-dependent manner to a single stranded region of the substrate and translocates towards the opposite end of the RNA in multiple consecutive steps. During the translocation step, the complementary strand is removed. (B) RNA helicases can not only displace nucleic acids but also displace proteins from RNA and thereby remodel RNA-protein complexes.

This fundamental process is required in almost all aspects of nucleic acid metabolism in living cells (Jankowsky, 2011). Indeed, RNA helicases have been implicated virtually in every step of RNA metabolism, from transcription, ribosomal biogenesis, splicing, RNA localization, translation, to RNA surveillance and turnover (see figure 2) (Bleichert & Baserga, 2007), (Fairman-Williams et al., 2010), (Jankowsky & Fairman, 2007), (Rocak & Linder, 2004), (Wahl et al., 2009). RNA helicases are present in all three kingdoms of life as well as in many viruses and represent the most abundant group of enzymes involved in RNA metabolism in eukaryotes (Anantharaman et al., 2002). Homology searches revealed that 95 helicases are encoded within the human genome, 64 of these represent RNA helicases and the remaining 31 represent DNA helicases (Umate et al., 2011). Further 47 out of the poly(A) mRNA-interacting proteins, contain a helicase domain (Baltz et al., 2012), (Castello et al., 2012). RNA helicases are very often part of multi-subunit complexes. Well established examples are Brr2, which is stably associated with the catalytic core of the spliceosome, eIF4A3 (also known as DDX48), a component of the exon junction complex (EJC), and UPF1, which acts in the surveillance complex and the cap binding complex subunit eIF4A (Ballut et al., 2005), (Bessonov et al., 2008), (Kashima et al., 2006), (Linder & Jankowsky, 2011). All these RNA helicases have in common that they impact on their associated protein complexes by inducing NTP-dependent conformational changes.

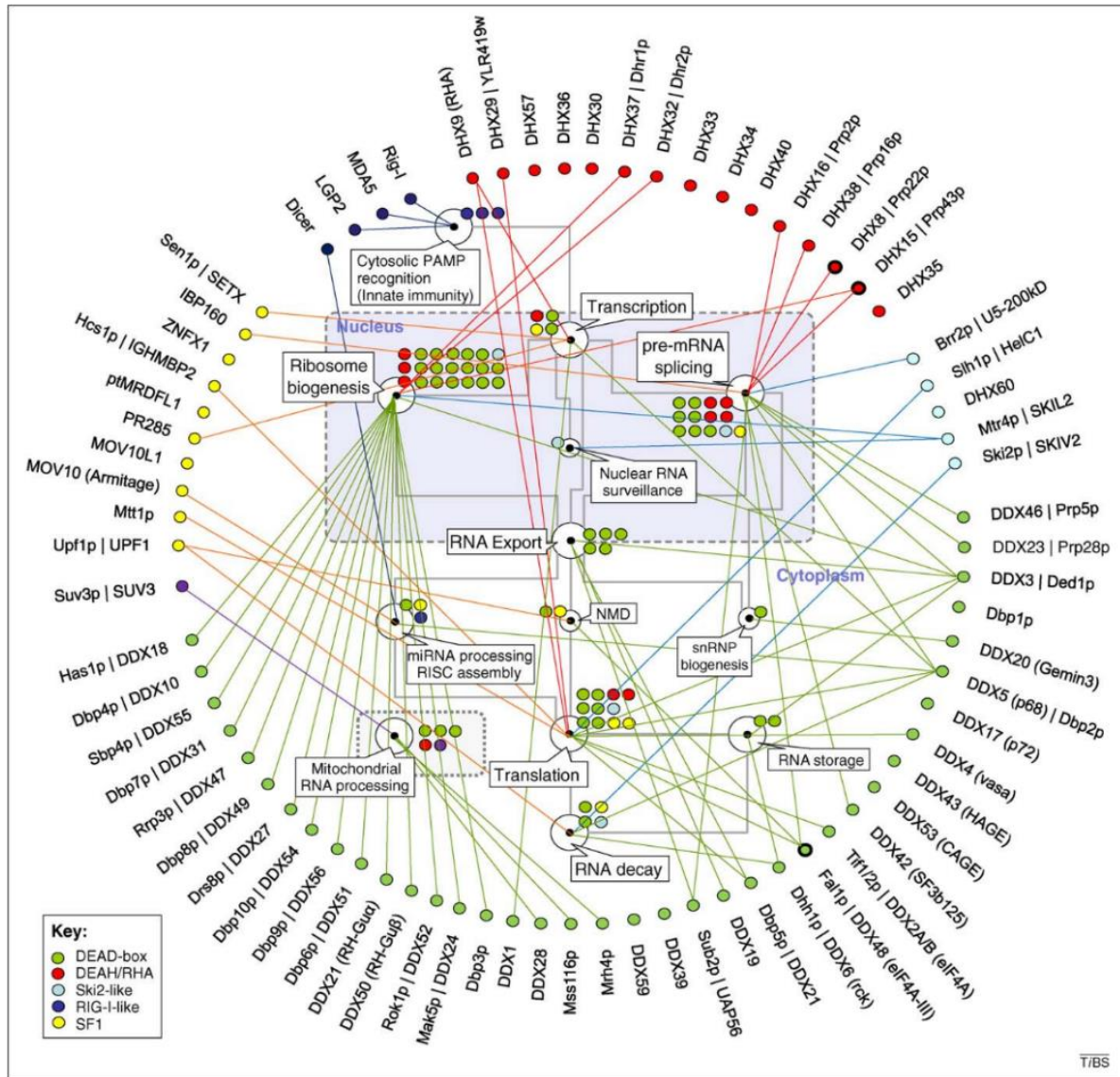


Figure 2: Overview of cellular processes eukaryotic RNA helicases are involved. The relation between each process (white boxes) is marked by the gray lines. The colored circles represent the RNA helicases involved in each process. The helicases (yeast and human nomenclature) are summarized according to their helicase family (bottom box on the left). Figure adopted by (Jankowsky, 2011).

3.2 Helicase families and their mechanism of action

Based on the sequence analysis, DNA and RNA helicases are classified into six super families (SF) termed from SF1 to SF6 (Fairman-Williams et al., 2010). RNA and DNA helicases are closely related and can be divided in two categories, those that are forming rings (mostly hexameric) and those that do not. The classification of the helicases is based on their sequence, structure, and function. All non-ring forming helicases, are part of the SF1 and 2 that harbor two RecA domains, while from SF3 to SF6 either harbor only one RecA or a AAA+-like domain (Taichert et al., 2017). These first two SFs also contain all eucaryotic helicases. Ring forming helicases are in the SFs 3 to 6. All currently known RNA helicases, with the exception of some viral RNA helicases, are part of the SF1 or SF2 and they can be found in the subfamilies Ski2- like, RIG-I-like, DEAD-box, DEAH/RHA, NS3/NPH-II, Upf1-like (see figure 3 A). They share similar dual RecA-like domains, 1A and 2A, that make up the helicase core (Jankowsky & Fairman, 2007).

The helicase core contains at least 12 characteristic sequence motifs at defined positions (Q, I, Ia, Ib, Ic, II, III, IV, V, Va, Vb and VI), that directly participate in NTP-binding and hydrolysis (Q, I, II and VI), RNA recognition (Ia, Ib, Ic, IV, V and Vb) and connection between the two sites (III and Va) (see figure 3 B) (Fairman-Williams et al., 2010). Motif I and II, known as Walker A and Walker B motifs, are the two most conserved motifs and structurally located in a NTP-binding pocket formed between the two RecA-like domains and residues from both motifs interact closely with bound NTP (Cheng et al., 2007), (Linder & Jankowsky, 2011), (Pyle, 2008), (Sengoku et al., 2006). The structurally conserved helicase core is surrounded by C- and N-terminal domains, which are essential for functional aspects of the protein, like substrate-binding domains, oligomerization, protein-interactions and cellular localization. In humans, the largest two RNA helicase families are the DEAD (DDX) proteins and DEAH (DHX) proteins both belonging to the SF2 (Jankowsky, 2011), (Umate et al., 2011), (Fairman-Williams et al., 2010). They are defined by their Asp-Glu-Ala-Asp (DEAD) or Asp-Glu-Ala-His (DEAH) amino acid sequences (Rocak & Linder, 2004).

DEAD box RNA helicases typically show a bidirectional unwinding activity, meaning they can unwind RNA duplexes in both directions ($3' \rightarrow 5'$ and $5' \rightarrow 3'$). Furthermore, they are considered non-processive, and hence do not translocate along longer stretches of RNA. Instead, they perform their function through a clamping-mode to facilitate local strand unwinding or complex remodeling of RNA-bound complexes (Jankowsky & Fairman, 2007), (Linder & Jankowsky, 2011). Members of this class are likely acting as “RNA chaperones” or “maturases” to ensure that the correct interactions are formed or as energy-dependent “facilitators” to drive multistep reactions to completion (Jarmoskaite & Russell, 2011).

In contrast, DEAH-box RNA helicases display processivity and thus are able to unwind nucleic acid double stands in either $3' \rightarrow 5'$ or $5' \rightarrow 3'$ direction. Accordingly, DEAH helicases have been described to unwind either RNA-RNA duplexes, RNA-DNA duplexes or both (Jankowsky & Fairman, 2007), (Kawaoka et al., 2004), (Kawaoka & Pyle, 2005), (Pang et al., 2002). For their activity, these enzymes require a free 5' or 3' RNA overhang for initial binding, which enables moving along the RNA molecule to displace the other strand. During this action, the RNA becomes unwound and secondary structures are resolved. In contrast to the DEAD-box helicases, DEAH-box helicases lacking the Q-motive (confers ATP specificity) and harbor an additional β -hairpin (triangle) which is important for the processivity (see figure 3 B) (Cordin & Beggs, 2013).

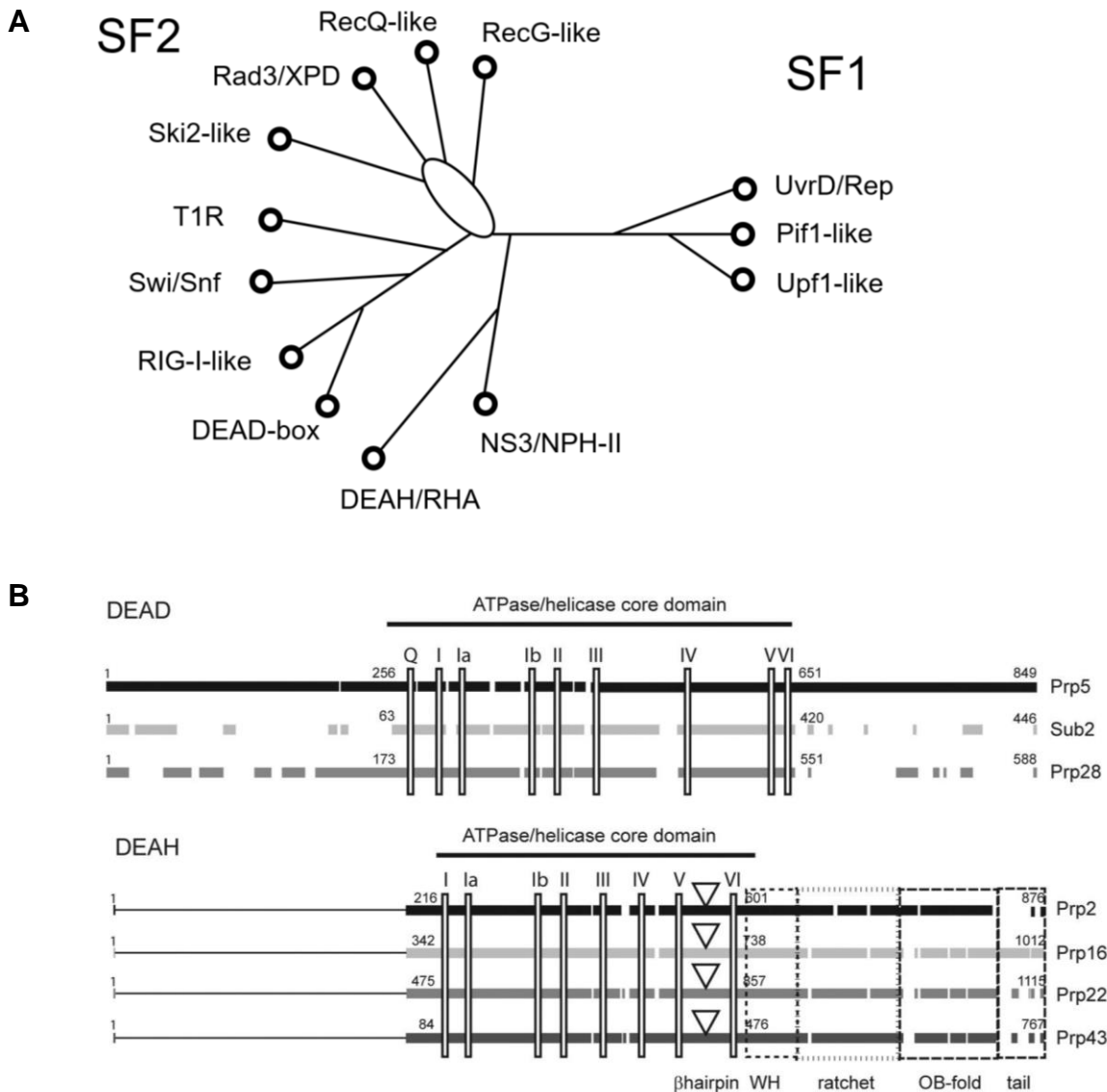


Figure 3: Overview of members of the SF1 and SF2 helicase families. (A) The oval indicates significant uncertainty of the protein topology in this region. The first two SFs contain all eukaryotic helicases including all currently known RNA helicases, with the exception of some viral RNA helicases. RNA helicases can be found in the subfamilies Ski2-like, RIG-I-like, DEAD-box, DEAH/RHA, NS3/NPH-II, Upf1-like. Figure derived from Jankovsky, 2011. (B) Sequence comparison of DEAD-box helicases and DEAH-box helicases from *S. cerevisiae*. The black and grey parts represent the conserved regions in each family. The position of conserved motives is indicated by the vertical lines. The DEAH-family lacking the Q-motive and harbor an additional β -hairpin (triangle) which is important for the processivity. Figure adopted from (Cordin & Beggs, 2013).

Recent structural studies on the basis of different conformational states of RNA helicases have been elucidated as to how the NTP-binding and hydrolysis is coupled with the binding of the RNA substrate in the helicase core and how the RNA unwinding is facilitated (Pyle, 2008). SF1 and SF2 share common features consisting of two dual RecA-like domains that shape together a nucleotide binding site, where the RNA is bound (see figure 4) (Fairman-Williams et al., 2010). Mechanistic models for the RNA translocation have shown that during the transition along the nucleic acid RecA2 performs an opening and closing motion between the nucleotide-free and bound states. During these conformational extremes, the RNA bases are assembled in the RNA binding pocket between a long β -hairpin in RecA2 and a conserved loop in RecA1 (termed “Hook-turn”). During the transition between these two states the β -hairpin and two other RNA-binding patches in RecA2 shift 1 nucleotide towards the 5' end of the RNA (Studer et al., 2020).

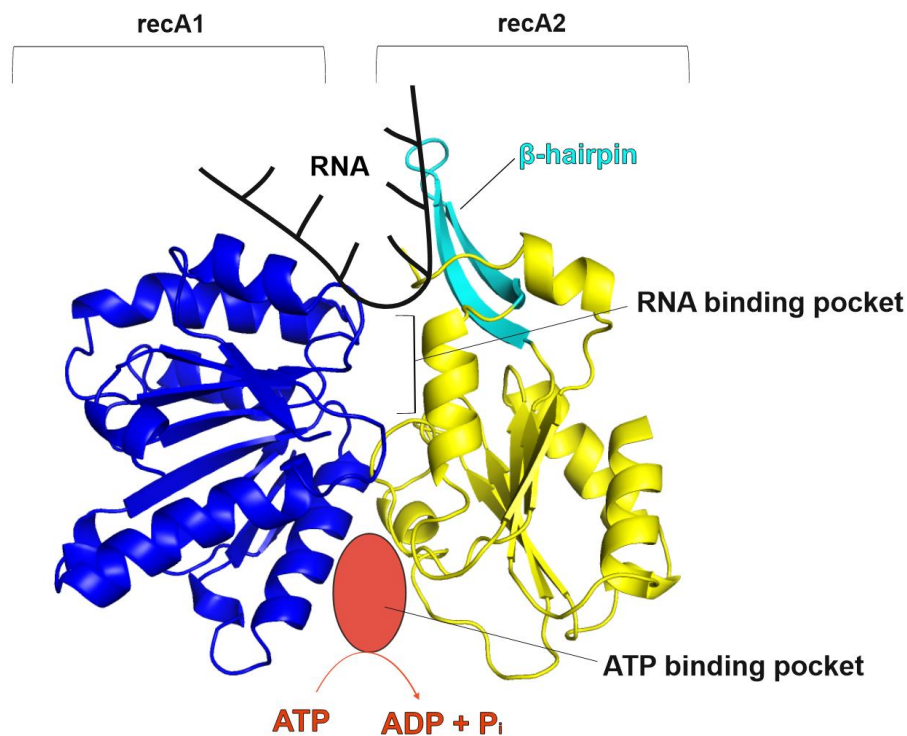


Figure 4: Overview of the helicase core of DEAH-box helicases. Model generated by SWISS-MODEL (details in figure S1). The recA1 and recA2 domains form a RNA binding pocket, where the RNA substrate gets tethered in a ATP dependent manner. See text for details.

3.3 RNA helicases in translation

RNA helicases are a major and important protein family in the context of RNA metabolism. RNA helicases are of immense importance especially during mRNA translation (see figure 2). The key regulatory events are occurring during the initiation phase of translation, where the translation rate is affected by the structure within the 5' UTR and the presence or absence of initiation and regulatory factors. A well characterized RNA helicase involved in translation initiation is the eIF4A (DDX2) subunit of the cap-binding complex eIF4F. Its crucial role is in unwinding secondary structures that may form the 5' UTR of the mRNA during translation initiation (Jaramillo et al., 1990).

Also other RNA helicases were identified as modulators of translation at the state of initiation such as DHX29 (also known as Ded1), DHX9 (also known as RHA) and DDX6 (also known p54 or RCK) (Shen & Pelletier, 2020). None of these helicases alone possess a processive activity that is sufficient enough to melt secondary structures of the 5' UTR to allow the ribosome to scan towards the initiation codon. It is hypothesized that several helicases are needed at the same time for the recruitment of binding partners to amplify the helicase processivity to fulfill this function *in vivo* (Merrick, 2010). Another RNA helicase involved in translation initiation is DHX29 whose main role is to promote translation initiation of mRNAs with moderate to strong 5' UTR secondary structures (Pisareva et al., 2008). DHX29 cycles between NTP- and nucleoside 5'-diphosphate (NDP)-bound states, results in the opening and closing of the 40S ribosome mRNA entry channel. In addition to this structural remodeling of the ribosome DHX29 can directly unwind mRNA secondary structures (Abaeva et al., 2011).

Whereas the above-mentioned RNA helicases act globally on a broad range of mRNAs, DHX9, also known as RNA Helicase A (RHA) unwinds secondary structures in the 5' UTR of very specific mRNA classes (Hartman et al., 2006). This specificity is determined by motifs outside of the helicase core, which target the so-called 5' post-transcriptional control element (PCE) (Hartman et al., 2006).

This control element can be found in the RNA genome of retroviruses like HIV-1 or human T-lymphotropic type 1 viruses) and is used by DHX9 to facilitate translation of the viral RNA, as well as to enhance the infectivity of progeny virions (Bolinger et al., 2010), (Brady et al., 2019). PCE exists also in cellular mRNAs, for example in the mRNA encoding the JUND growth-control protein, which contains a highly structured 5' UTR and initiates translation in a cap-dependent mechanism (Short & Pfarr, 2002). It has been proposed that DHX9 stimulates ribosome scanning through its helicase activity and controls the RNA–protein rearrangements, and thus facilitates translation initiation (Tettweiler & Lasko, 2006). Other studies showed that DHX9 is able to bind its substrate mRNA via its N-terminal domain and to rearrange the highly structured 5' UTR (Ranji et al., 2011).

RNA helicases may also negatively regulate the translation such as DDX6 (also known as p54 or RCK), which has been proposed as a translation repressor involved in promoting the decapping of mRNAs, which targets mRNA for degradation (Fischer & Weis, 2002). DDX6 exerts its function by inhibiting the assembly of the 48S pre-initiation complex on the mRNA, which hinders the process of translation initiation (Coller & Parker, 2005).

3.4 Signaling pathways associated to translation

The translational output of a given cell can also be modulated by altering the activity of the translation machinery itself. Changes in the cellular environment can have an impact on the signaling cascades that result in downregulation, modification, sequestration, or degradation of components of translation factors (Deribe et al., 2010). One of the most important mechanisms of global translational control is phosphorylation of translation initiation factors and ribosomal proteins. Two major signaling pathways known to be implicated in this process are the mTOR/PI3K/Akt pathway and the mitogen activated protein kinase (MAPK) pathway (Saxton & Sabatini, 2017).

The main function of the mammalian target of rapamycin (mTOR) cascade are growth factors, hormonal stimuli and nutrient availability and the promotion of protein synthesis under favorable cellular conditions.

mTOR is a serine/threonine kinase and interacts with the protein GβL and forms two distinct complexes, mTORC1, with Raptor (regulatory associated protein of mTOR) and MTORC2, with Rictor (rapamycin insensitive companion of mTOR) (Hara et al., 2002), (Kim et al., 2002). These two complexes can phosphorylate the ribosomal protein S6 kinase (S6K) and the serine/threonine kinase Akt respectively (Sarbasov et al., 2005). S6K and MTORC1 may also directly phosphorylate translation initiation factors or other binding proteins resulting in an increasing of translational output whereas phosphorylated Akt promotes the MTORC1 activity (Laplante & Sabatini, 2012).

These signaling cascades are of particular importance for mRNAs which are translated in a growth dependent manner, in particular those encode for proteins of the translation apparatus. They contain the unusual m⁷GpppC cap followed by a stretch of 4 to 14 pyrimidine collectively termed TOP mRNAs (Meyuhas & Kahan, 2015). The TOP motif is present in all 79 human ribosomal proteins as well as non-ribosomal proteins involved in translation including multiple subunits of eIF3, eIF4A, eEF2, and poly(A) binding protein (PABP) (Iadevaia et al., 2008). It acts as a *cis*-regulatory element that in itself is sufficient for the regulation of translation in response to growth stimuli or nutrient deprivation. A prime main regulator of the translation of 5'TOP mRNAs is the RNA binding protein LARP1. This protein is also a target of mTORC1 and interacts physically with mTORC1 via RAPTOR (Fonseca et al., 2015). Via this interaction LARP1 is able to directly interact with the 5'TOP motif and modulates their translation (Cockman et al., 2020).

3.5 The RNA helicase DHX30

The subject of this PhD thesis is the RNA helicase DHX30. The *DHX30* gene encodes for a putative ATP dependent RNA helicase DHX30 which is a member of the superfamily 2 (SF2) of RNA helicases (Umate et al., 2011). The essential gene product of *DHX30* is a 134 kDa protein which is organized in a modular manner. The central helicase core of DHX30 consists of two domains that resemble the bacterial recombination protein recombinase A (referred to as RecA-1 and RecA-2).

These two core helicase domains contain eight highly conserved sequence elements which play an important role in either RNA binding, or ATP binding and hydrolysis. Besides the helicase core DHX30 harbors two N terminal double-stranded RNA-binding domains (dsRBD 1 and 2). Furthermore, a winged helix domain (WHD), a ratchet-like (RL) domain, and an oligosaccharide binding (OB) domain are present at the C-terminus (see figure 5) (Lessel et al., 2017).

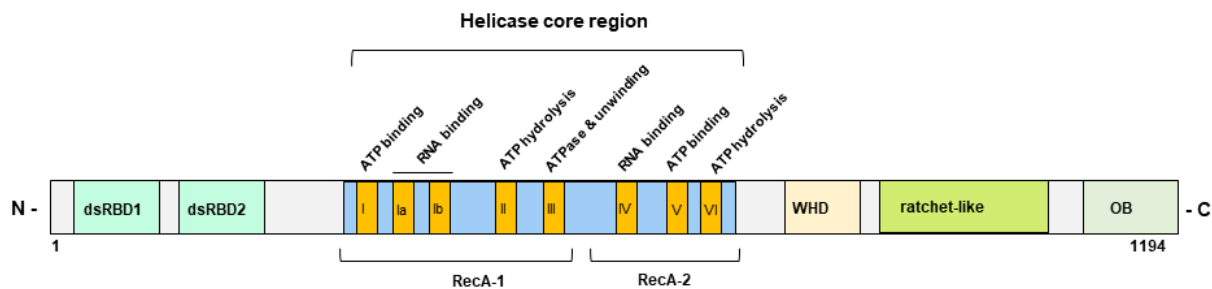


Figure 5: Domain organization of DHX30. DHX30 belongs to the Superfamily 2 helicase and contains a highly conserved helicase core with the typical RecA-1 and RecA-2 domains, containing sequence elements (I, Ia, Ib, II, III, IV, V, VI) important for RNA binding, or ATP binding and hydrolysis. The N-terminus harbors two double-strand RNA binding domains (dsRBD1 & dsRBD2) and the C-terminus a winged helix domain (WHD), a ratchet-like (RL) domain and an oligosaccharide building (OB) domain.

Although DHX30 was classified as an RNA helicase based on sequence similarities to other RNA helicases, it was at the beginning of this work unknown whether this protein actually possessed helicase activity.

3.5.2 Putative cellular functions of DHX30

DHX30 has been shown to localize mainly to the cytoplasm (Lessel et al., 2017). Consistent with this localization, a recent study identified DHX30 as a ribosome associated factor (Simsek et al., 2017). Studies showed that the depletion of DHX30 results in a constitutive change in polysome-associated mRNAs. Further it was showed that a knockdown of DHX30 results in an enhancing of the translation of mRNAs coding for cytoplasmic ribosomal proteins and a reduction in translation efficiency of nuclear-encoded mitoribosome mRNAs. It is further proposed that the mitoribosome transcripts as direct targets of DHX30 (Bosco et al., 2021). DHX30 may exert its function upon binding to a specific *cis*-element called CGPD (CG-rich motif for p53-dependent death) found in 3'UTRs of mRNAs which are associated to cell fate upon apoptosis. Higher expression of DHX30 caused reduced translation of GCPD-motif-containing transcripts in HCT116 cells (Rizzotto et al., 2020).

In the context of viral infections DHX30 was described as a factor interacting with the antiviral zinc-finger protein ZAP via its N-terminus. ZAP is a host factor which inhibits viral replication by eliminating viral mRNAs in the cytoplasm and the interaction with DHX30 is important for the activity of ZAP (Ye et al., 2010). There are two DHX30 isoforms present in cells, however, only one harbors a mitochondrial localization signal (Bosco et al., 2021). This isoform impacts on mitochondrial ribosome maturation and assembly via its interaction with the Fas-activated serine-threonine kinase (Antonicka & Shoubridge, 2015). DHX30 shows a high expression level in neural cells and somites during embryogenesis in mice suggesting an important role in neuronal development (Zheng et al., 2015). However, its precise function is currently unknown.

3.5.3 DHX30 is linked to neurodevelopmental disorder NEDMIAL

DHX30 is an essential gene in mice and its knockout results in developmental defects in the central nervous system (CNS). In accordance with these findings in mice, Lessel et al. reported 12 unrelated patients, with mutations in *DHX30* displaying a severe neurodevelopmental disorder. This rare autosomal dominant neurodevelopmental disorder called “Neurodevelopmental Disorder with severe Motor Impairment and Absent Language” or also called NEDMIAL is linked to *de novo* missense mutations in the *DHX30* gene. The main clinical features of this disease are global developmental delay, intellectual disability, severe speech impairment, and gait abnormalities. Additional symptoms include autistic features, behavior challenges, sleep disorder, seizures, hyperflexible joints, involuntary movements, distinctive facial features, and strabismus.

Six different *de novo* missense mutations were identified by whole-exome sequencing within the helicase core region of *DHX30*, which is predicted to mediate either ATP binding/hydrolysis or RNA recognition (see figure 6). They could confirm that the 5 mutations were present in the ATP binding motifs II or VI and showed reduced ATPase activities compared to the wild-type. One remaining variant located in the putative RNA-binding motif Ia did interfere with the binding capacity toward some target RNAs. Overexpression of mutated forms of *DHX30* resulted in an abnormal accumulation of the mutant *DHX30* in cytoplasmic stress granules, which was associated with a global decrease in translational output. It was hence suggested that the mutations of *DHX30* result in a state of a chronic cellular stress condition, which in combination with a misregulated translation results in the diseased phenotype.

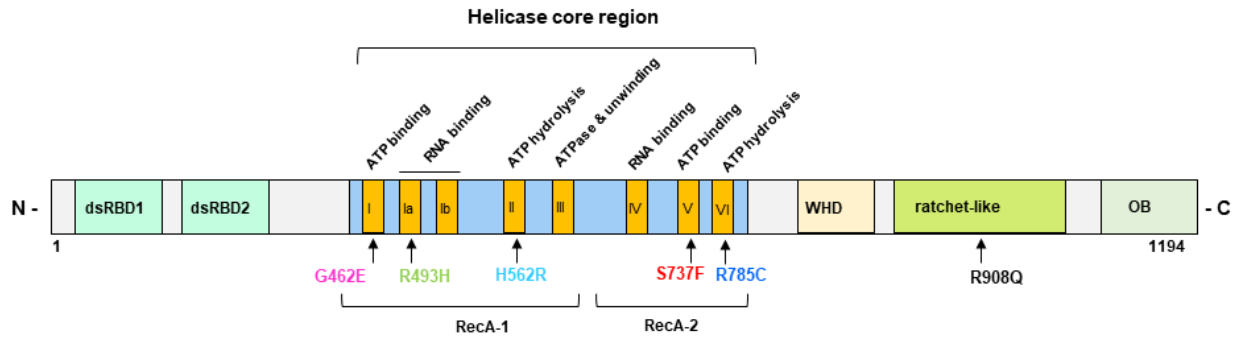


Figure 6: Overview of identified mutations of DHX30 in NEDMIAL patients. Schematic protein structure of DHX30 with a highly conserved helicase core with the typical RecA-1 and RecA-2 domains, containing sequence elements (I, Ia, Ib, II, III, IV, V, VI) important for RNA binding, or ATP binding and hydrolysis. The mutations identified in the patients are localized in different sequence elements of the conserved helicase motifs. One mutation (R908Q) is localized in the ratchet-like domain.

3.6 Aim of this study

The DHX30 gene encodes for a putative DEAH-box RNA helicase and recent studies identified DHX30 as a candidate gene for a human neurodevelopmental disorder (Eldomery et al., 2017), (Zheng et al., 2015). The main goal of this study was to link DHX30 to a specific cellular pathway and to gain a better understanding of the potential function of this RNA helicase on a molecular level. As an initial step towards this end, attempts were made to characterize its enzymatic activities *in vitro*. The basis for these studies is the availability of recombinant functional protein in large amounts and an enzymatically active state. For this purpose, an efficient bacterial expression and purification strategy was established. Since DHX30 contains a highly conserve helicase core and belongs to the SF2 helicases, a major focus of these studies was put on the characterization of DHX30 putative ATPase and nucleic acid unwinding activities.

The second focus of this work was to shed light on the role of DHX30 in cellular RNA metabolism, an aspect which has been almost unexplored so far. For this purpose, eukaryotic stable cell lines were established and DHX30 protein complexes were purified to identify and characterize the cellular DHX30 interactome. The third focus of this work was to elucidate the impact of DHX30 depletion on cellular mRNA metabolism. By performing a transcriptome analysis in polysome gradients upon DHX30 knockout, deregulated RNAs on a transcriptional and on the post-transcriptional level were identified and characterized. In the last part of this work, pathogenic variants of DHX30 were expressed along the same line as already established for the wild-type protein and compared with the wild-type protein in terms of their enzymatic activities. Lastly, the pathogenic DHX30 variants were investigated for their interaction with its cellular partners.

4. Results

4.1 Purification and biochemical characterization of DHX30, a putative member of the Helicase Superfamily 2

DHX30 has been classified as a member of the DEAH-family in the Superfamily 2 of helicases. According to the sequence similarity of DHX30 to other RNA helicases and the presence of eight highly conserved motifs, which are predicted to mediate either ATP binding/hydrolysis or RNA recognition it is proposed that DHX30 has an RNA unwinding activity. As an initial step for detailed analysis of its enzymatic activities an expression and affinity purification strategy for a full-length recombinant DHX30 from bacterial cells was established. The recombinantly expressed and purified DHX30 was used for the enzymatic assays of DHX30 as a RNA helicase, namely ATP hydrolysis activity and unwinding activity on RNA substrates.

4.1.1 Expression and Purification of recombinant full-length DHX30

The availability of native and enzymatically active DHX30 was the prerequisite for its detailed functional characterization. To this end, an expression protocol in *E. coli* was established. To achieve that, the full-length sequence of DHX30 wild-type, as well as pathogenic variants were inserted into a pet-28M vector and transformed into a *E. coli* Rosetta strain. The recombinant protein was expressed as a fusion containing a N-terminal hexahistidine tag (6xHis-tag) and an adjacent SUMO tag to improve its solubility and allowing the isolation via Ni-NTA affinity chromatography and Superdex75/100 gel filtration (see figure 7).

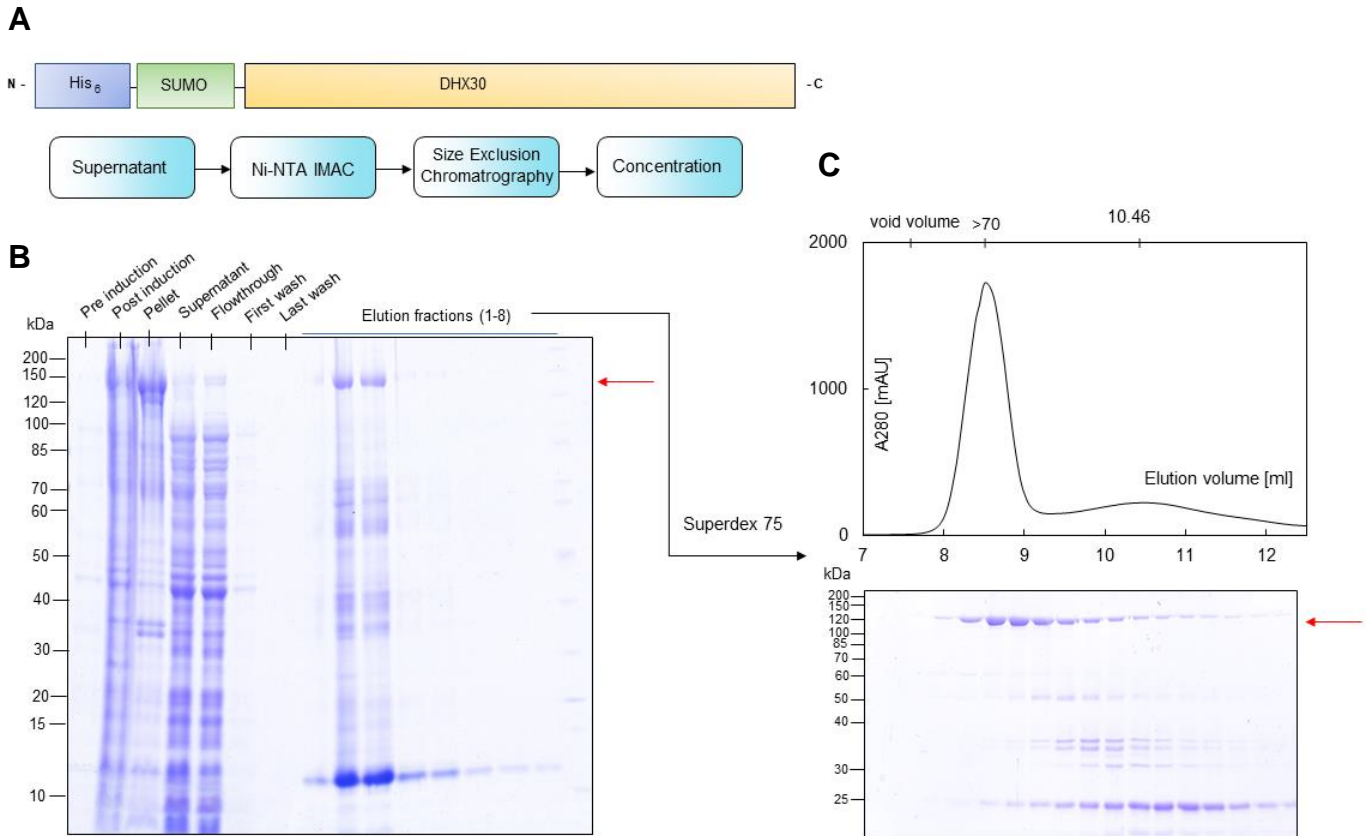


Figure 7: Strategy for expression and purification of DHX30 in *E. coli*. (A) The pet-28M vector containing the full length DHX30 flanked by a N-terminal Hexahistidine SUMO tag was transformed into *E. coli* strain Rosetta pLys pRARE. In the first step, the cells were lysed and the supernatant containing the target protein was applied to Ni-NTA beads. The eluate from the Ni-NTA column was loaded on a size exclusion chromatography column (Superdex 75/100). The respective fractions containing the target protein were collected and concentrated with a Vivaspin 500 column. (B) Ni-NTA purification of recombinantly expressed DHX30 in *E. coli*. Protein expression was induced with 1 mM IPTG at 14°C overnight. The lysate was fractionated by high-speed centrifugation and the supernatant was incubated with Ni-NTA agarose beads. The bound proteins were eluted with imidazole (elution fractions 1 - 8). The target protein is clearly visible at ca. 135 kDa (red arrow). Proteins were analyzed by 12% Bis-Tris PAGE and visualized by Coomassie staining. (C) Gel-filtration chromatography of recombinantly expressed full-length 6xHis-SUMO DHX30 using a Superdex 75/100 column. The peak between 8 ml and 9 ml contains recombinant 6xHis-SUMO DHX30 (ca. 140 kDa) (red arrow). Peak fractions were analyzed by SDS-PAGE (12% Bis-Tris) and Coomassie staining.

Under optimal conditions (induction with 1 mM IPTG at 14°C for 16h) a fraction of the expressed protein was soluble and could be isolated by means of affinity chromatography and gel filtration. As shown in figure 7, the full-length 6xHis-SUMO DHX30 was efficiently recovered from the resin. The elution fractions containing the target protein were pooled, concentrated with a concentration column (Vivaspin 500) and applied on a Superdex 75/100 gel filtration column to remove remaining contaminants (figure 7C). The target protein elutes close to the void volume, corresponding to a mass of around 140 kDa, and thus is likely monomeric and non-aggregated. The peak fractions containing the purified 6xHis-SUMO DHX30 were pooled and concentrated with a concentration column (Vivaspin 500) for functional and enzymatic studies. The purity of the recombinant protein was estimated to be about 85% by Coomassie blue staining and the total yield of purified 6xHis-SUMO DHX30 was about 0.3 mg obtained from a 2L *E.coli* culture.

4.1.2 RNA unwinding activity of recombinant DHX30

To test whether the recombinantly expressed full-length DHX30-WT is enzymatically active an RNA unwinding assay was established. For this, a synthetic [³²P]-labeled RNA molecule which carries a sequence with a strong propensity to self-annealing and forms a double helix which was synthesized by T7 transcription (see figure 8 A).

Analysis of this RNA substrate by non-denaturing PAGE resulted in a single band of low electrophoretic mobility, corresponding to the dimer linked by the double helical segment. Upon pre-incubation at 95°C, this dimer converted into its monomeric form and consequently migrated in the gel with higher mobility. To determine which is the minimal protein amount of the DHX30-WT necessary to resolve the dimeric form, a titration analysis was performed. A constant concentration of RNA substrate was incubated with increasing amounts of recombinant protein. In the presence of ATP, 10 nm of DHX30-WT was sufficient to resolve the dimer almost completely into the monomeric form after 30 min (see figure 8 B). This reaction was entirely ATP dependent thus confirming that the purified His-SUMO DHX30-WT possesses an ATP-dependent RNA helicase activity (see figure 8 B).

To determine the specificity of the unwinding activity, a DHX30 version carrying a mutation in the ATP binding site (G462E) which was purified in the same manner as the WT was used. This control shows that the unwinding reaction was solely catalyzed by the protein and not due to any contaminating component in the reaction mixture (see figure 8 C).

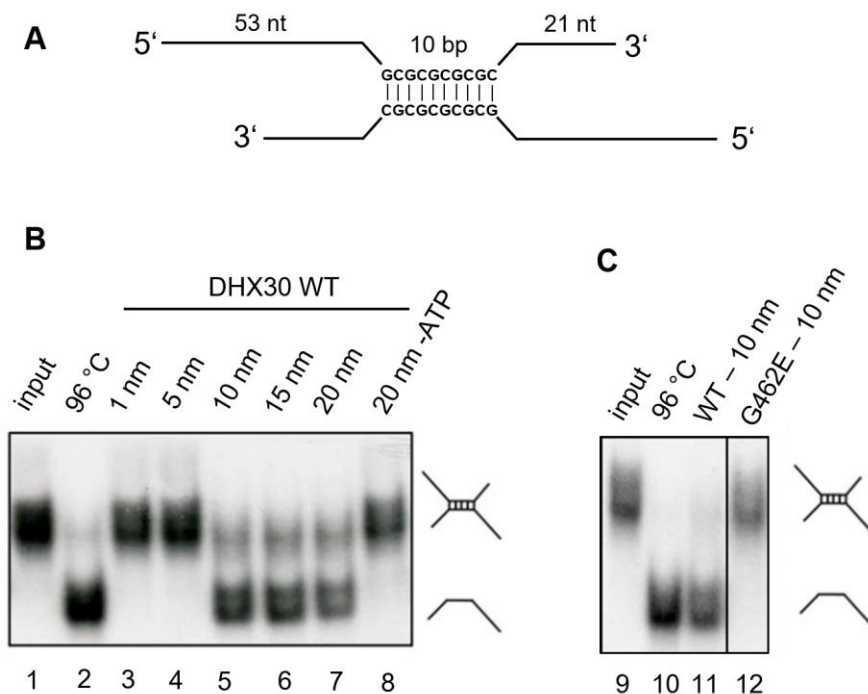


Figure 8: ATP-dependent RNA unwinding activity of recombinant DHX30. A radiolabeled RNA duplex containing a 5' and 3' overhang (A) was incubated with increasing amounts of recombinant His-SUMO DHX30-WT protein in the presence of ATP (B lane 3 – 7) and analyzed by native RNA gel electrophoresis. The positions of duplex and single-stranded RNA are indicated. The [³²P]-RNA duplex in the absence of protein is shown in lane 1 (input) and in the absence of ATP in lane 8. The single-stranded RNA products are determined by comparison with those generated by denaturing the RNA duplex alone at 96°C (lane 2). (C) To determine the specificity of the unwinding activity, a DHX30 version carrying a mutation in the ATP binding site (G462E) was used (lane 12).

4.2 Cellular localization of DHX30 via immunofluorescence microscopy

To gain insight into a potential cellular function of the RNA helicase DHX30, I next tried to find the localization of the protein in U2OS cells by indirect immunofluorescence microscopy. U2OS cells were cultured on coverslips, fixed, stained with DHX30 primary antibody (Bethyl) and subsequently visualized with fluorescent-labeled secondary antibodies. Using confocal laser microscopy, a predominant localization of DHX30 in the cytoplasm was detected and only very small amounts in the nucleus. In the cytoplasm DHX30 seems to be part of granular structures around the nucleus (see figure 9, green channel). These results are in line with previous findings which showed that DHX30 is predominantly localized in the cytoplasm (Lessel et al., 2017).

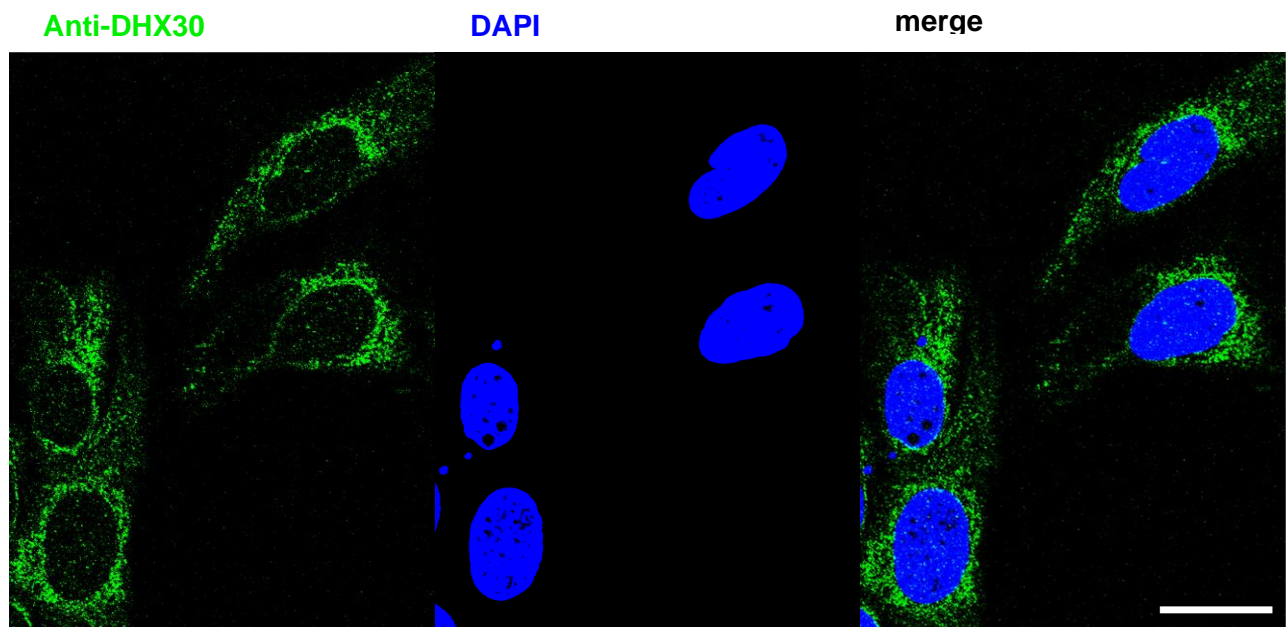
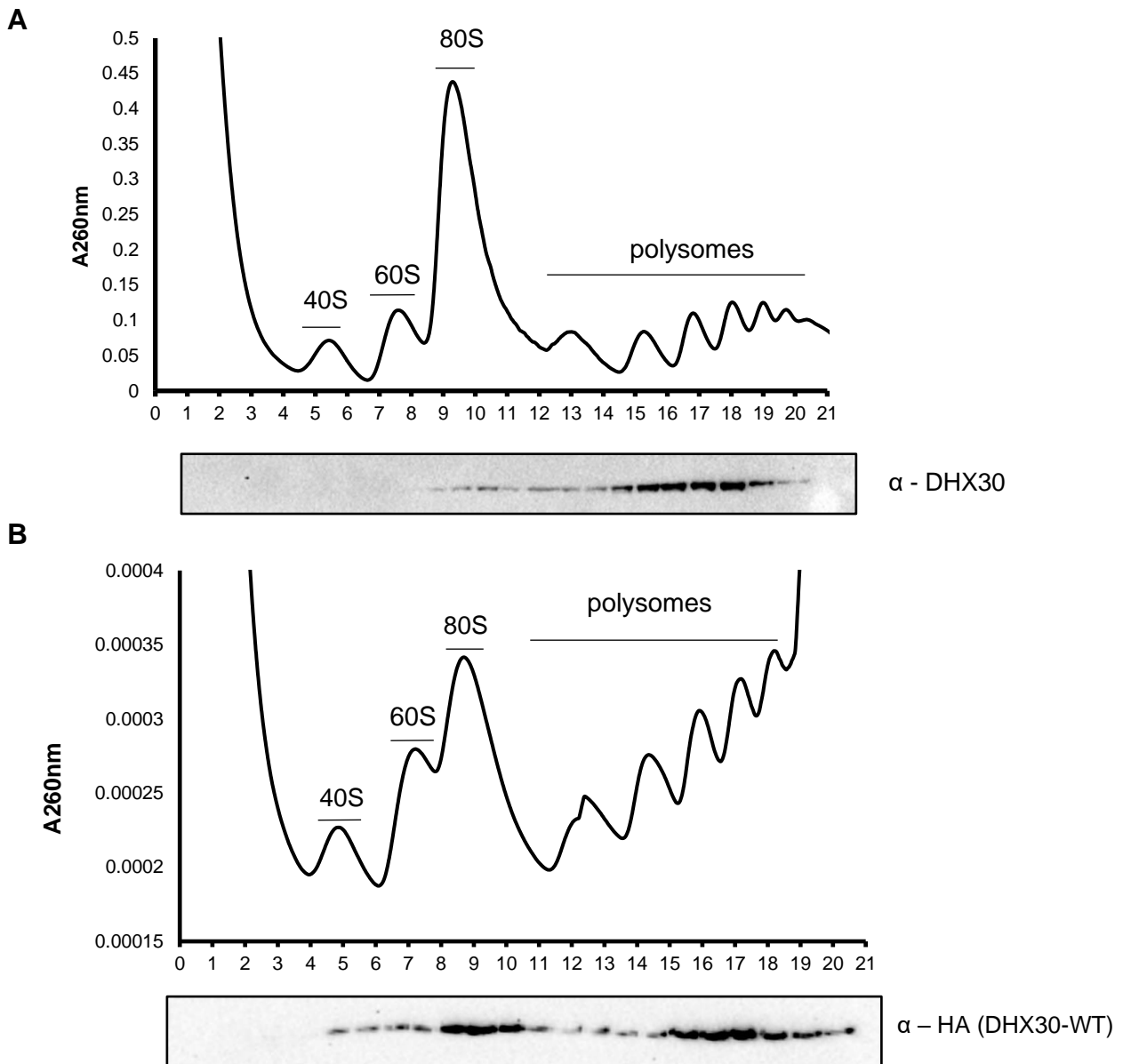


Figure 9: Cellular localization of DHX30 via immunofluorescence microscopy. U2OS cells were cultured on cover slips, fixed by 4% formaldehyde, permeabilized and blocked in 8% BSA containing 0.3% triton X-100. Cells were incubated with anti-DHX30 antibody (Bethyl) and subsequently with Alexa Flour 488-conjugated secondary antibody followed by counterstaining with DAPI. Nuclei are visualized via DAPI staining (blue). Scalebar: 20 μ m

4.3 DHX30 co-migrates with ribosomes

The enzymatic RNA helicase activity of DHX30 in conjunction with its cytosolic localization raised the possibility that this factor is connected to the cellular translation machinery or other cytosolic RNA metabolic events. In order to determine whether DHX30 is part of known macromolecular entities acting in these pathways I performed sucrose-gradient centrifugation studies with native cellular extracts. With this technique, it is possible to separate cellular components from a crude cellular lysate through a gradient based on their shape and molecular size.

Therefore, HEK293T cells were lysed under near- physiological conditions and extracts were separated over a 5 % to 45 % sucrose gradient by centrifugation. After harvesting the gradient, the fractions were separated by SDS-PAGE and the protein was visualized by Western blot with an anti-DHX30 antibody. As shown in figure 10, the majority of DHX30 co-migrates with polyribosomes (fraction 15 to 20), especially in the heavier fractions. A minor fraction of DHX30 co-migrates also with the 80S ribosomal particle (fraction 9 and 10). The same experiment was performed in a Flp-In T-REx 293 cell line overexpressing DHX30-FLAG/HA. The co-sedimentation of the overexpressed DHX30-FLAG/HA (figure 10 B) shows a similar pattern like endogenous DHX30 (figure 10 A). The major portion of DHX30-FLAG/HA co-sediments with heavy polysomes and 80S and only a minor population with ribosomal subunits.



Next, I wanted to test whether DHX30 binds directly to ribosomes and also co-sediments with the translation machinery. *E. coli* purified His-SUMO-DHX30-WT full-length protein was incubated with purified HeLa ribosomal particles (40S, 60S and 80S) in a molar ratio of 1:1 and subsequently analyzed by sucrose gradient centrifugation. The gradients were harvested, individual fractions separated by SDS-PAGE and proteins analyzed by Western blotting (figure 11).

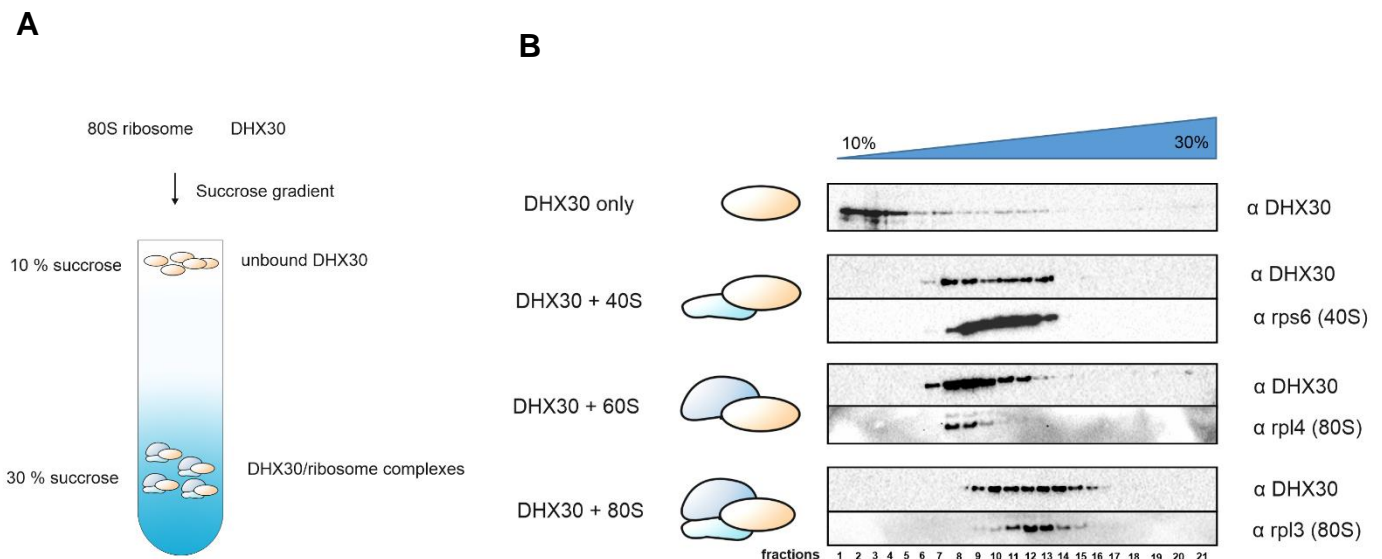


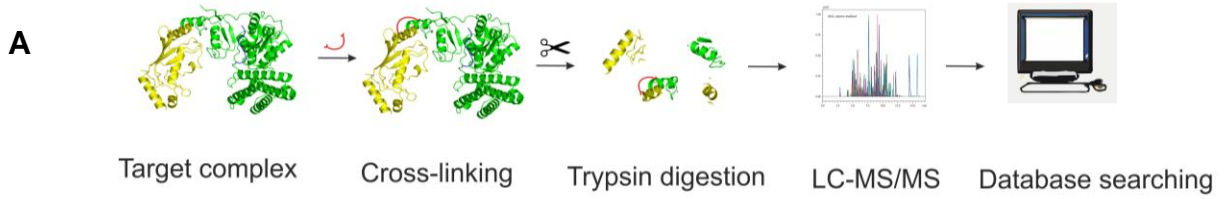
Figure 11: DHX30 forms a complex with ribosomal particles *in vitro*. (A) Purified His-SUMO-DHX30-WT was incubated with purified ribosomal particles (40S, 60S and 80S) from HeLa cells and loaded on a 10 to 30% sucrose gradient. DHX30/Ribosome complexes run in heavier fractions than the unbound protein. (B) Western Blot analysis of the sucrose fractions against DHX30 and ribosomal subunits show that DHX30 is co-migrating with 40S, 60S and 80S ribosomal particles (fractions 7 to 16).

As shown in figure 11 B, the His-SUMO-DHX30 control remains in the top fractions (fraction 1 to 4) of the gradient due to its low S-value confirming that the recombinant protein does not form larger aggregates. A shift to higher S-values was observed upon incubation of His-SUMO-DHX30 with either 40S, 60S or 80S ribosomal particles (fraction 7 to 16). Since DHX30 co-migrated under these conditions with ribosomal particles these results strongly indicate binding to ribosomes and its subunits *in vitro*.

4.4 DHX30 directly interacts with ribosomes via its N-terminal dsRNA-binding domain

Next, I performed experiments aiming to gain insight into the mode of interaction between DHX30 and the translation machinery. To this end, a chemical crosslinking-approach was combined with an analysis of protein fragments by means of mass spectrometry. This approach is based on the application of the bifunctional reagent bis-sulfosuccinimidyl suberate (BS3), which covalently links adjacent lysines in a given protein complex under physiological conditions. Reconstituted His-SUMO-DHX30-ribosome complexes from the sucrose-gradients were crosslinked with 0.3 mM BS3 crosslinker for 1h at 4°C. The crosslinked sample was then analyzed by an established cross-linking/mass spectrometry analysis in the Group of Henning Urlaub (Max Planck Institute for multidisciplinary natural sciences, Göttingen) (see figure 12).

Among several weak X-link sites, two major crosslinks between DHX30 and ribosomal proteins were identified. The crosslink with the highest score (1,43) was between amino acid 108 of the ribosomal protein RPS3, and the amino acid 48 of the N-terminal dsRNA-binding domain 1 (dsRBD1) of His-SUMO DHX30 (see figure 12 B + C). The ribosomal protein 3 (RPS3) is part of the small ribosomal subunit (40S) and is located at the mRNA entry channel at the A site of the 80S ribosome (figure 12 D). Another crosslink with a lower score (score 0,7) was identified between the dsRBD1 of DHX30 and the ribosomal protein 8 (RPL8), which is in contrast to RPS3 a structural part of the large ribosomal subunit (60S). RPL8 is located in between the 40S and 60S ribosomal subunits (see figure 12 E). These X-link data confirm that DHX30 indeed interacts with both subunits and that this interaction is highly specific. The fact that the crosslinks are on two sites of the ribosome could be an indication for different functions of DHX30 at the ribosome, either the modulation of mRNA translation or a function in the interface of the two ribosome subunits for example during the ribosomal subunit joining.



B

Ribosomal subunit	Protein 1	Protein 2	AbsPos1	AbsPos2	Max of Score
40S	sp Q7L2E3 DHX30_HUMAN	sp P23396 RS3_HUMAN	48	108	1.43
	sp P23396 RS3_HUMAN	sp Q7L2E3 DHX30_HUMAN	108	48	1.43
60S	sp Q7L2E3 DHX30_HUMAN	sp P62917 RL8_HUMAN	138	234	0.7
	sp P62917 RL8_HUMAN	sp Q7L2E3 DHX30_HUMAN	234	138	0.7

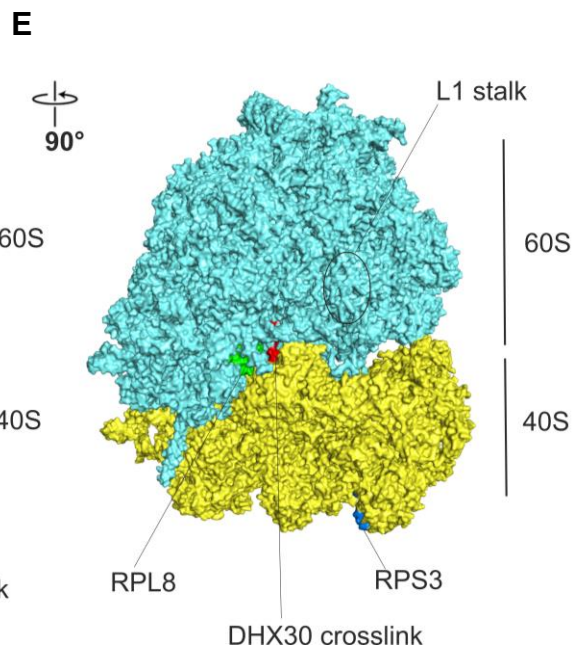
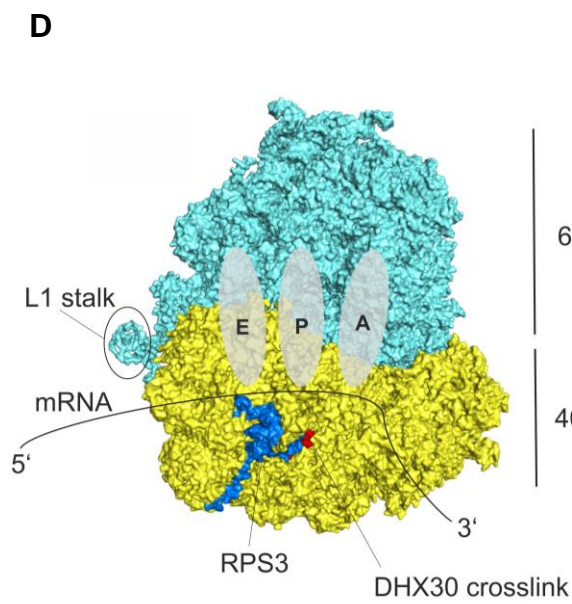
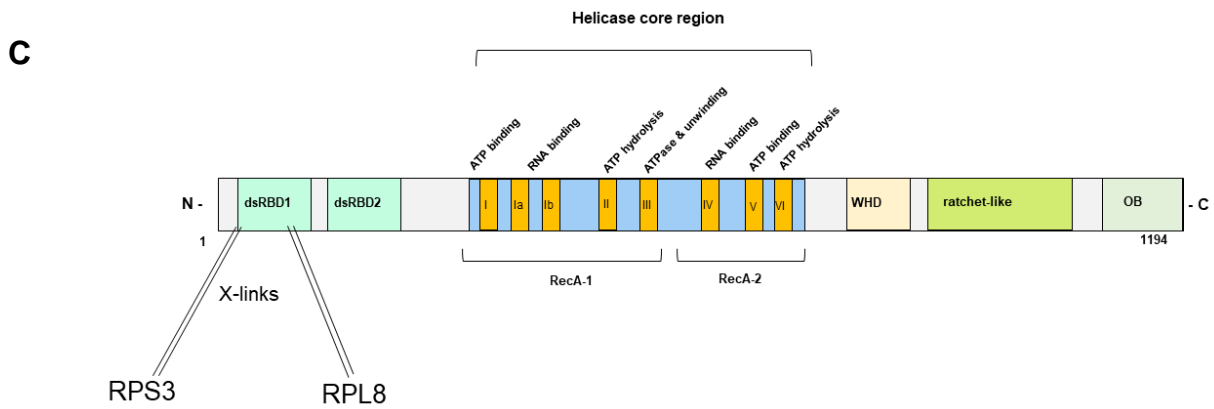


Figure 12: Cross-linking/mass spectrometry of DHX30/Ribosome complexes. (A) Workflow of cross-linking/mass spectrometry analysis to identify protein-protein crosslinks within a protein complex. The target complex is cross-linked and digested with trypsin into peptides which were analyzed by liquid chromatography coupled high-resolution mass spectrometry (LC-MS/MS). A database search was performed to identify the cross-linked peptides based on their fragmentation spectra. (B) Overview of the identified crosslinks between recombinant DHX30 and ribosomal proteins with the position of the crosslinked amino acid and the respective score. (C) Location of the crosslinks between dsRBD1 and ribosomal proteins within the domain structure of DHX30. (D) Crosslink between DHX30 and RPS3 located in the 80S ribosome (PDB: 5T2C). The 60S subunit is colored in cyan and the 40S subunit in yellow. The A, P and E site of the ribosome are marked in grey. The crosslink between DHX30 and RPS3 (blue) (Score 1,43) is marked in red and is located at the mRNA entry channel. The L1 stalked is highlighted for better visualization by turning it 90°. (E) 80S ribosome from D turned by 90° to visualize the second crosslink (red) at the ribosomal interface (RPL8) (green).

4.5 Determination of the DHX30 interactome - purification of DHX30 protein complexes

The data obtained so far point to a role of DHX30 in the context of translation. To gain a better understanding of this putative function I performed experiments aiming to identify the interactome of DHX30. For this purpose, stable Flp-In T-Rex 293 cell lines expressing either the full-length DHX30 WT or catalytic inactive mutants (R493H, H562R) were generated (see 6.2.2.3). These cell lines expressing the C-terminal FLAG/HA-tagged protein of interest upon induction with tetracycline. The expression was verified by a Western blot against the FLAG/HA tag (see supplementary figure S2). For immunopurification of DHX30 from these cells the stable cell lines were grown to a 70% confluency and the expression of the FLAG/HA-tagged DHX30 was induced with tetracycline. 16 hours after the induction cells were lysed and an immunoprecipitation (IP) was performed with anti-FLAG antibody coupled agarose beads. After native elution of the bound proteins with FLAG-peptide, protein complexes were separated in a 5% to 45 % sucrose gradient. Gradient fractions were loaded on a SDS-PAGE and proteins visualized by silver staining. As shown in figure 13 A, DHX30-FLAG/HA co-sediments with a group of proteins in complexes with a sedimentation coefficient of approximately at 80 S. Based on this S-value and the protein pattern, it was likely that endogenous DHX30 was bound to ribosomes, which was later confirmed by mass spectrometry.

The complex found in the heavier (i.e. >80S) fractions likely represents DHX30 associated with polyribosomes as also observed for the endogenous protein. Of note, the incubation of the lysate with enzyme MNase, prior to gradient centrifugation shifted DHX30 to the 80S fraction (figure 13 B) further supporting the idea that it interacts with ribosomes.

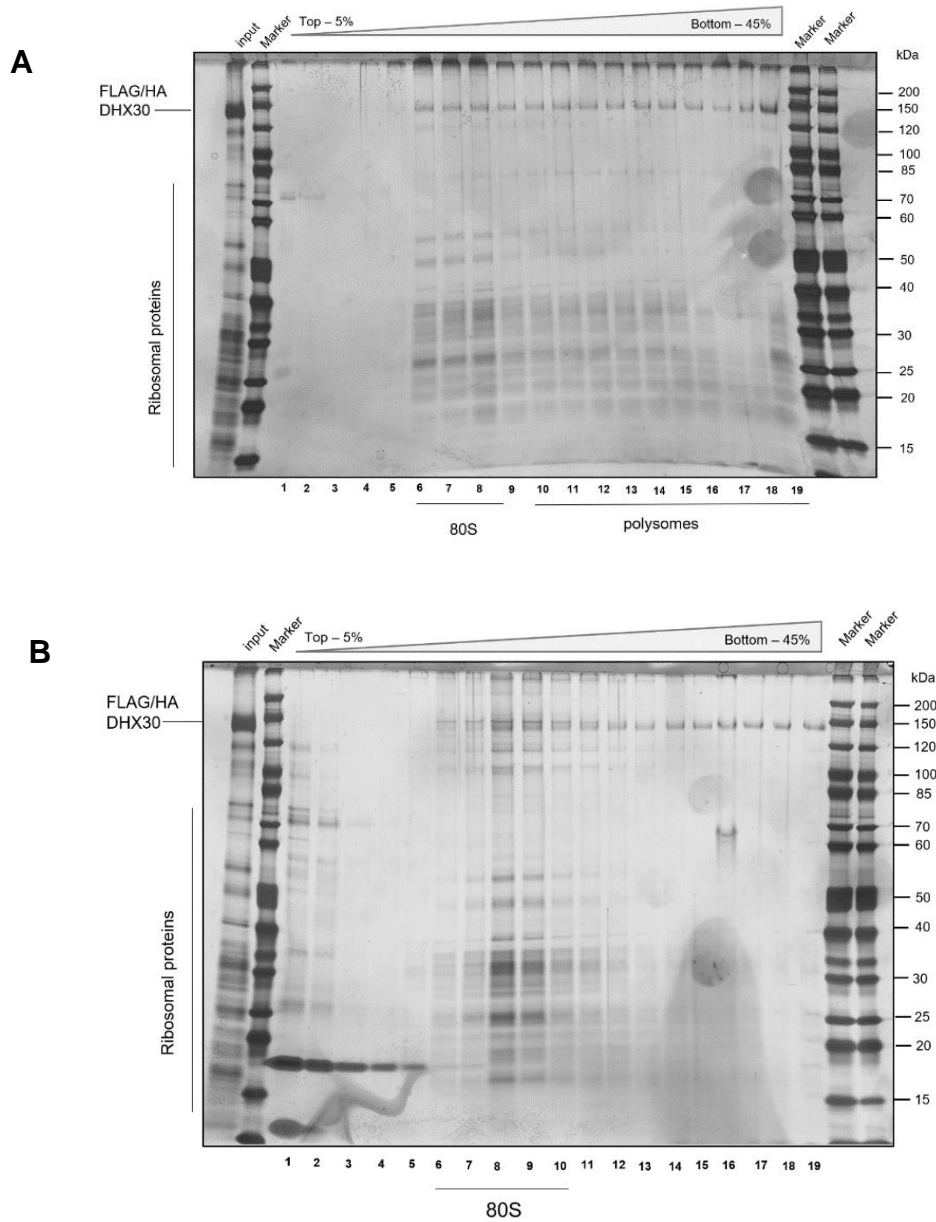
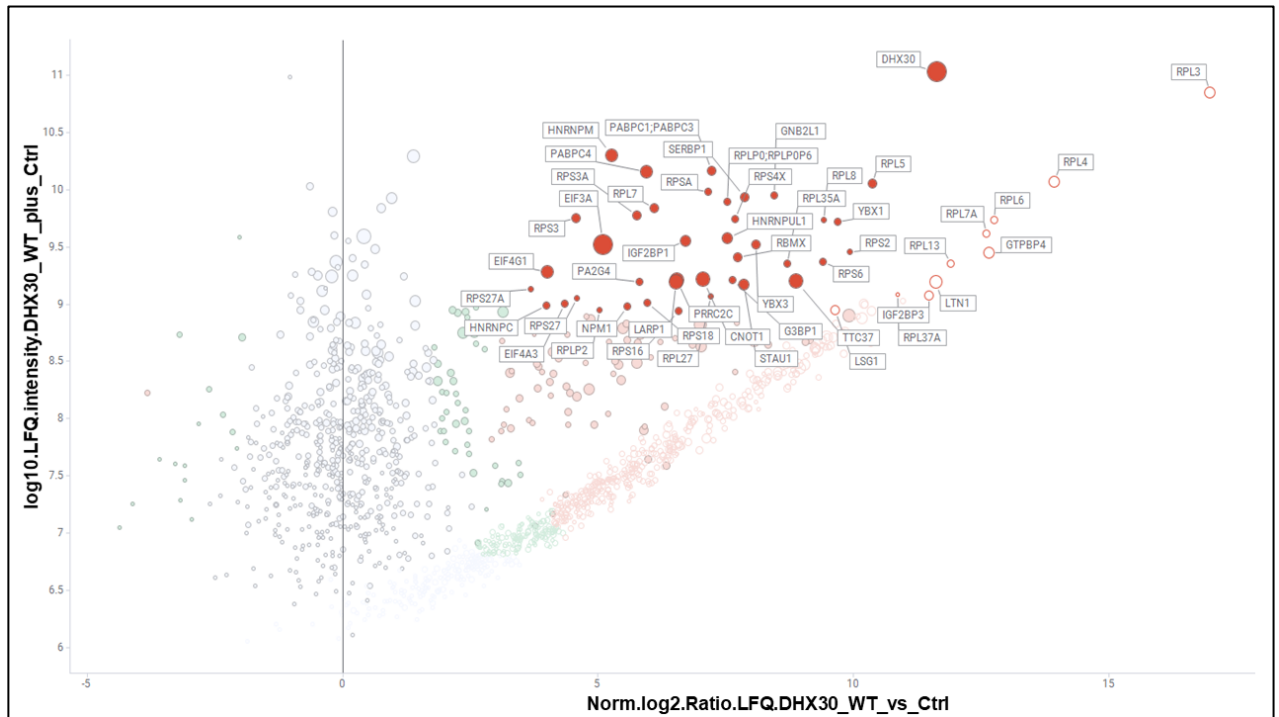


Figure 13: Purification of DHX30 protein complexes using Flp-In T-REx 293 cells. (A) Silver stained SDS-PAGE of a 5% - 45% sucrose gradient of purified DHX30 protein complexes from Flp-In T-REx 293 cells shows that DHX30 is part of a ribonucleoprotein complex. DHX30 is present in a lighter 80S complex (fraction 6-8) and in a heavier polysomal complex (fraction 10-19). (B) The heavier DHX30 complex can be dissolved by MNase treatment.

I reasoned that the composition of the DHX30-ribosome complex as determined by mass spectrometry may give a first indication as to what function DHX30 may accomplish. Towards this end, I isolated DHX30 complexes from cells by means of anti-FLAG-tag immuno-affinity chromatography and identified its interactome by mass spectrometry. This was accomplished by a detailed bioinformatic and statistical evaluation of the mass-spectrometry data of DHX30 affinity purifications. These studies were performed in collaboration with Stephanie Lamer (AG Schlosser, Rudolf-Virchow Center of Würzburg, Proteomics unit). The enrichment of the proteins in the anti-FLAG/HA IP was calculated in comparison to a control IP (empty Flp-In T-REx 293 cells, expressing no bait,). This analysis revealed a significant enrichment of a total of 364 associated proteins in the DHX30 IP over the control IP (see figure 14 A, details in table S1).

The most enriched interactors are labeled in figure 14 A and listed in figure 14 B. Consistent with the previous findings the majority and most highly enriched interactors of DHX30 are proteins of the small and the large ribosomal subunit (RPL and RPS proteins) and general factors of the translation machinery. Especially proteins involved in translation initiation could be identified (EIF3A, EIF4A3, EIF4G1, LARP1, PABPC1 and PABPC4), which is in line the finding that DHX30 co-sedimented with 80S ribosomes. Other highly enriched proteins were, factors involved in mRNA decay (CNOT1, G3BP1, STAU1, TTC37 and proteins of the exosome) and ribosome recycling (EIF4A, LTN1, NEMF, HBS1). This suggests that DHX30 may have a role in mRNA decay and/or ribosome turnover pathways.

A



B

Large ribosomal proteins	Small ribosomal proteins	Proteins involved in translation initiation	others	
RPL235A	RPS16	EIF3A	CNOT1	NEMF
RPL27	RPS18	EIF4A3	G3BP1	NPM1
RPL3	RPS21A	EIF4G1	GNB2L1	PA2G2
RPL31A	RPS21A	LARP1	GTPBP4	PA2G4
RPL4	RPS3	PABPC1	HBS1	PRRC2C
RPL5	RPS3A	PABPC4	HNRNPC	RBMX
RPL6	RPS4X		HNRNPM	SERBP1
RPL7A	RPS6		HNRNPUL1	STAU1
RPL8	RPSA		IGF2BP3	TTC37
RPLP0			LSG1	YBX1
RPL13			LTN1	YBX3

● mRNA decay pathways
● ribosome recycling factors & ribosome quality control

Figure 14: Quantitative mass spectrometry of the DHX30 interactome. (A) Scatter Blot of the identified peptides from immunoprecipitated DHX30-FLAG/HA complexes from Flp-In T-REx 293 cells. The specific interactors diameters correlate with the number of identified razor and unique peptides. Labeled are the identified peptides which had the highest enrichment in the DHX30-FLAG/HA IP over control IP. (B) List of proteins which showed the highest enrichment in the DHX30-FLAG/HA IP over control IP. Most peptides are ribosomal proteins and proteins involved in translation initiation. Also proteins involved in mRNA decay (red) and ribosome quality control (green) were among the top hits.

Next, a gene ontology enrichment analysis was performed for the 200 most enriched proteins, using the program ShinyGO v0.741 (<http://bioinformatics.sdstate.edu/go/>). As expected, this analysis identifies the translation as the pathway where DHX30 is mainly involved in (see figure 15 A). In addition, mRNA/RNA catabolic processes meaning pathways resulting in the breakdown of RNA was among the top GO terms (see figure 15 B). These data suggest that DHX30 associates with the translation machinery during initiation and/or termination/ribosome recycling.

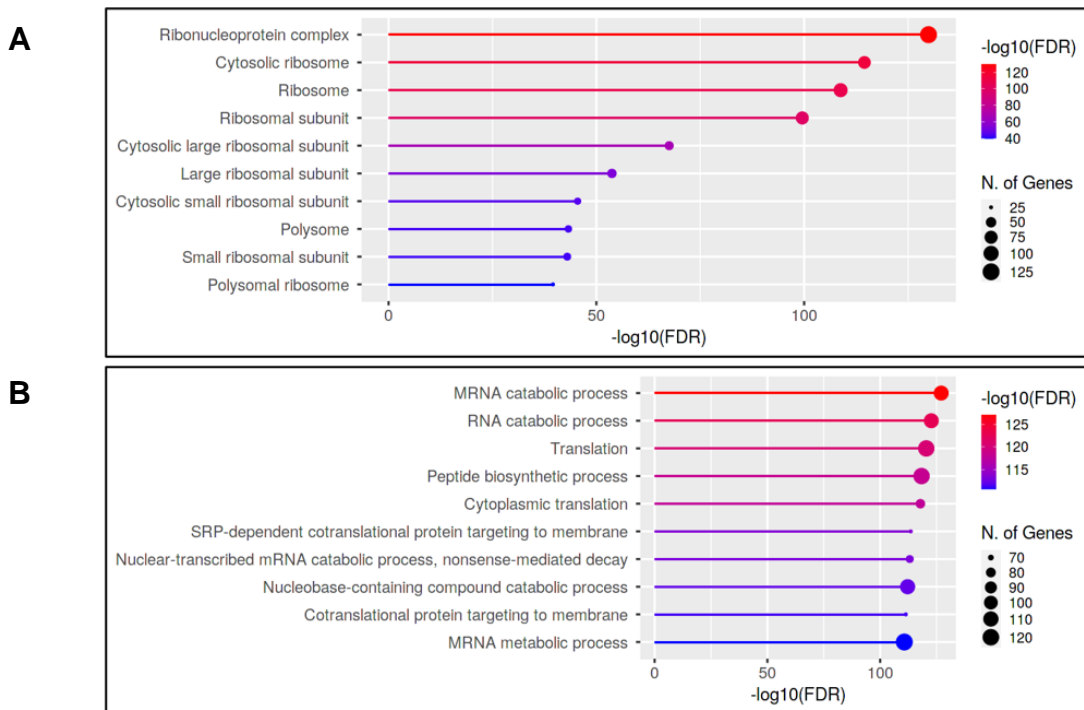


Figure 15: Gene ontology enrichment analysis of the DHX30 interactome. Analysis was performed with the top 200 proteins identified in the DHX30-FLAG/HA IP over control IP by mass spectrometry with ShinyGO v0.741. mRNA translation and mRNA/RNA catabolic processes were identified as the pathways DHX30 is mainly involved in. (A) GO term analysis of the cellular components. (B) GO term analysis of the molecular functions.

4.6 Studies on the cellular function of DHX30 upon amino acid and serum starvation

The experiments described in the preceding sections clearly linked DHX30 with ribosomes and polysomes in the cytoplasm, suggesting that it participates in the translation process, rather than ribosome biogenesis. In addition, the crosslinking data indicate that DHX30 directly interacts with ribosomal subunits via its N-terminal double stranded RNA binding domain 1. In the following chapter I describe experiments that I have performed addressing the question whether DHX30 regulates translation of specific sets of mRNAs in response to metabolic changes.

4.6.1 DHX30 shifts from polysomes into monosomes upon amino acid starvation and serum starvation

To investigate how specific proteins and protein complexes change their composition under various growth conditions, Dr. Cornelius Schneider (researcher in the Fischer lab) performed a *gradient profiling by sequencing* (Grad-seq) experiment with extracts derived from HEK293 cells. For this method, a gradient centrifugation is used to separate the proteins and RNAs from cells under defined conditions. Proteins and RNAs of each fraction of the gradient are then analyzed by RNA-seq and liquid chromatography-tandem MS (LCMS/MS), respectively. This method enables the analysis of how individual proteins and RNAs change their sedimentation as a consequence of defined treatments (Gerovac et al., 2021).

To test whether DHX30 changes its sedimentation and hence its interaction pattern in response to altered metabolic conditions, cells were exposed to amino acid starvation (1h) and serum starvation (2h), respectively. Hereafter the cells were treated with cycloheximide to arrest translation, lysed and separated on a 5 to 45% sucrose gradient. After harvesting the gradients, each fraction was analyzed by mass spectrometry and RNA seq (see figure 16 A). It has been shown previously that in cells the starvation of amino acids and/or serum leads to major changes in the translation pattern of mRNAs.

Under normal conditions the majority of cellular mRNA are associated with polysomes, which is an indication of their active translation (Janapala et al., 2019). Upon exposure to diverse stress stimuli translation is reduced at the global level and the population of polysomes is decreasing and the 80S peak increases. Figure 16 B shows the polysome profiles of the analyzed polysome gradients, where it is clearly visible that upon amino acid starvation and serum starvation, the polysome peaks decline and the 80S peak increases, respectively. As reported earlier, this is an indication for the successful starvation-treatment.

I first tested whether amino acid starvation and/or serum starvation affects the association of DHX30 with ribosomal complexes. Under non-starvation conditions, DHX30 co-sediments with polysomes (see figure 16 C, green graph). Upon amino acid starvation or serum starvation however, an almost quantitative shift of DHX30 from polysomes (fraction 16 to 21) to the 80S peak (fraction 9 to 10) was observed (see figure 16 C, blue and yellow graph). This effect, which was independently confirmed by Western blot analysis using antibodies against DHX30 (see figure 16 C, bottom) suggests a role of the helicase in starvation-induced translational control.

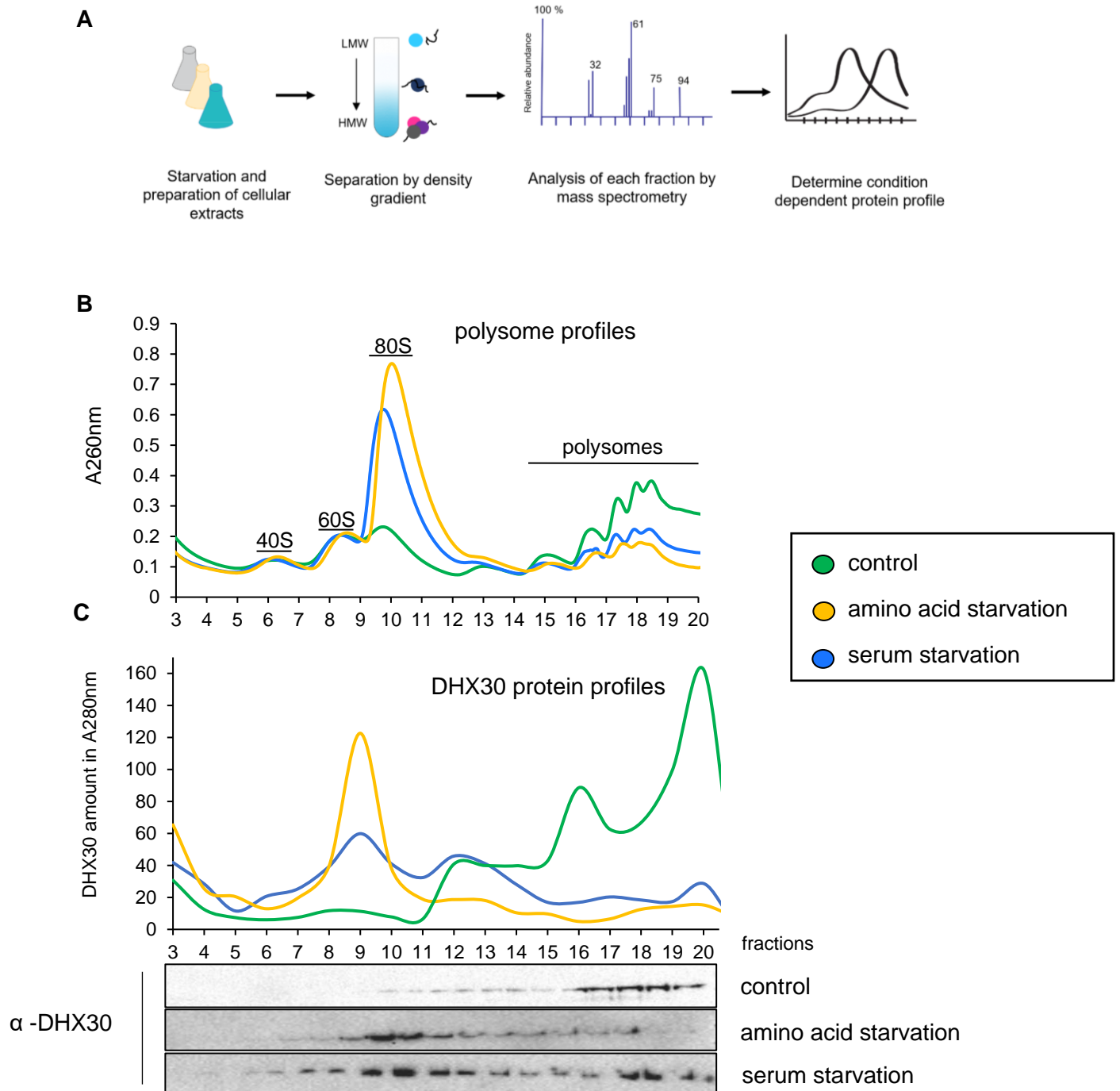


Figure 16: Grad-seq experiment in HEK293 cells upon starvation conditions. (A) Workflow of the grad-seq experiment performed by Dr. Cornelius Schneider. (B) A₂₆₀ profiles of the polysome gradients from the grad-seq experiment. Upon amino acid starvation and serum starvation the polysomes decrease and the 80S peak increases, which is an indicator for a successful treatment. (C) Protein profiles of DHX30 under control conditions (green), amino acid starvation (yellow) and serum starvation (blue) show the shift of DHX30 from polysomes to the 80S peak upon the applied stress treatments.

4.6.2 DHX30 shifts from polysomes into monosomes upon starvation independently of LARP1

The shift of DHX30 from polysomes to monosomes points to a regulatory event in multicellular organisms commonly referred to as “TOP-response”. This describes the regulation of the eukaryotic translation machinery in response to conditions of cell growth such as starvation where mRNAs coding for proteins of the translational machinery and translation initiation factors are selectively withdrawn from polysomes. This is mediated by a specific *cis*-regulatory RNA element found in these mRNAs termed the 5'terminal oligopyrimidine (5'TOP) motif. It is composed of an invariant m⁷GpppC cap followed by an uninterrupted tract of 4–14 pyrimidine nucleotides (Lahr et al., 2017).

To reduce the translational output of 5'TOP mRNAs during starvation 5'TOP mRNAs shift from the pool of actively translated mRNAs (polysomes) to the 80S region of the gradient. During this process, the RNA binding protein LARP1 plays a crucial role. During starvation LARP1 binds to 5'TOP mRNAs and shifts together with these mRNAs from polysomes to 80S (see figure 17). Data from Dr. Cornelius Schneider revealed that the shift of 5'TOP mRNAs from polysomes to 80S is LARP1 dependent (data not shown).

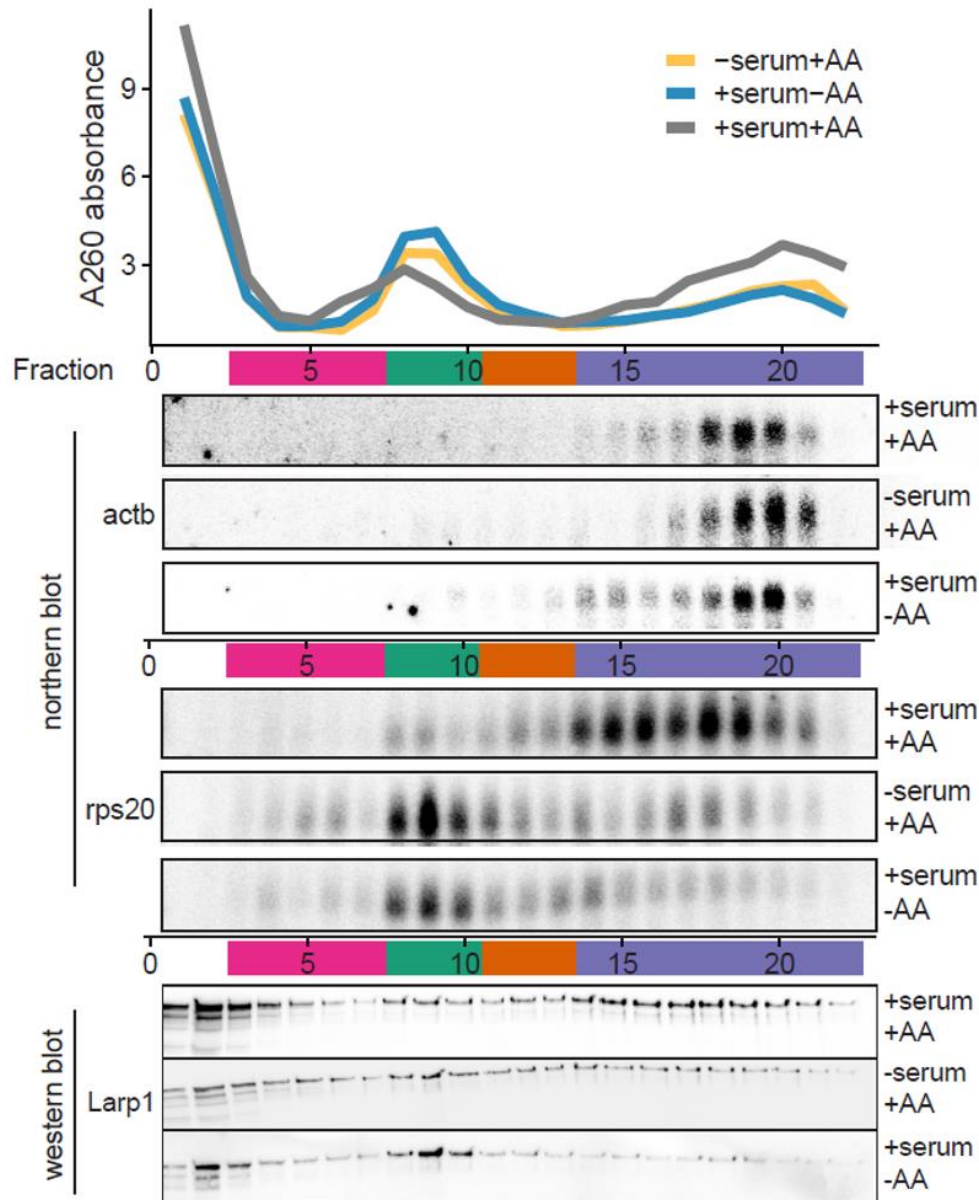


Figure 17: LARP1 and 5'TOP mRNA shift from polysomes to 80s upon starvation as a result of the TOP-response. A260 absorbance profile of polysomes gradients (top). Sedimentation profiles of a 5'TOP (RPS20) and a non-5'TOP transcript (ACTB) by northern blotting of gradient fractions from log phase (control), serum (-serum) and amino acid (-AA) starved cellular lysates (middle). Sedimentation profile of the LARP1 protein by Western blotting of gradient fractions from log phase, serum and amino acid starved cellular lysates (bottom). Experiment and figure by Dr. Cornelius Schneider.

Since the experiments described above revealed a pronounced shift of DHX30 from polysomes to the 80S fraction upon starvation I wanted to investigate whether this shift is functionally connected to the TOP-response. To test this hypothesis a polysome gradient of extracts derived from control and LARP1 KO cells was performed after treatment with Torin and analyzed by a Western blotting using a DHX30 antibody. Torin is a mTOR inhibitor which is able to effectively block phosphorylation of mTORC1 and mTORC2 and thus mimicking starvation (Thoreen et al., 2009). As figure 18 shows, DHX30 shifts from polysomes into the 80S peak not only in control cells but also in LARP1 KO cells upon mTOR treatment. This result led to the conclusion that DHX30 shifts independently of 5'TOP mRNAs from polysomes to 80s upon starvation.

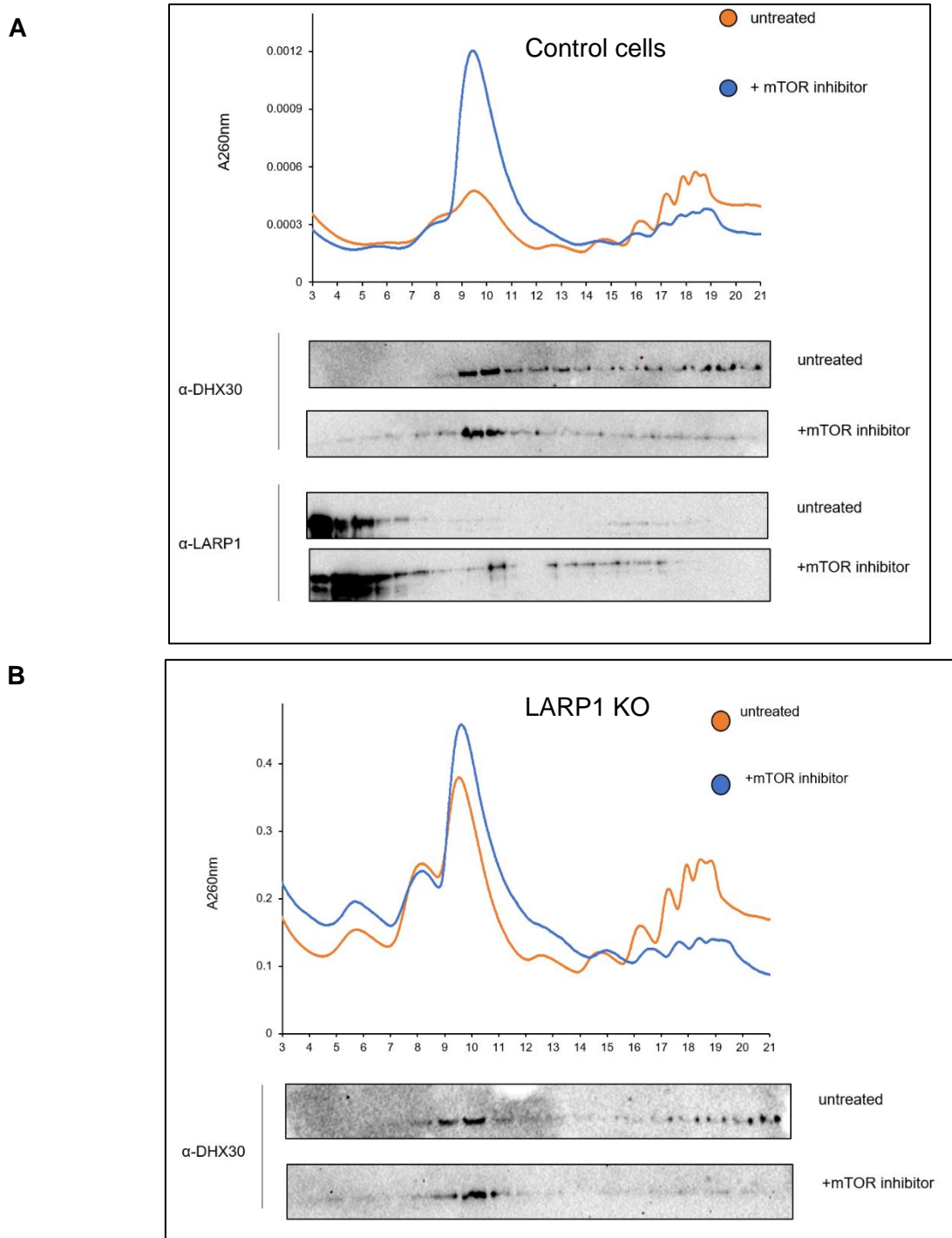


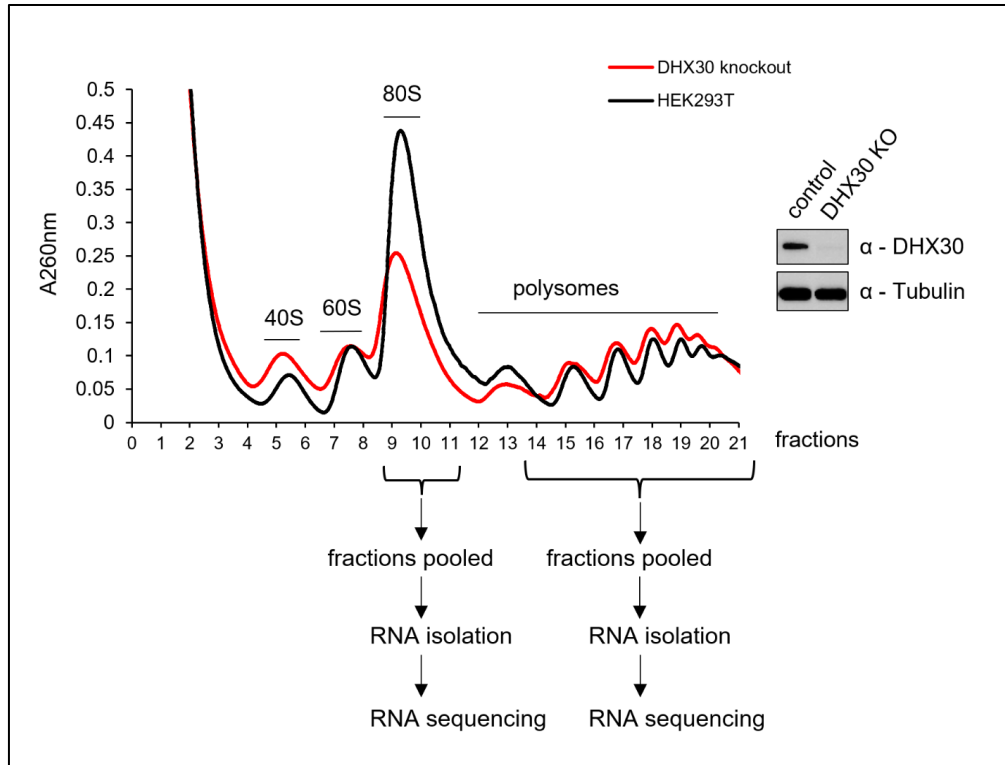
Figure 18: Polysome sucrose gradient distribution of DHX30 in dependence of LARP1. Cellular starvation was mimicked by treating the cells with mTOR inhibitor Torin. (A) Polysome gradient and Western blot against DHX30 and LARP1 show a shift of DHX30 and LARP1 to the 80S peak upon mTOR inhibitor treatment. (B) Polysome gradient of LARP1 KO cells and Western blot against DHX30 show that DHX30 shifts to the 80S peak independent of LARP1.

4.7 The depletion of DHX30 results in the accumulation of RNAs in the 80S peak and changes in the polysome profile

Next, I investigated a potential function of DHX30 during translation initiation, in particular during the formation of initiation complexes. In case of a role of DHX30 in this pathway, one would expect to observe changes in the polysome profiles under DHX30 knockout conditions. For these experiments, I used HEK293T wild-type and DHX30 knockout cell lines for sucrose gradient sedimentation analysis. The results show that in DHX30 KO cells the 80S peak is reduced by about 50% and the level of 40S ribosomes (fraction 4 to 6) and the polysomes (fraction 12 to 21) are slightly increased (see figure 19 A).

These results show that the depletion of DHX30 has an impact on the total amount of 80S ribosomes. As this may hint to a role of DHX30 in translation initiation, I next performed RNA sequencing experiments in DHX30 depleted cells from mRNA pools representing different stages of translation. Total RNA as well as RNA from the 80S peak (initiating ribosomes) and the polysome fractions (actively translating ribosomes) were isolated and sequenced. I first asked whether the overall distribution of RNAs over the analyzed pools are different in control and DHX30 KO cells. For this the ratio between the overall RNA reads in each fraction were compared between DHX30 KO and control cells (see figure 19 B). It was found that the overall mRNA content is increased in the 80S peak of DHX30 KO cells. This suggests that mRNAs accumulate in the 80S in DHX30 KO cells even though the total amount of 80S ribosomes is decreased.

A



B

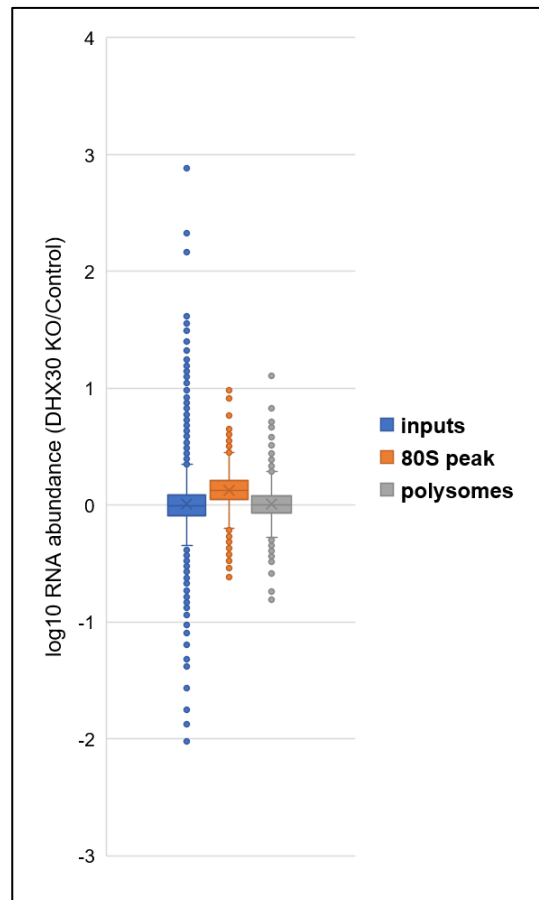


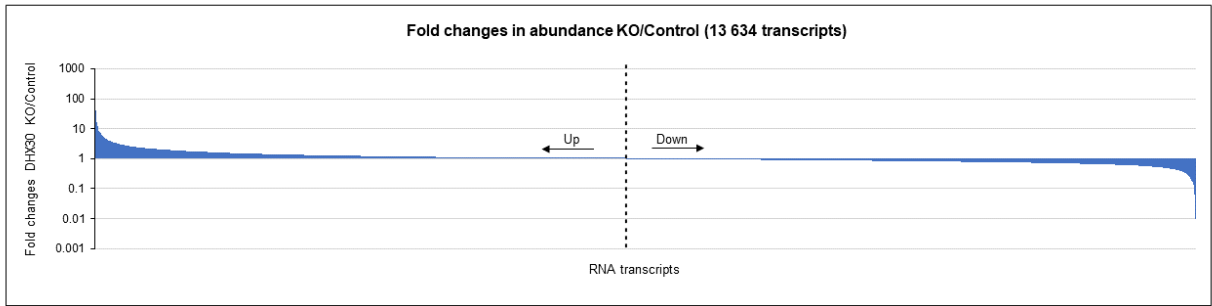
Figure 19: Polysome sucrose gradients of DHX30 KO cells and HEK29T control cells. (A) Polysome gradients (5% to 45%) with HEK293T and DHX30 KO cells show a strong decrease of the 80S peak and a slight increase of 40S and polysomes upon DHX30 KO. Shown is the workflow for RNA sequencing of RNAs from polysome gradients. The respective fractions were pooled, the RNA was isolated by TRIzol and sent for RNA sequencing analysis. (B) Comparison of the average RNA abundance between DHX30 KO and control cells. The RNA reads were normalized to actin- β mRNA. Shown are the mean values from triplicates. The depletion of DHX30 results in an accumulation of mRNAs in the 80S peak.

4.7.1 DHX30 depletion results in the deregulation of mRNAs involved in neurogenesis and nervous system development.

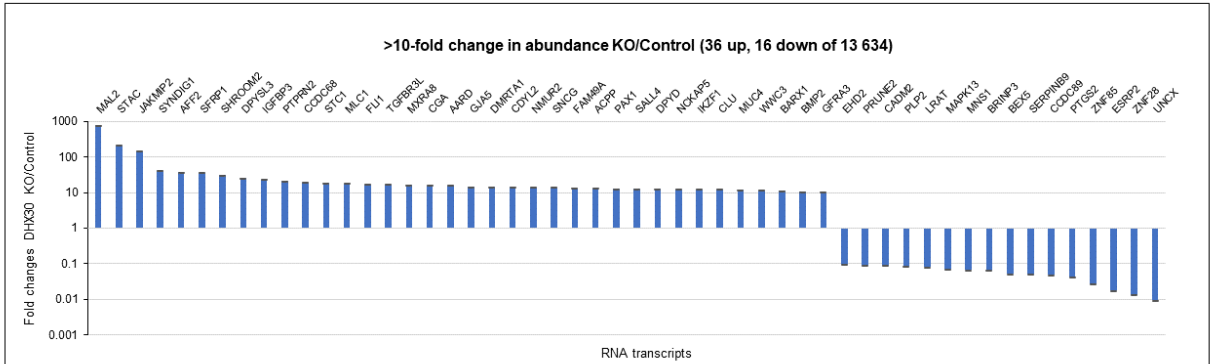
In the first step of the analysis of the RNA sequencing results I focused only on the RNA reads collected from the total RNAs. Changes in these mRNAs reflect a regulation on the level of transcription. This analysis gives a broad picture about global effects of DHX30 depletion on the transcriptome in HEK293T cells. In this analysis 13 634 transcripts were considered, which are coding for full length proteins whereas miRNAs, antisense transcripts, lncRNAs and pseudogenes were excluded. For the selected mRNAs, the ratio between the reads of the DHX30 KO and the control cell line was formed to calculate the relative transcript abundance upon DHX30 depletion. All reads were normalized to the reads of actin- β mRNA, which was expected to be unaffected by the KO.

The level of the majority of the analyzed mRNAs changed only marginally (see figure 20 A). By contrast, a small set of mRNAs were found to be drastically deregulated upon DHX30 KO. These encompass 36 transcripts, which are heavily upregulated (at least 10-fold) and 16 transcripts heavily downregulated (see figure 20 B). The top 4 upregulated genes (MAL2, STAC, JAKMIP2 and SYNDIG1) have a fold-changes between 41 and 769 in the DHX30 KO cells over the control. The top 4 downregulated genes (UNCX, ZNF28, ESRP2 and ZNF85) have fold changes between 37-fold and 110-fold (see figure 20 B). The fold-changes of some mRNAs were confirmed by quantitative real-time PCR (qPCR) from total RNAs of the used cell lines (figure 20 C + D).

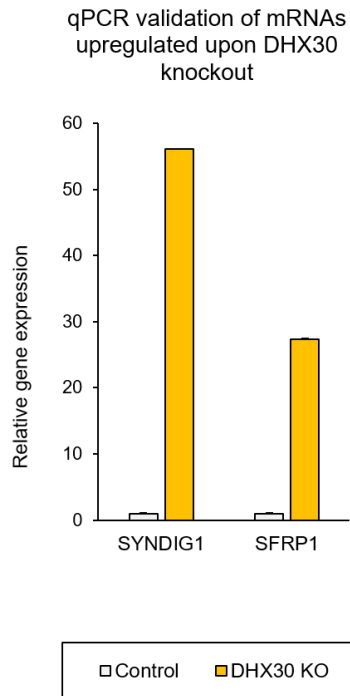
A



B



C



D

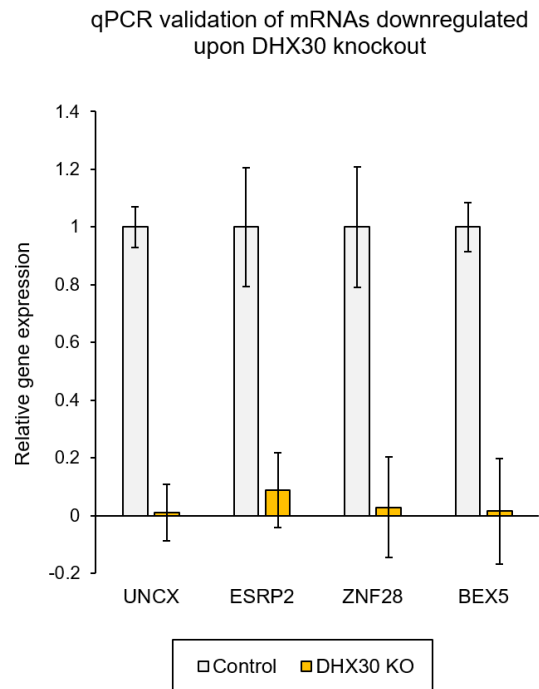


Figure 20: RNA sequencing of total RNAs upon DHX30 KO. (A) Fold changes (y-axes) of the analyzed 13 634 mRNAs upon DHX30 KO. The RNA reads were normalized to actin- β mRNA and the inputs. Shown are the mean values from triplicates. (B) Most drastic (>10 fold) deregulated mRNAs upon DHX30 KO. (C) Validation of selected mRNAs upregulated upon DHX30 KO with qPCR. Relative gene expression levels were normalized to actin- β (D) Validation of selected mRNAs downregulated upon DHX30 KO. Relative gene expression levels were normalized to actin- β .

To obtain a deeper understanding of the deregulated transcripts and to find a potential common biological function of these transcripts a GO term analysis was performed. For this a list of transcripts which were at least 50% down-regulated upon DHX30 was generated. This list contains 427 transcripts and was analyzed for significant GO terms to get information about the biological process and molecular function they are involved in. The same procedure was performed with all transcripts which were at least 5-fold enriched in DHX30 KO cells over control. As shown in figure 21 A and B the majority of the deregulated mRNAs are linked to the biological processes of neurogenesis, cell/neuron differentiation and nervous system development, which is in line with the neuropathogenic phenotype which can be seen in the NEDMIAL patients.

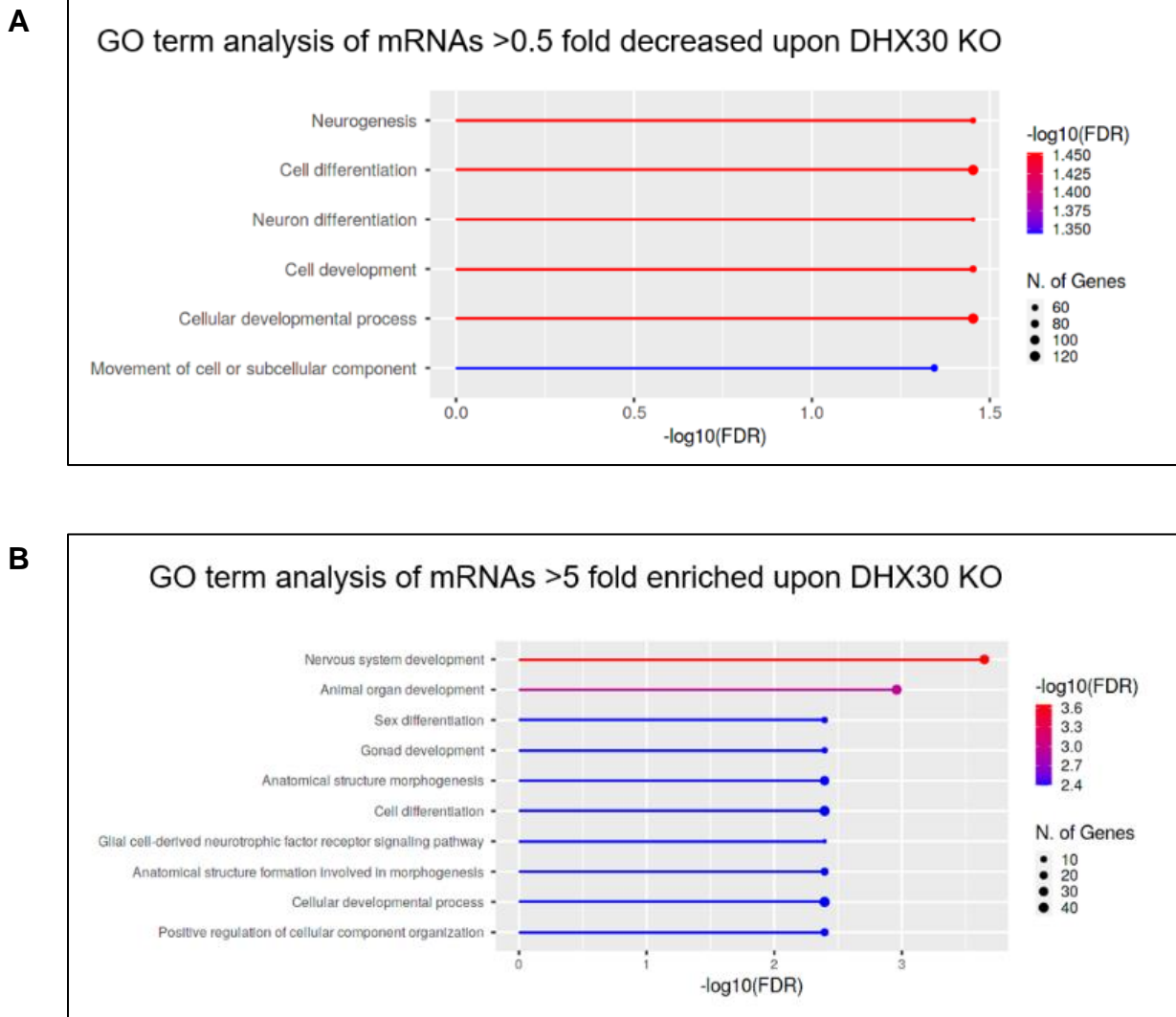


Figure 21: Gene ontology enrichment analysis of candidate mRNAs upon DHX30 KO from total RNAs identified by RNAseq. (A) GO term analysis of all mRNAs which are at least decreased by 50 % upon DHX30 KO over control (427 transcripts), show a strong enrichment of genes involved in neurogenesis, cell/neuron differentiation and cell development. (B) GO term analysis of all mRNAs which are at least 5 fold increased upon DHX30 KO over control (114 transcripts), show a strong enrichment of genes involved in nervous system development.

4.7.2 DHX30 KO affects the abundance of 5'TOP mRNAs in the 80S peak and in the polysomes

RNA sequencing of total cellular mRNAs showed a strong deregulation of candidate mRNAs upon DHX30 KO at a transcriptional level. Next I analyzed if there are mRNA candidates which are deregulated on a post-transcriptional level. For this analysis I focused on mRNAs showing changes in the 80S and polysomal mRNA pool respectively but not on the transcriptional level (total RNA). A ratio between the reads of the DHX30 KO cell line and the control cell line was formed to calculate the relative transcript abundance upon DHX30 depletion in each RNA pool. All reads were normalized to actin- β mRNA and the input mRNAs.

I found 959 transcripts in the 80S peak and 3094 in the polysomes being reduced upon DHX30 depletion. The analysis further revealed that among the most downregulated transcripts in the 80S peak are mRNAs coding for components of the translation machinery and translation factors. The majority of these mRNAs belong to the 5'TOP mRNA class (see figure 22 A). These mRNAs were also reduced in the polysomal fractions by up to 50% (see figure 22 B). Since the 5'TOP mRNAs in these cells were largely unaltered on a transcriptional level (see figure 22 C) these data suggest that 5'TOP mRNAs are selectively withdrawn from the translation machinery upon DHX30 KO.

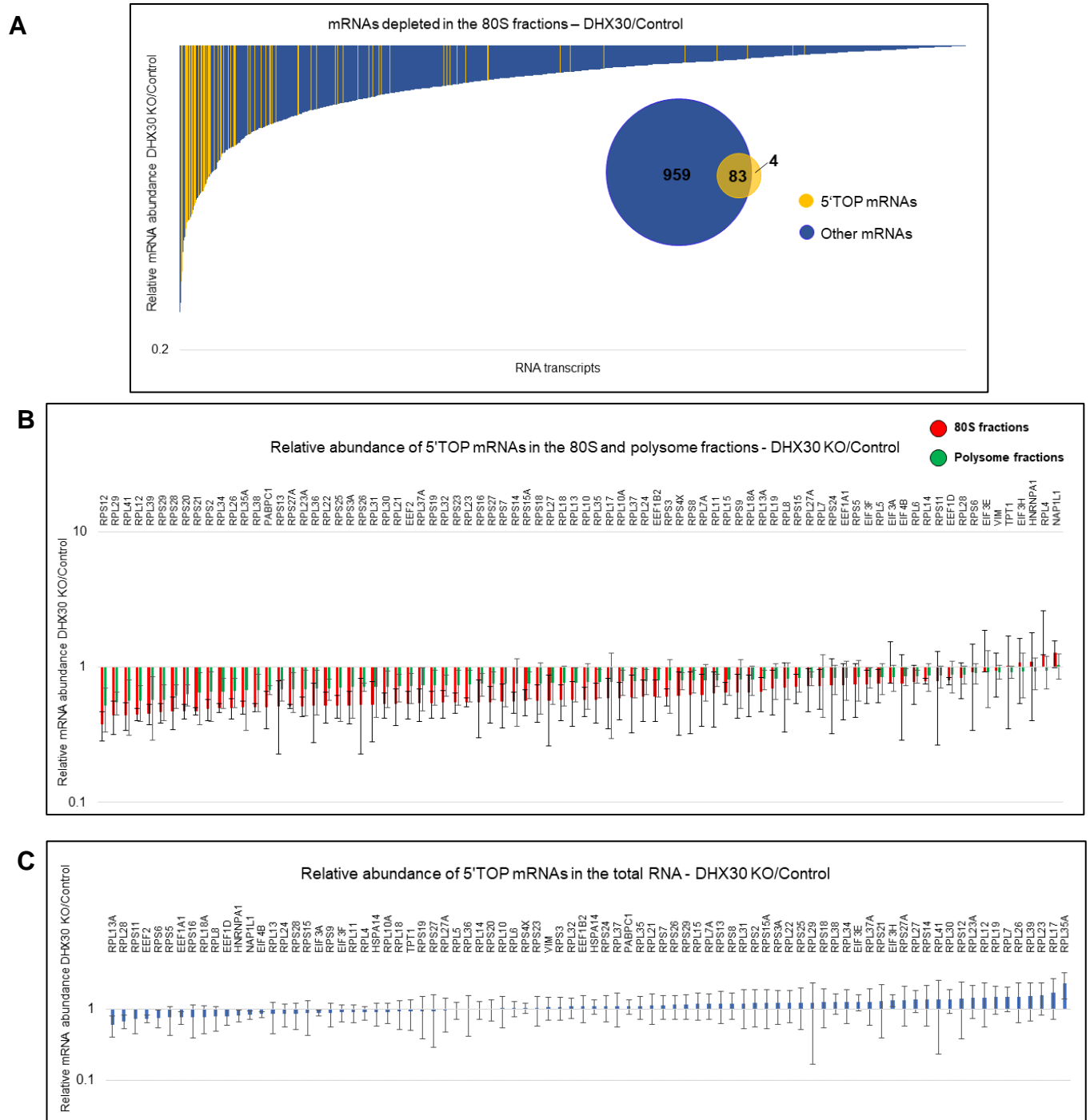


Figure 22: DHX30 KO affects the abundance of 5'TOP mRNAs in the 80S peak and in the polysomes. The RNA reads were normalized to actin- β mRNA and the inputs. Shown are the mean values from triplicates. (A) In total 959 transcripts are downregulated in the 80S peak upon DHX30 KO. Among the most drastic deregulated transcripts the majority are 5'TOP mRNAs (yellow). (B) Relative expression levels of 5'TOP mRNAs in the 80S peak (red) and in the polysomes (green) show a decrease in both mRNA pools. All values normalized to the inputs. (C) Relative expression levels of 5'TOP mRNAs in the input fractions show no drastic changes on a global level upon DHX30 KO.

4.8 Biochemical characterization of pathogenic missense mutations of DHX30

The biochemical investigation summarized in the chapters above identified DHX30 as a ribosome associated RNA helicase with a likely impact on the translation of a defined set of cellular mRNAs. Since DHX30 is associated with the neurodevelopmental disease NEDMIAL, my findings raised the possibility that altered translation is a molecular defect in cells of these patients. Hence, the following experiments were performed to analyze the influence of pathogenic missense mutations within DHX30 on the enzymatic activities and functional association with the translation machinery.

The pathogenic missense mutations were identified by whole-exome sequencing and are located in different motifs of the helicase core: G462E in motif I, R493H in motif Ia, H562R in motif II, S737F in motif V, R785C in motif VI. One mutation, namely R908Q, is not located in the helicase core but in the ratchet-like domain (figure 23 A). The aim of the next experiments is to find out if the disease phenotype can be correlated with a lack of activity in terms of ATP hydrolysis and RNA substrate unwinding.

4.8.1 Pathogenic missense mutations in the helicase core of DHX30 interfere with its ATPase activity and helicase activity

Plasmids containing DHX30 with pathogenic missense mutations were generated by *site directed mutagenesis* to allow the expression and purification of the DHX30 variants in *E.coli* as recombinant protein with an N-terminal 6xHis-SUMO tag. The purification was performed in the same manner as described for wild-type DHX30 (see chapter 4.1.1) and proteins were analyzed by SDS-PAGE (see figure 23 B). Using this expression and purification strategy, recombinant mutant DHX30 variants could be obtained with similar purity as the wild-type protein. To test the helicase activity of the recombinant DHX30 mutants in comparison to the wildtype I used the already described helicase assay (see chapter 4.1.2). A synthetic [³²P]-labeled RNA duplex was incubated with the purified DHX30 mutants in the presence of ATP and the unwinding products were analyzed by a non-denaturing PAGE.

All variants harboring mutations in the helicase core, showed an impaired helicase activity that failed to unwind the RNA:RNA duplex *in vitro*. In contrast, the R908Q variant which harbors a missense mutation in the ratchet-like motive showed no impact on the helicase activity (see figure 23 C).

Since the unwinding activity is coupled to the ATPase activity the next question was if the impaired unwinding activity results from defects in the hydrolysis of ATP. The ATPase activity of the recombinant DHX30 mutants was measured in comparison to the wildtype using an *in vitro* ATPase assay. The recombinant proteins were incubated with α -[P³²]-ATP at 37°C for 30 minutes in the presence of a double stranded RNA duplex and the hydrolysis of α -[P³²]-ATP into α -[P³²]-ADP was monitored by thin-layer chromatography. All pathogenic variants of DHX30 harboring missense mutations in the helicase core failed to hydrolyze ATP *in vitro* (see figure 23 D).

In contrast, the R908Q mutant was still able to hydrolyze ATP *in vitro*. These results are consistent with the fact that helicase activity requires energy produced by hydrolysis of ATP to unwind substrates. In conclusion these results indicate that NEDMIAL-related missense mutations located in crucial catalytic motifs result in a reduction of its enzymatic activity. These data show that loss of helicase activity of DHX30 is alone necessary and sufficient to cause the NEDMIAL phenotype. However, the pathogenic variant R908Q displayed enzymatic activity comparable to the wild-type protein. The mechanism by which this variant causes the disease is currently unknown.

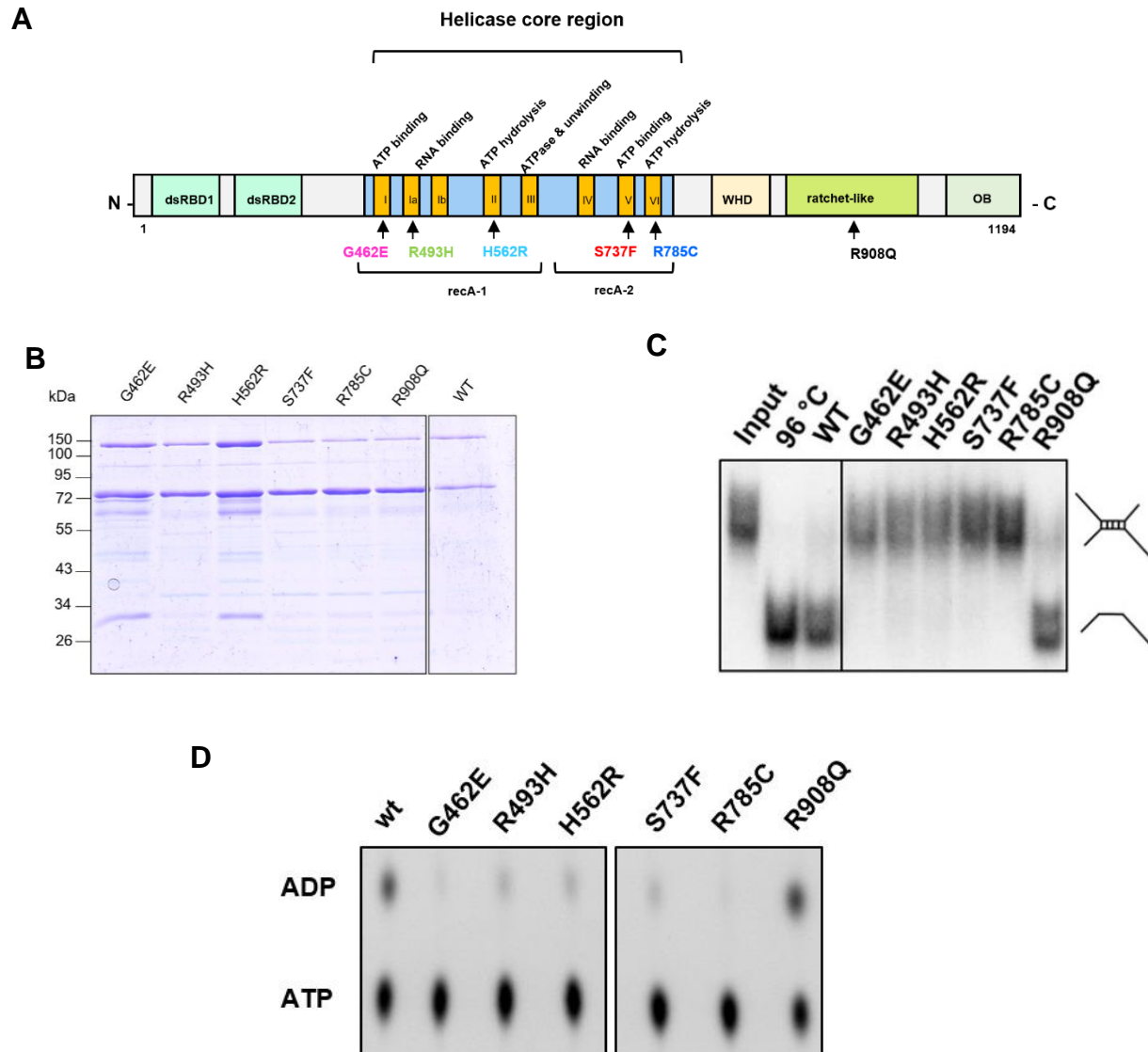


Figure 23: ATPase activity and unwinding assays of pathogenic DHX30 variants. (A) Schematic representation of the 6 pathogenic missense mutations in DHX30 used in this study. Five missense mutations are located in conserved motifs within the helicase core and one in the ratchet-like domain. (B) Expression and purification of recombinant His-SUMO DHX30 mutants. DHX30 protein mutants were expressed and purified as described for wild-type His-SUMO DHX30. (C) Pathogenic missense mutations in the helicase core disrupt the unwinding activity of DHX30 *in vitro*. (D) Pathogenic missense mutations located in the helicase core of DHX30 interfere with its ATPase activity *in vitro*.

4.8.2 Co-migration of DHX30 with ribosomes is independent from its catalytic activity

Previous experiments showed that DHX30 co-sediments with ribosomes and polysomes in polysome sucrose gradients. Since many pathogenic missense mutations of DHX30 interfere with its enzymatic activity, I wanted to test whether they also impact the association with the translation machinery. To test this, polysome gradients of extracts derived from cell lines overexpressing either FLAG/HA tagged DHX30 or two variants harboring pathogenic point mutations (H562R, R493H) were performed. A Western blot analysis revealed that wild-type and mutant DHX30 only slightly differ in their association with polysomes and the 80S ribosome (see figure 24 bottom). Association of DHX30 with the translation machinery is therefore independent of its catalytic activity and not drastically disturbed in the disease.

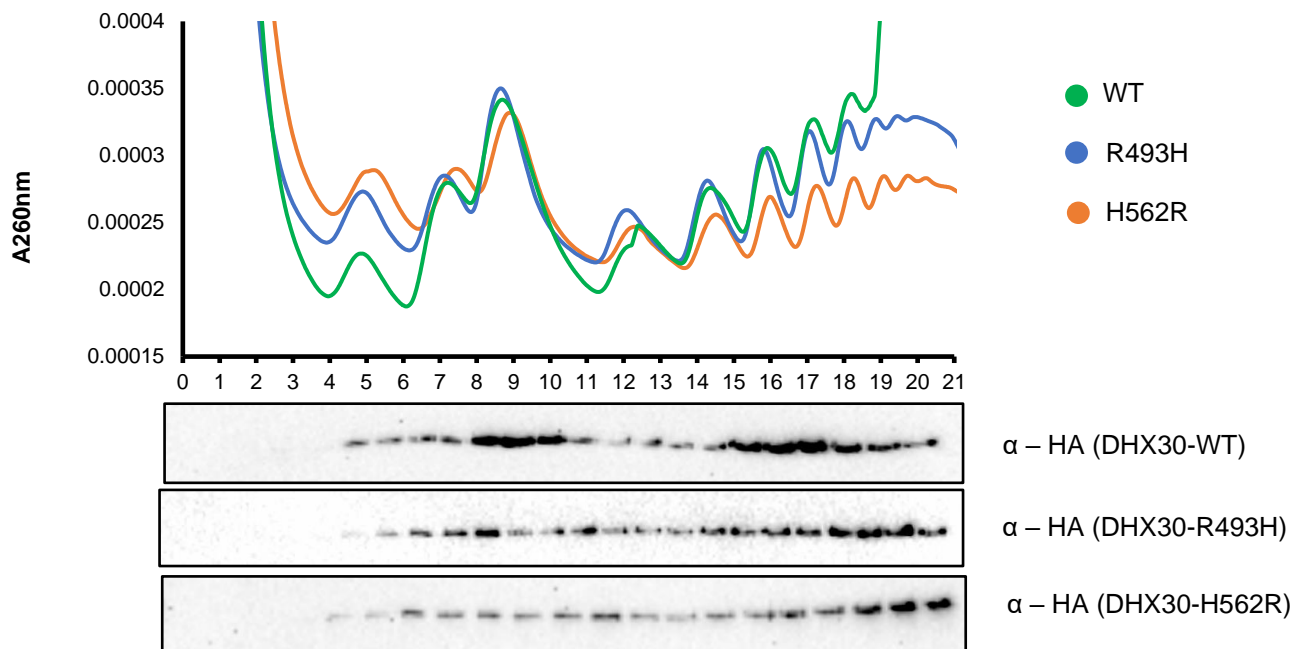


Figure 24: Sucrose gradient distribution of pathogenic DHX30 variants after ultracentrifugation. Polysome gradients of cell lines overexpressing different versions of FLAG/HA tagged DHX30. Pathogenic versions of DHX30 (R493H and H562R) showing a similar co-sedimentation behavior like the DHX30-WT.

4.8.3 Comparative analysis between the interactome of DHX30 wild-type and disease-causing mutants

The data above show that many pathogenic DHX30 variants are enzymatically defective but retain their affinity to the translation machinery. The question arose if wild-type and mutant DHX30 display differences in their protein interactome. To test this immunoprecipitations with cell lines overexpressing DHX30-FLAG/HA WT and catalytic inactive mutants (R493H and H562R) were performed and analyzed by mass spectrometry. The enrichment of the proteins in the anti-FLAG/HA IP was calculated in comparison to a control IP (empty Flp-Trex cells, expressing no bait).

The bioinformatic and statistical evaluation of the data were performed in cooperation with Stephanie Lamer (AG Schlosser, Rudolf-Virchow Center of Würzburg, Proteomics unit). The normalized values of each IP (WT, H562R and R493H) were blotted against each other to have a direct comparison between each interactome (see figure 25). As shown in figure 25, the interactome of the WT and the mutants showed no significant difference. This result shows that the protein-interactome of DHX30 is independent from its enzymatic activity.

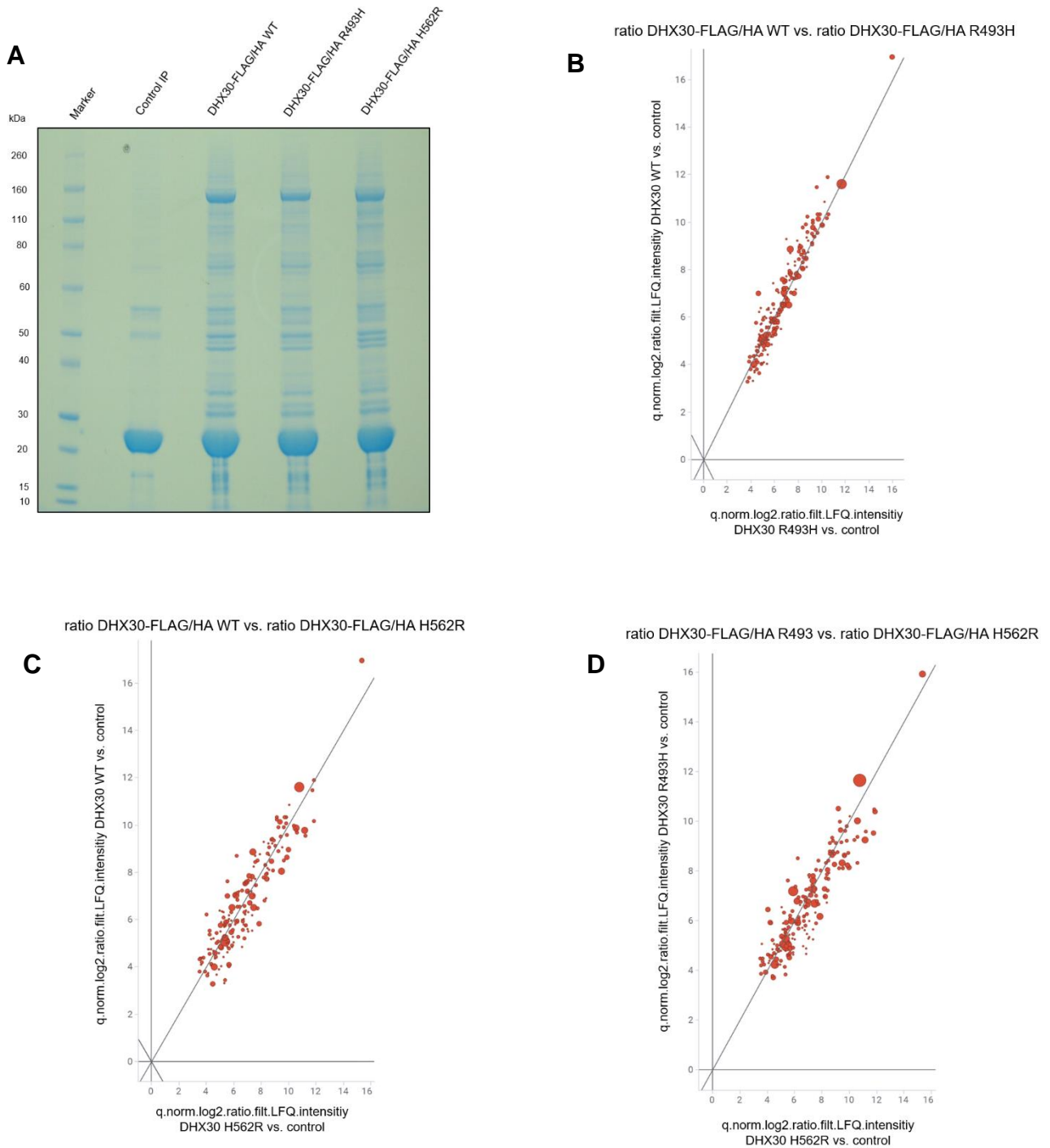


Figure 25: Comparative Analysis of mass spectrometry data of the protein interactome of pathogenic DHX30 variants. (A) Coomassie stained SDS gel of the DHX30-FLAG/HA IP eluates (WT and mutants) and control IP. (B) Scatter plot of the identified peptides from DHX30-FLAG/HA WT (y-axis) and R493H mutant (x-axis). (C) Scatter plot of the identified proteins from DHX30-FLAG/HA WT (y-axis) and H562R mutant (x-axis). (D) Scatter plot of the identified proteins from DHX30-FLAG/HA R493H mutant (y-axis) and H562R mutant (x-axis).

4.8.4 Unwinding activity of DHX30 on RNA:DNA and DNA:DNA duplexes.

The previous experiments identified DHX30 as a RNA helicase associated with the translation machinery. Consistently immunofluorescence microscopy localized the majority of DHX30 in the cytoplasm (see figure 9). However, a minor fraction of DHX30 could also be detected in the nucleus where it appears in distinct dot-like structures. The question therefore was whether DHX30 also has a nuclear function and if so, what substrates it targets. Apart from dsRNA and dsDNA also DNA:RNA hybrids form in the nucleus. The latter, termed R-loops are RNA:DNA hybrids which consist of two DNA strands and one complementary RNA. In cells, R-loops are formed during transcription elongation. The nascent RNA molecule from the transcribing DNA template re-annealed with one of the two strands in a double stranded DNA molecule (Pan et al., 2014).

In D-loop structures the RNA strand is displaced by a DNA strand. D-loops occur during DNA repair, in telomeres and as semi-stable structures in mitochondrial circular DNA molecules (Nicholls & Minczuk, 2014). To test whether DHX30 can unwind any of those structures, I performed *in vitro* assays using radiolabeled nucleic acid scaffolds as substrates (see 6.2.5.8). In total 6 different substrates including R-loops and D-loops which contained either a 3' overhang, a 5' overhang or no overhang were generated. To examine the activity of recombinant DHX30-WT on the respective substrate, each substrate was incubated with an increasing amount of the full-length protein and loaded on a 6% native RNA PAGE after incubation. As shown in figure 26, DHX30 is capable of unwinding not only a pure RNA substrate as shown previously but also R-loops with a 3' overhang. In contrast, R-loops harboring a 5'-overhang or no overhang were not unwound. Furthermore, it could be observed that DHX30 is unable to unwind any substrate consisting of DNA only.

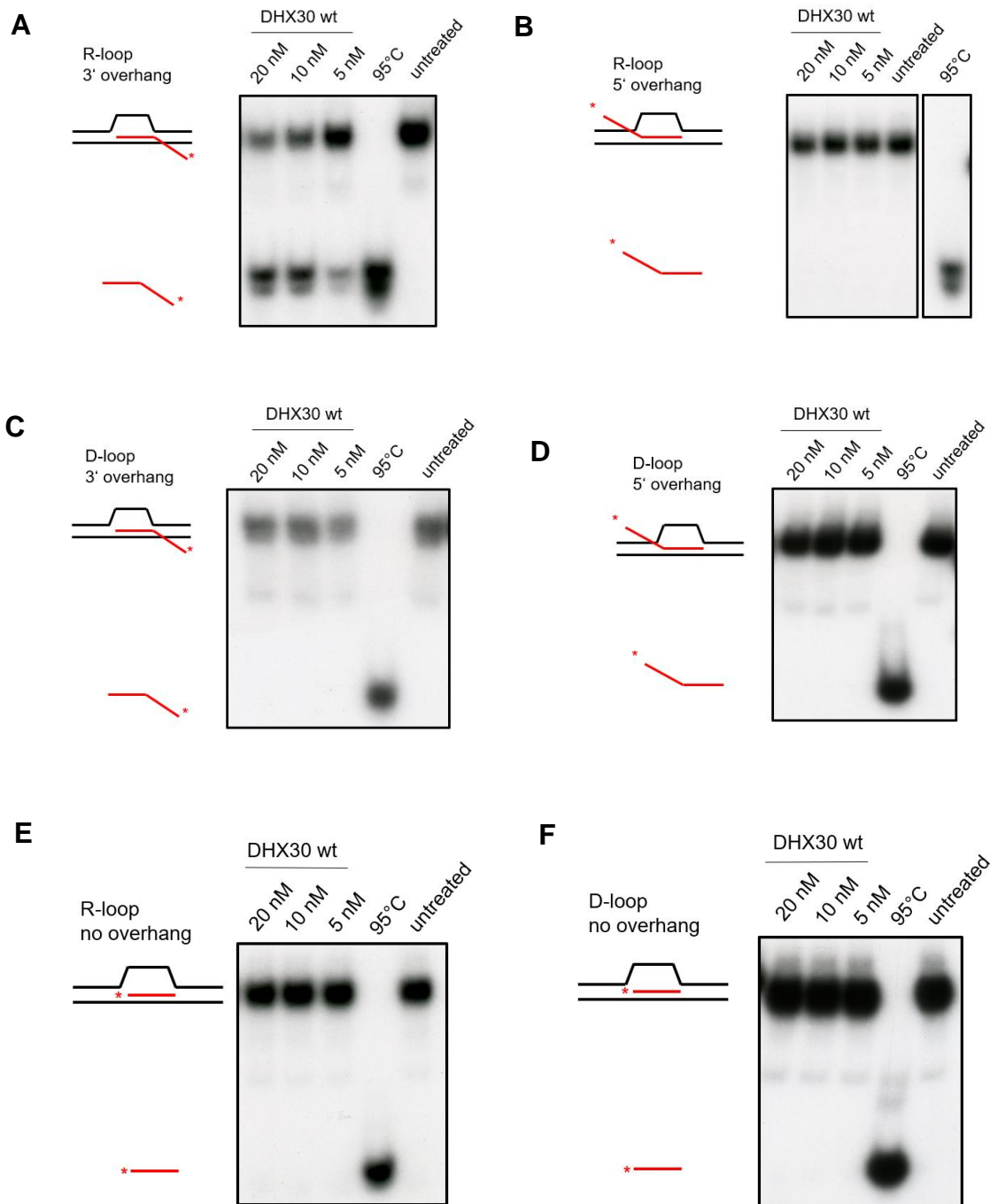


Figure 26: Unwinding assays of recombinant DHX30 with different R-loop and D-loop substrates. R-loop and D-loop constructs with different overhangs were incubated with increasing amounts of 6xHis-SUMO DHX30-WT recombinant protein and analyzed on a 6% native PAGE. Position of the substrate and fully unwound single-stranded oligonucleotide products are marked. (A) DHX30-WT is capable to unwind R-loop structures with 3' overhangs in a dose dependent manner. (B to F) DHX30-WT is unable to unwind R-loop structures with 5' overhang or no overhang, further it is unable to unwind any D-loop DNA structures. To confirm that the R-loop and D-loop structures are properly formed, the substrates were incubated with the enzyme RNase H (see supplemental figure 3).

To test for the specificity of this reaction the R-loop containing a 3' overhang was incubated with the catalytic dead H562R mutant and as expected no unwinding activity was detected (figure 27). In conclusion, these experiments show clearly that DHX30 is a 3' → 5' RNA helicase which is able to unwind RNA:RNA and RNA:DNA duplexes but not DNA:DNA duplexes.

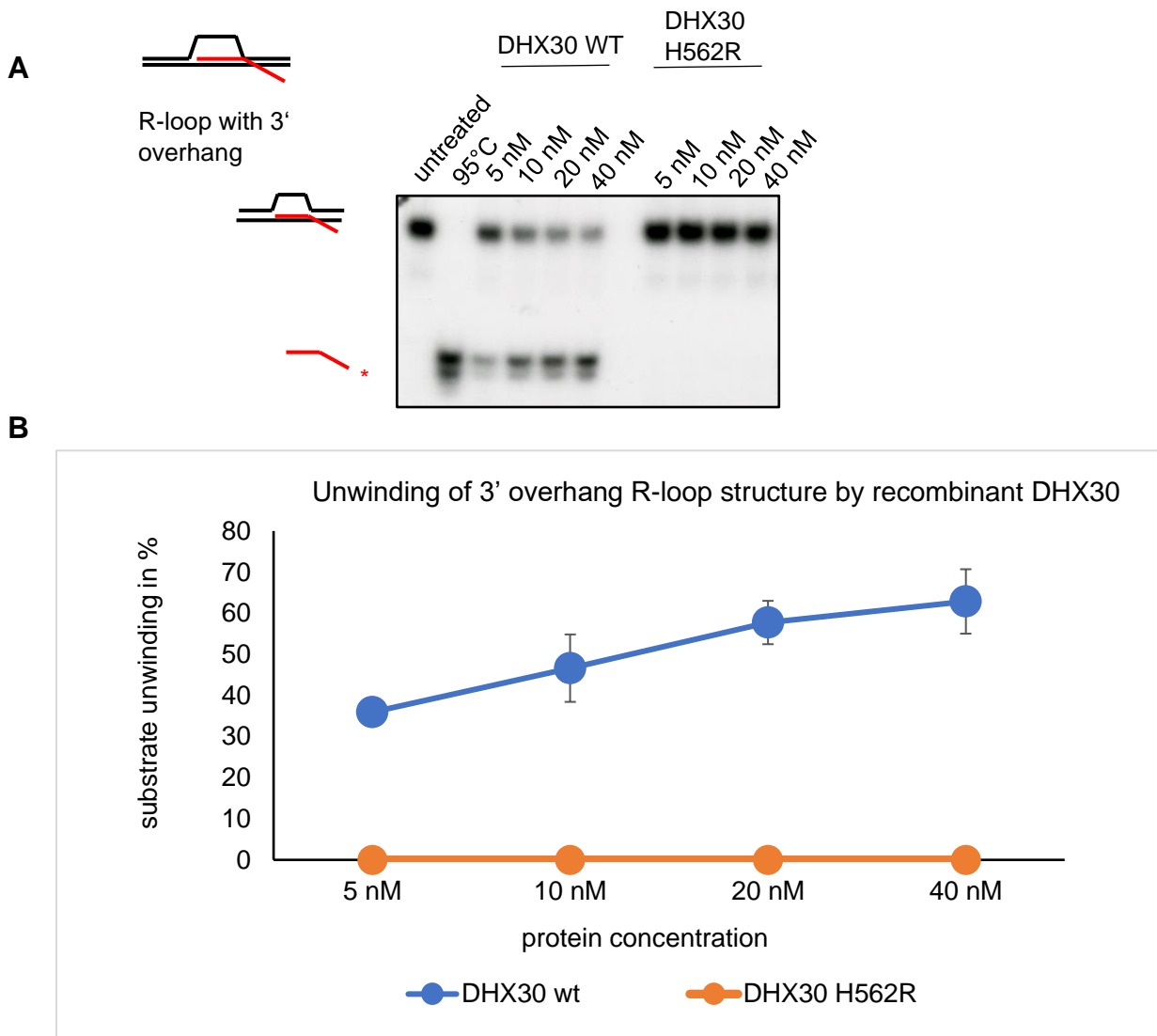


Figure 27: Unwinding assays of recombinant DHX30 (WT and inactive mutant) with 3'-R-loop substrate. (A) Radiolabeled R-loop with 3' overhang was incubated with increasing amounts of DHX30-WT or DHX30-H562R respectively and analyzed on a 6% native-PAGE. DHX30-WT shows an unwinding activity in a dose dependent manner in contrast to the catalytic inactive DHX30-H562R construct. (B) The substrate unwinding in % was calculated and blotted against the protein concentration of DHX30-WT and DHX30-H562R.

5. Discussion

Mutations in the *DHX30* gene causes the autosomal dominant disease “Neurodevelopmental Disorder with severe Motor Impairment and Absent Language” (NEDMIAL; OMIM #617804) (Lessel et al., 2017). Even though *DHX30* has been studied in some detail in the past years, only little was known about its enzymatic properties, cellular function and targets affected in NEDMIAL. The major goal of this work was to characterize the enzymatic properties of *DHX30* and to identify the cellular pathway where it exerts its function. In this thesis I have provided evidence that *DHX30* is an ATP-dependent 3' → 5' RNA helicase capable to unwind RNA:RNA and RNA:DNA duplexes. This function is impaired in *DHX30* variants containing NEDMIAL-causing missense mutations. Furthermore, the finding that *DHX30* is a ribosome-associated factor provided insights into a potential function of *DHX30* during translation and/or turnover of cellular mRNA. Preliminary data suggest that this function is highly specific and affects 5'TOP mRNAs and mRNAs involved in neuronal function. The capability of *DHX30* to unwind RNA:DNA substrates in conjunction with the observation that a fraction of cellular *DHX30* localizes to the nucleus further suggested that the helicase has a function during transcription. My data identified *DHX30* as a helicase implicated in cellular mRNA production and provided insights into the etiology of NEDMIAL.

5.1 Enzymatic properties of *DHX30*

Based on its primary sequence and structure predictions, *DHX30* had been classified as a member of the helicase Superfamily 2 (SF2). This protein family is characterized by a helicase domain composed of the highly conserved RecA1 and RecA2 core including the typical eight highly conserved sequence elements (Lessel et al., 2017). In addition, *DHX30* harbors two N-terminal double-stranded RNA-binding domains (dsRBD 1 and 2), a winged helix domain (WHD), a ratchet-like (RL) domain, and an oligosaccharide binding (OB) domain (see figure 5). To characterize the enzymatic properties of *DHX30* a two-step purification strategy was established, which allowed the production of *DHX30* to near homogeneity and in an enzymatically-active state in *E.coli* (see figure 7).

Two findings suggested that the recombinantly expressed protein is correctly folded and biologically active. First, the purified protein was in a non-aggregated state as concluded from gel filtration studies. Second, the recombinant protein was able to hydrolyse ATP and unwind RNA duplexes as well as RNA:DNA substrates (see figure 8 & figure 26). Importantly, DHX30 variants harboring missense mutations in crucial elements of the helicase/ATPase domain did not show any activity when purified in the same manner as the wild-type protein (see figure 8 & figure 23). This indicated that the activities measured in the *in vitro* ATPase and helicase assays did not arise from co-purifying contaminants but rather reflect the true activity of DHX30.

A detailed analysis of the enzymatic activity of DHX30 revealed that it unwinds its substrates in a 3' → 5' direction (see figure 26). This finding is consistent with studies, showing that DEAH-box helicases function as translocating helicases, advancing in the 3' → 5' direction to disrupt nucleic acid duplexes or secondary/tertiary structures (Schwer, 2008), (Tanak et al., 2005), (Smaldino et al., 2015). The helicase assay performed with the full-length DHX30 protein showed that the RNA:RNA duplex is completely unwound without any detectable re-annealing (see figure 8). This is likely due to the fact that DHX30 has RNA-binding activity and thus shields the individual single-stranded RNA strands from re-forming of RNA duplexes. Based on the amino acid sequence and functional motifs of DHX30, there are four main paralogs in humans. The protein identity is ranging between 30% to 20% and the most similar one is DHX36 (Rizzotto et al., 2020). Biochemical studies showed that the main substrate of DHX36 are DNA G-quadruplexes with comparable efficiencies as observed for DHX30 (Yangyuru et al., 2018). However, the biochemical activity assays performed in this study were mostly qualitative rather than quantitative. Understanding of the exact kinetics and processivity of DHX30 would require additional quantitative enzymatic investigations that could not be performed in the context of this work.

5.2 DHX30 interactome and direct interaction with the ribosome

Elucidating the cellular pathway DHX30 is acting upon was a major goal of this study. To this end, I provided several lines of evidence that linked DHX30 to translation of specific mRNA classes. First, I could confirm from the previous studies that DHX30 majorly localizes in the cytoplasm (see figure 9). Second, the analysis of the DHX30 interactome revealed that its main interactors are proteins of the translation machinery and factors involved in translation initiation (see figure 13). Third, and most importantly, we found that DHX30 is able to directly interact with ribosomes through its N-terminal dsRNA-binding domain 1 (see figure 12).

Chemical crosslinking of reconstituted His-SUMO-DHX30-ribosome complexes revealed two crosslinks between DHX30 and ribosomal proteins. The most significant interaction is between the ribosomal protein RPS3, which is part of the 40S ribosomal subunit (amino acid 108 in humans) and the dsRNA binding domain 1 of DHX30. RPS3 is a ribosomal protein which is located at the mRNA entry channel, next to the A site in the assembled 80S ribosome and contacts mRNA via conserved residues. Studies show that RPS3 promotes the interaction between the mRNA and 40S at the entry channel and enhances the initiation accuracy (Dong et al., 2017). This interaction would be in line with a function of DHX30 during mRNA translation initiation, probably by re-shaping the mRNA to be translated. This scenario is supported by RNA sequencing data, which revealed a strong impact on the abundance of specific mRNAs in translating ribosomes when DHX30 is depleted (see figure 22).

Despite several attempts, DHX30 could not be directly localized at the ribosome using cryo-EM. When highly pure and homogeneous ribosome-DHX30 samples isolated from cells or reconstituted *in vitro* were analyzed, only the ribosome structure could be reconstituted. This indicates that DHX30 binds in the periphery of the ribosome in a flexible manner so that it remains invisible in 3D reconstructions. Alternatively, and not mutually exclusive with the first scenario, DHX30 may only be loosely associated with the ribosome and hence dissociates during cryo-EM sample preparations.

The non-ribosomal proteins identified in the DHX30 interactome study gave first hints towards its function. Among the highly enriched proteins, factors were identified which are involved in mRNA decay (CNOT1, G3BP1, STAU1, TTC37) and ribosome recycling (HBS1L, LTN1, NEMF, PELO and TCF25) (see figure 14 & 15). During ribosome recycling the ribosomal subunits are separated from each other and the bound mRNA, and the produced polypeptide chain is then degraded. This process occurs when a ribosome stalls during the translation and has to be “rescued” by resolving them to prevent the blockage of translation (Young & Guydosh, 2022).

The presence of ribosome recycling factors in the interactome studies could indicate that DHX30 interacts with stalled ribosomes and helps to resolve translational “roadblocks” of certain mRNAs. Alternatively, the activity of DHX30 may be of importance during the process of ribosome splitting and recycling. Another indication for one of these two scenarios is the finding that DHX30 is mainly associated with heavy polysomes in sucrose gradients from cellular lysates (see figure 10). Heavy polysomes are expected to contain very long mRNAs, which may form extended secondary structures and thus cause ribosomal stalling.

An interesting but thus far unexplained finding of this work was that the amount of free 80S ribosomes was strikingly reduced in DHX30 KO cells (see figure 19). This could be concluded from the observation that the mRNA content in the 80S peak by RNA sequencing was dramatically increased in the DHX30 KO cells as compared to control cells (see figure 19). One interpretation of this finding is that under DHX30 KO conditions ribosomes are prevented from splitting and re-initiation of translation. Ribosome profiling, which uses next-generation sequencing to identify ribosome-protected mRNA fragments, would directly address this possibility and such experiments are currently underway.

5.3 DHX30 depletion results in the deregulation of mRNAs involved in neurogenesis and nervous system development.

The analysis of the global RNA pool in DHX30 KO cells by RNA sequencing revealed that the KO of DHX30 drastically deregulates a subset of transcripts either directly or indirectly (see figure 20). These mRNAs, which were validated by qPCR, were classified as important for nervous system development, neurogenesis, and cell differentiation by GO-term analysis (see figure 21). These results are in line with the neuropathogenic phenotype which can be observed in NEDMIAL patients. One mRNA that has been identified as being strongly upregulated upon DHX30 KO encodes SYNDIG1. Its expression has been linked to excitatory synapse development. In addition, it has been shown that an inhibition of neuronal activity in rat hippocampal neurons results in an enrichment of this protein along dendrite spines (Kalashnikova et al., 2010). Another upregulated candidate is SFRP1, which functions mainly in developmental contexts like control of cell specification, proliferation and differentiation (Bovolenta et al., 2008). Interestingly SFRP1 is a factor which is excreted and upregulated during inflammation in neuronal cells, a phenotype frequently observed in neuronal diseases like Alzheimer's disease (Esteve et al., 2019), (Bai et al., 2020).

The most downregulated mRNA, which was identified during this analysis was the transcript of the *UNCX* gene. This gene encodes for a homeobox transcription factor and was shown to be important during somitogenesis and neurogenesis (Nittoli et al., 2019). This gene is also required for the maintenance and differentiation of specific elements of the axial skeleton (Sanchez & Sanchez, 2013). Interestingly *UNCX* is expressed in neuronal progenitor cells of the dorsal neural tube in regions, which give rise to the spinal cord and regions of the telencephalon (Saito et al., 1996). Additional factors, which are massively de-regulated upon DHX30 KO are BRINP3, BEX5 and SYNCG. BRINP3 is strongly downregulated, which may interfere with its reported role as negative regulator for neuronal cell proliferation during the cell cycle transition (Shorts-Cary et al., 2007). Likewise, downregulation of BEX5, may affect its role in neuronal development (Kazi et al., 2015).

Additional factors, which are massively de-regulated upon DHX30 KO are BRINP3, and SYNCG. BRINP3 is strongly downregulated, which may interfere with its reported role as negative regulator for neuronal cell proliferation during the cell cycle transition. Lastly, I found an increase of Synucleins (SYNCG) upon DHX30 KO. These highly conserved proteins are especially abundant in neurons and typically enriched in presynaptic terminals. These proteins are associated with pathological lesions of neurodegenerative diseases (Surguchov et al., 2001). Also the mRNA encoding for ESRP2 was identified as heavily downregulated in our dataset. This gene is an important splice factor during the development of several organ systems and a downregulation results in widespread developmental defects (Beebe et al., 2015).

Since a pathological hallmark of NEDMIAL patients is a low muscle tone (reduced muscle strength) the obtained datasets were also screened for deregulated transcripts linked to muscular function. Potentially interesting mRNAs encode for the STAC and STC-1 protein. STAC is important for the control of calcium release and the process of muscle contraction (Suzuki et al., 1996), (Flucher & Campiglio, 2019), (Rufenach & Van Petegem, 2021). The latter has been implicated in skeletal muscle development. Studies showed that the overexpression of the STC-1 protein in mice results in a retarded muscle and bone growth (Filvaroff et al., 2002), (Jiang et al., 2000). An important question was whether the upregulated mRNAs are translated in DHX30 KO cells and thus give rise to an increase in the encoded protein product. The finding that the transcripts were not only upregulated in the input fractions but also in the 80S and polysome fraction, suggests that this is indeed the case (data not shown). However, direct evidence for translation through ribosome profiling, pulse chase experiments and/or Western blotting has not been obtained thus far.

An interesting observation was that many of the identified deregulated transcripts in DHX30 KO cells are coding for transcription factors (for example UNCX, ZNF28, ZNF85, AFF2, FLI1). It has been shown that the regulation of transcription is highly important for the control of neural development in vertebrate embryos (Lee et al., 2014).

Deregulation of these transcription factors (or subsets thereof) may hence be an upstream event in DHX30 deficient cells that results in the deregulation of other (downstream) target genes that are under control by these factors. Several scenarios are possible: DHX30 deficiency may result in changes of the stability of the mRNA of one or more transcription factors, which results in changes of their mRNA levels and their translation. These changes could have dramatic consequences on other mRNAs as a secondary effect. In the literature several RNA helicases have been described which are involved in the stabilization and/or destabilizing of mRNAs (Khemici & Linder, 2018). It is also possible that DHX30 deficiency impacts the translation efficiency by the lack of recruiting of other translation factors which are necessary for the proper translation of some transcripts, which results in a changed proteome. Further experiments are needed to determine the order of events that lead to deregulation of DHX30 target mRNAs. These studies would also pave the way for the analysis of cell samples of the NEDMIAL patients.

5.4 Depletion of DHX30 results in the reduced abundance of 5'TOP mRNAs in 80S and polysomes

The transcriptome studies identified mRNAs whose abundance is altered in DHX30 cells as a consequence of transcription/stability or both (see figure 20). In a separate approach, I focused on mRNAs, whose deregulation was likely due to post-transcriptional regulation rather than transcriptional/stability mechanisms. RNA sequencing of polysome gradients upon DHX30 KO conditions were performed, assuming that those mRNAs that are associated with polysomes are actually translated. This analysis showed a strong and selective decrease of 5'TOP mRNAs in the 80S and polysomes upon the DHX30 KO (see figure 22). 5'TOP mRNAs encode for ribosomal proteins and translation initiation factors and are characterized by an m⁷GpppC-cap followed by a stretch of 4 to 14 pyrimidine residues (the so-called TOP motif) (Meyuhas & Kahan, 2015). This motif acts as a *cis*-regulatory element that rapidly switches between on or off translation of these mRNAs in response to growth stimuli or nutrient deprivation.

A basic idea of how RNA helicases could regulate the translation of specific mRNAs is that these proteins are involved in the unwinding of exceptionally strong 5' UTR secondary structures to promote the translation like for example DHX29 or DDX3X (Parsyan et al., 2011). This scenario in the context of 5'TOP mRNAs is rather unlikely since it is reported that 5'TOP mRNAs possess short and structured 5'UTRs (Gandin et al., 2016). Recent studies showed that the translation of 5'TOP mRNAs is regulated by the La-related protein 1 (LARP1) by interacting with the active eEIF4F complex and mTORC1 (Tcherkezian et al., 2014). LARP1 was proposed to be a translation repressor for 5'TOP mRNAs (Fonseca et al., 2015), (Lahr et al., 2017).

One function of DHX30 could be to rearrange proteins bound to 5'TOP mRNAs in a manner to ensure a proper translation of 5'TOP mRNAs. In this scenario DHX30 would assist in the displacement of translational repressors including LARP1 from 5'TOP mRNAs to control their translation. In such case DHX30 would rather work as a RNPase, which is remodeling a mRNA protein complex then a processive RNA unwinding helicase. The translational control of 5'TOP mRNAs is not only relevant during starvation but also plays a crucial role in regulation of neural circuits. Studies showed that 5'TOP mRNAs are upregulated during synaptic plasticity in vertebrate synapses (Tsokas et al., 2005) (Tsokas et al., 2007). The cell body of neurons is highly polarized including extensive characteristic spatial compartmentation.

This complex morphology requires the ability of distal axons and dendrites to quickly respond to external cues excluding the direct communication with the soma (Agrawal & Welshhans, 2021). Especially in axons and dendrites the mRNA localization and translation at distal sites is highly important (Agrawal & Welshhans, 2021). This dynamic signaling is coordinated by the localization of the translation machinery, including mRNA transcripts, ribosomes and RNA-binding proteins to specific subcellular regions (Jung et al., 2014), (Holt et al., 2019). Recent studies showed that in axons 5'TOP mRNAs are locally translated and integrated into ribosomes, which demonstrates that the local synthesis of components of the translational machinery is essential for the axonal translation (Nagano et al., 2020), (Shigeoka et al., 2019).

Changes of the local translation in the stages of neural development have emerged as important implications to decipher the etiology of neurological disorders (Agrawal & Welshhans, 2021). The experiments of this work gives a hint that changes in the translation of 5'TOP mRNAs could contribute to the phenotype which can be seen in NEDMIAL patients.

5.5 Pathogenic variants of DHX30 lose their enzymatic activities *in vitro*, but are still associated with ribosomes

To elucidate the malfunction of DHX30 in NEDMIAL patients, pathogenic mutants of DHX30 were tested for their enzymatic activities and their ability to associate with ribosomes. For the enzymatic characterization of DHX30 patient mutations, plasmids containing DHX30 with patient mutations were cloned, expressed, and purified in the same manner as the DHX30 wildtype (see figure 23). The results showed that the ATPase activity and the unwinding activity in all pathogenic variants of DHX30 harboring missense mutations in the helicase core are abolished.

In contrast, the R908Q variant which harbors a missense mutation affecting a highly conserved residue within the ratchet-like motive was still able to hydrolyze ATP and unwind RNA duplexes *in vitro* (see figure 23). One has to mention that the individual where the R908Q mutation was identified showed a milder form of NEDMIAL, with a normal ability to speak and a late onset of ataxia (Mannucci et al., 2021). One plausible explanation for the pathogenicity of this mutant could be that this mutation results in a lower steady-state level of DHX30 in this NEDMIAL patient. This hypothesis is supported by the identification of four affected individuals carrying variants that result in either haploinsufficiency or a truncated protein. These patients presented a milder phenotype compared to the patients harboring the missense mutations in the helicase core (Mannucci et al., 2021). Although the missense mutations in the helicase core result in a loss of activity, the association with their respective protein interactome stays intact (see figure 24).

The analysis of the interactome of two mutants (R493H and H562R) in comparison to the wildtype showed no significant changes in interacting proteins by mass spectrometry (see figure 25). Even the pathogenic forms of DHX30 show a co-migration with ribosomes although the amount of DHX30 associated with 80S was slightly reduced (see figure 24). This indicates the ATPase and helicase activity is not crucial for the association of DHX30 with translating ribosomes. Interestingly this finding is similar to studies about the pathogenic nature of the motor neuron disease SMARD1, which is caused by missense mutations of a ribosome associated RNA helicase, called IGHMBP2 (Grohmann et al., 2001). As observed for DHX30, missense mutations in the helicase core of IGHMBP2 results in the abolishment of the ATPase and helicase activity but still allows binding to ribosomes (Guenther et al., 2009). Taken together, there is an indication that the loss of DHX30 ATPase and helicase activity results in non-functional DHX30 mRNP/ribosome complexes which may be a pathological hallmark of NEDMIAL.

5.6 A potential function of DHX30 in the nucleus - enzymatic activity of DHX30 on R-loop and D-loop substrates

Although the majority of DHX30 localizes to the cytoplasm, a clear but minor pool could also be found in the nucleus (see figure 9). In a recent study, proteins interacting with RNA/DNA hybrids in human cells were identified and included among other DEAH-box helicases such as DHX9, DHX15 and DHX36 also DHX30 (Cristini et al., 2018). RNA/DNA hybrids mostly occur in so-called R-loops structures, which are stable triple-stranded nucleic acid structures formed in the nucleus during transcription when the nascent RNA hybridizes back to the double stranded DNA (Wang et al., 2021). These structures need to be resolved by enzymes in order to restore the native DNA double helix and to resolve transcription/replication conflicts. In fact, these structures are present in various key biological processes, such as genome stability maintenance, transcriptional regulation and DNA damage repair (Aguilera & Garcia-Muse, 2012), (Grunseich et al., 2018), (Lang et al., 2017).

A dysfunction in the R-loop regulation is linked to multiple human diseases including cancers, neurological diseases and immune disorders (Crossley et al., 2019), (Brambati et al., 2020). The availability of enzymatically active DHX30 allowed me to test whether it can resolve these or potential other nuclear DNA/RNA structures. The experiments shown in figure 26 and 27 gave a clear answer to this question: DHX30 was found not only to unwind RNA:RNA duplexes but also R-loop structures *in vitro*. Since DHX30 is not active on DNA:DNA substrates, the results strongly suggest that the activity of DHX30 essentially requires an RNA moiety in its substrates.

Since the resolution of R-loops is linked to transcriptional control, it is also thinkable, that a non-functional DHX30 has impact on the transcription of certain mRNAs, like those identified by RNAseq in DHX30 KO cells (see figure 20). R-loops can also occur in mitochondria, which is of relevance for mitochondrial replication and gene expression (Holt, 2019). In this regard it is interesting that a mitochondrial isoform of DHX30 has recently been identified. It is hence possible that this isoform may have a potential function in mitochondria on R-loops. The nuclear function of DHX30 is the focus of current research that we are doing in collaboration with the group of Prof. Ying Liu (University of Copenhagen).

5.7 The Pathomechanism of NEDMIAL: a Hypothesis

In recent years links between RNA metabolism and disease in general and in neuronal disorders in particular came into focus. This is because tight control of gene expression at the transcriptional and post-transcriptional level is believed to be of particular importance for the proper formation of neurons (Swanger & Bassell, 2011). In line with this, a group of mRNA binding proteins have been identified over the past years that are directly involved in a wide range of neurodevelopmental disorders. The prototypic disease linked to mRNA metabolism is the “Fragile X syndrome” (FXS; OMIM#300624), the most common genetic cause of mental retardation in humans (Fernandez et al., 2013), (Hagerman et al., 2017). This disease is caused by reduced levels of functional FMRP, an RNA binding protein involved in several aspects of mRNA metabolism including mRNA

transport and translation (Fernandez et al., 2013). Another example of a disease linked to mRNA metabolism is “Spinal Muscular Atrophy with Respiratory Distress 1” (SMARD1; OMIM#604320). In this disease the degeneration of α -motoneurons is caused by mutations in the *IGHMBP2* gene (Grohmann et al., 2001). *IGHMBP2* encodes for a Upf1-like 5' \rightarrow 3' RNA helicase, is ribosome associated and functionally linked to translation and thus resembles in its biochemical properties DHX30 analyzed in this study. Furthermore, as observed DHX30 in NEDMIAL, disease-causing mutations in *IGHMBP2* interfere with its enzymatic function (Guenther et al., 2009).

The data presented in this thesis suggest that defects in mRNA metabolism may also be a key event in the etiology of NEDMIAL. Based on the experiments performed in this work I propose a general model of DHX30 function in cellular RNA metabolism and its possible implication for the etiology of NEDMIAL: DHX30 is a RNA helicase which is able to resolve RNA:RNA duplexes and RNA:DNA hybrids. In the cytoplasm it forms a complex with ribosomes. Pathogenic DHX30 mutants, in contrast, fail to accomplish at least some of these activities: ATPase/Helicase inactive forms of the protein are likely to be unable to resolve RNA:DNA hybrids in the nucleus and RNA duplexes in the cytoplasm. This may result in drastic changes in the transcription efficiency of specific mRNAs and an unbalanced transcriptome, as it has been observed in this study in DHX30 KO cells (see figure 28 – 1). In the cytoplasm, an inactive DHX30 could impact the active translation of mRNAs (including 5'TOP mRNAs) (see figure 28 – 2). An imbalanced proteome is likely the consequence, which could trigger further misregulation in the transcriptome (including the transcription of mRNAs involved in neurodevelopment) and potentially other cellular events (like mRNA translation) (see figure 28 – 3). The overall misregulation of specific transcripts on the transcriptional and translational level could result in a malfunctional mRNA metabolism and neurodevelopmental diseases (see figure 28 – 4).

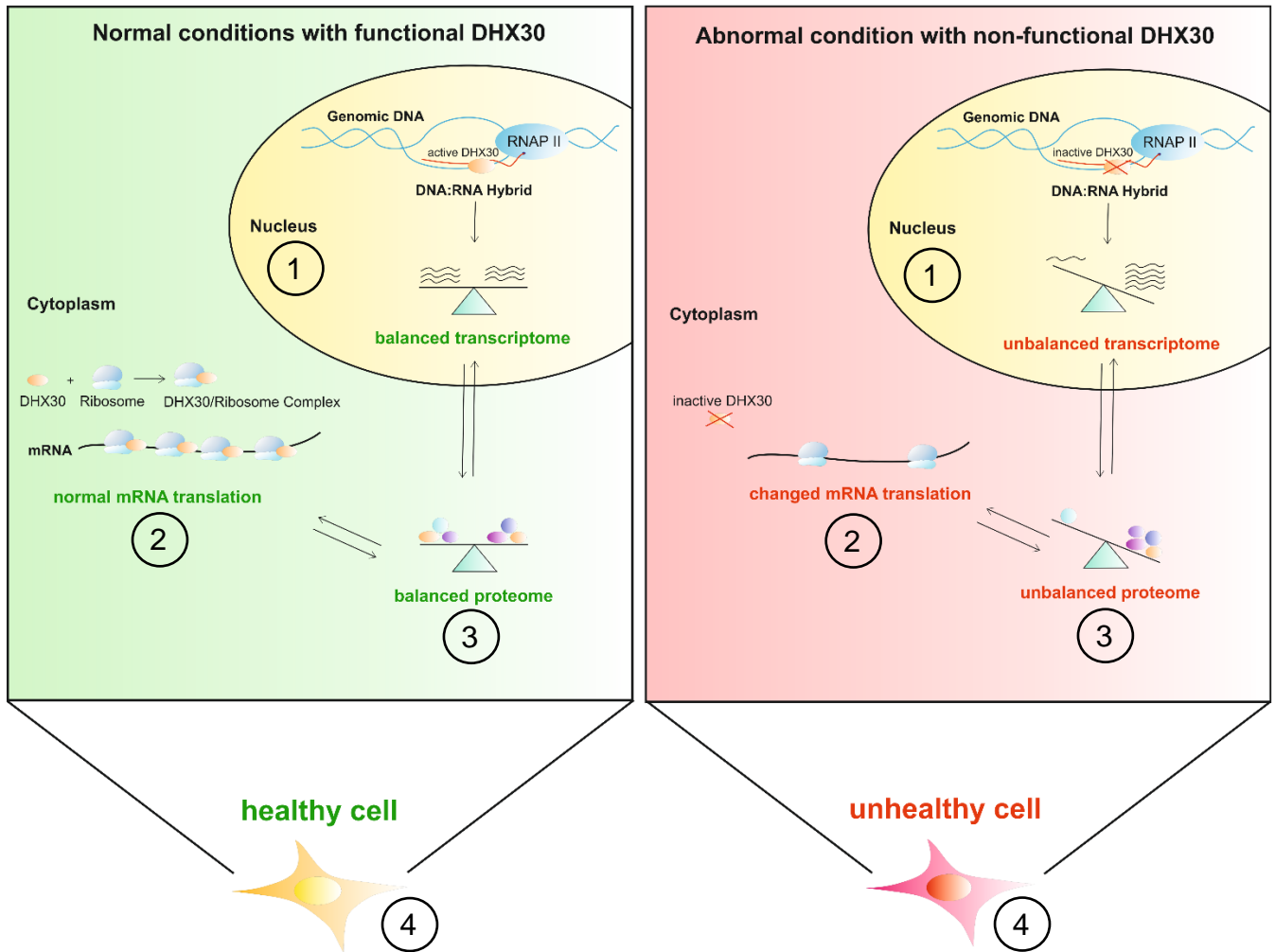


Figure 28: Model of the potential function of DHX30 in the RNA metabolism of human cells. For description see text.

Further experiments along the same lines as described in this work and in patient-derived cell lines are needed to substantiate this model and to obtain insight into the order of events that eventually lead to the pathophysiological changes in NEDMIAL.

6. Material & Methods

6.1 Material

All chemicals used were purchased from Merck, BD Biosciences, Serva, Sigma-Aldrich, Riedel-de Haen, Boehringer Ingelheim and Roth. Radioisotopes were obtained from Hartmann Analytic. Laboratory consumables were obtained from Hartenstein, Macherey-Nagel, Eppendorf, Sarstedt, Sartorius stedim, Dispomed and Geiner.

6.1.1 Nucleotide and Protein Ladders

GeneRuler™ DNA Ladder Mix	Thermo Fisher Scientific
GeneRuler™ 100 bp DNA Ladder	Thermo Fisher Scientific
PageRuler™ Prestained Protein Ladder	Thermo Fisher Scientific
PageRuler™ Unstained Protein Ladder	Thermo Fisher Scientific

6.1.2 Buffers and Solution

DNA loading buffer (6x)	30% (v/v) Glycerol 0.25% Bromophenol Blue 0.25% Xylene Cyanol FF
Native loading buffer (5x)	50% (v/v) Glycerol 0.5x TBE 0.02% (w/v) Bromophenol Blue
5x Tris/EDTA/borate (TBE)	445 mM Tris-HCl, pH 8.3 445 mM Boric acid 10 mM Na ₂ EDTA
CaCl ₂ -Buffer	60 mM CaCl ₂ 15% (v/w) Glycerol 10 mM PIPES, pH 7.0
10x Lämmli	250 mM Tris-Base 1.92 M Glycine 35% SDS
10x NET buffer	500 mM Tris-Base 50 mM NaEDTA 1.5 M NaCl 0.5% Triton-X 100
NET-Gelantine	2.5 g Gelantine

	1x NET Buffer
10x Phosphate buffered saline (PBS)	1.4 M NaCl 27 mM KCl 100 mM Na ₂ HPO ₄ 18 mM KH ₂ PO ₄
6x Protein sample buffer	300 mM Tris-HCl, pH 6.8 12% (w/v) SDS 30% (v/v) Glycerol 600 mM DTT 0.04% (w/v) Bromophenol Blue
5x DNA loading dye	5 mM Tris-HCl 0.05 mM EDTA 0.04% (w/v) Bromophenol Blue 0.04% (w/v) Xylene Cyanol
RNA loading buffer	95% Formamide 50 mM EDTA 0,03% (w/v) Bromophenol Blue
10x T7 Transcription buffer	400 mM Tris-HCl, pH 7.9 10 mM Spermidine 260 mM MgCl ₂ 0.1% Triton X
RNA gel elution buffer	0.5 M NH ₄ OAc 0.1 mM EDTA 2 mM MgCl ₂ 0.1% SDS
4x resolving gel buffer	1.5 M Tris-Base 0.4% SDS (w/v) pH 8.8 (HCl)
4x collecting gel buffer	250 mM Tris-Base 0.2% SDS (w/v) pH 6.8 (HCl)
Coomassie-staining solution 0.15%	(w/v) Serva Blue R 15% (v/v) Acetic acid 45% (v/v) Methanol
Coomassie-destaining solution	30% (v/v) Methanol 10% (v/v) Acetic acid
Amido black staining solution	0.3% (w/v) Amido black 10% (v/v) Methanol 2% (v/v) Acetic acid
Amido black de-staining solution	90% (v/v) Methanol 3% (v/v) Acetic acid

6.1.3 Cell Culture

6.1.3.1 Bacterial Cells

Strain	Chromosomal genotype	Supplier
<i>E. Coli</i> DH5 α	F- Φ 80lacZ Δ M15 Δ (lacZYA-argF) U169recA1 endA1 hsdR17 (rk-, mk+) phoA ^{sup} E44 λ -thi-1 gyrA96 relA1 λ -	Invitrogen
<i>E. Coli</i> BI-21-Rosetta	thi hsdR17 (rK-mK+) glnV44 relA1 lacF- ompT hsdSB(rB-mB-) gal dcm pRARE(CamR)	GE Healthcare

6.1.3.2 Eukaryotic Cell lines

Cell type	Description	Supplier
HEK 293	Human Embryonic Kidney cell line	DSMZ (ACC 035)
HEK 293T	Human Embryonic Kidney cell line	DSMZ (ACC 635)
HEK293T DHX30 KO	Human Embryonic Kidney cell line, DHX30 knockout introduced by Crispr/Cas9	Illaria Mannucci, UKE Hamburg
Flp-In TM T-REx TM 293	Human Embryonic Kidney cell line	Invitrogen (R780-07)
Flp-In TM T-REx TM 293 DHX30-WT	Human Embryonic Kidney cell line overexpressing C-terminal FLAG/HA tagged DHX30-WT	This work
Flp-In TM T-REx TM 293 DHX30-H562R	Human Embryonic Kidney cell line overexpressing C-terminal FLAG/HA tagged DHX30-H562R mutant	This work
Flp-In TM T-REx TM 293 DHX30-R493H	Human Embryonic Kidney cell line overexpressing C-terminal FLAG/HA tagged DHX30-R493H mutant	This work

6.1.4 Cell Culture Media

Bacterial Media	
Luria broth (LB)	1.0% (w/v) Tryptone 1.0% (w/v) NaCl 0.5% (w/v) Yeast Extract
Super broth (SB)	3.5% (w/v) Tryptone 0.5% (w/v) NaCl 2.0% (w/v) Yeast Extract set pH to 7.5 using NaOH

Selection media was prepared by combination of antibiotics (100 µg/ml Ampicillin (Roth), 50 µg/ml Kanamycin (Sigma-Aldrich), 50 µg/ml Chloramphenicol (Sigma-Aldrich) and media. Agar plates were made by addition of 2% (w/v) Bacto™ Agar.

Eukaryotic Cell media	
HEK 293	DMEM 10% FBS 1% (v/v) Pen/Strep
Flp-In™ T-REx™ 293	DMEM 10% (v/v) FBS 10 µg/ml Blasticidin 100 µg/ml Zeocin
Flp-In™ T-REx™ 293 for stable cell lines	DMEM 10% (v/v) FBS 10 µg/ml Blasticidin 100 µg/ml Hygromycin B

6.1.5 Antibodies

Primary Antibodies

Antibody	Supplier	Dilution (WB)
DHX30	Bethyl (A302-218A)	1:500 (WB), 1:50 (IF)
HA	HISS (MMS-101R)	1:1000 (WB)
rpS6	Abcam (ab59261)	1:1000 (WB)
rpL3	Abcam (ab154882)	1:1000 (WB)
Tubulin	Sigma-Aldrich (236-10501)	1:1000 (WB)
LARP1	Abcam (ab86359)	1:500 (WB)

Secondary Antibodies

Antibody	Supplier	Dilution
α -mouse glgG (whole molecule) peroxidase conjugate	Sigma-Aldrich (A4416)	1:5000 (WB)
α -rabbit glgG (whole molecule) peroxidase conjugate	Sigma-Aldrich (A6154)	1:5000 (WB)
Goat anti-Rabbit IgG (H+L) Highly Cross-Adsorbed Secondary Antibody, Alexa Fluor Plus 488	Invitrogen (A32731)	1:200 (IF)

6.1.6 Plasmids

Plasmid	Description	Cloning	Reference/Supplier
pFRT/TO/MCS Mammalian expression vector	pcDNA5/FRT/TO overexpression plasmid		(Küspert, 2014)
pFRT/TO/MCS::DHX30 WT	DHX30-WT incl. C-terminal FLAG/HA tag	HindIII/Acc65I	This work
pFRT/TO/MCS::DHX30-R493H	DHX30-R493H incl. C-terminal FLAG/HA tag	HindIII/Acc65I	This work
pFRT/TO/MCS::DHX30-H562R	DHX30-H562R incl. C-terminal FLAG/HA tag	HindIII/Acc65I	This work
pet-28M-SUMO1::DHX30-WT	DHX30-WT inc. N-terminal 6xHis-SUMO	Age/NotI	This work

pet-28M-SUMO1::DHX30-G462E	DHX30-G462E inc. N-terminal 6xHis-SUMO	Mutagenesis	This work
pet-28M-SUMO1::DHX30-R493H	DHX30-R493H inc. N-terminal 6xHis-SUMO	Age/NotI	This work
pet-28M-SUMO1::DHX30-H562R	DHX30-H562R inc. N-terminal 6xHis-SUMO	Age/NotI	This work
pet-28M-SUMO1::DHX30-S737F	DHX30-S737F inc. N-terminal 6xHis-SUMO	Mutagenesis	This work
pet-28M-SUMO1::DHX30-R785C	DHX30-R785C inc. N-terminal 6xHis-SUMO	Mutagenesis	This work
pet-28M-SUMO1::DHX30-R908Q	DHX30-R908Q inc. N-terminal 6xHis-SUMO	Mutagenesis	This work

6.1.7 DNA and RNA Oligonucleotides

DNA oligonucleotides for cloning and mutagenesis

Primer	Sequence 5'-3'
20_DHX30_forw_Agel	TCATCTACCGGTGGAACCGGTGGATCCGTGAGCAAGC TTCGAATTCGTCGACTGG
21_DHX30_rev_+stop_NotI	ATATAGCGGCCGCTTACCTAGATCCGGTGGATCCCGG C
DHX30_forw_hind3_FLP	ATATAAAGCTTGAGGAGATCTGCCGCCGC
DHX30_rev_ACC65I_flag ha_FLP	ATATGGTACTTATGCGTAATCTGGAACATCGTATGGG TAACCTCCACCGCCCCCTTTATCGTCATCGTCTTTGTA GTCGGATCCCGGCCGCGTAC
3_DHX30_mut_G462E_fwd	GGGACACGGGCTGTGAAAAGACCACGCGCATCCCCCA
4_DHX30_mut_G462E_rev	TGGGGGATGCGCGTGGTCTTTTACAGCCCGTGTCCC
5_DHX30_mut_S737F_fwd	CAACATTGCTGAGACTTTTATCACAATCAATGACATCGT GCATG
6_DHX30_mut_S737F_rev	CATGCACGATGTCATTGATTGTGATAAAAGTCTCAGCA ATGTTG
7_DHX30_mut_R785C_fwd	GGGGCCGGGCGGGCTGCTGCCAGT
8_DHX30_mut_R785C_rev	ACTGGCAGCAGCCCGCCCGGCCCC
9_DHX30_mut_R908Q_fwd	ACTGGTGGTCGTTTCTGCCTCACCCAGGACCCCTTCA
10_DHX30_mut_R908Q_rev	TGAAGGGGTCTGGGTGAGGCAGGAAACGACCACCAG T

DNA oligonucleotides for qPCR

Primer	Sequence 5'-3'	Reference/Supplier
ZNF28_human_for	GAGTGTGGCAAGACCTTCAGTC	OriGene
ZNF28_human_rev	CTCTCTGATGCTGTGCAAGGTG	OriGene
UNCX_human_for	AGAAGGCGTTCAACGAGAGCCA	OriGene
UNCX_human_rev	CGTGTTCTCCTTCTTCTCCAC	OriGene
ESRP2_human_for	GCAGAGACACAAGCACCACATG	OriGene
ESRP2_human_rev	TTCCCGTGACAAGAAACGAGCC	OriGene
BEX5_human_for	TGGTGAATACCAGGAGCCTGGA	OriGene
BEX5_human_rev	CATCTCCTCCATGAACCGTTCC	OriGene
SFRP1_human_for	CAATGCCACCGAAGCCTCCAAG	OriGene
SFRP1_human_rev	CAAACCTCGCTGGCACAGAGATG	OriGene
SYNDIG1_human_for	CCTCAGTGTCTTCTCCATGCTC	OriGene
SYNDIG1_human_rev	TGATGGACAGCACTGCCAGGAA	OriGene

DNA and RNA oligonucleotide substrates for unwinding assay

Name	Sequence 5'-3'	Reference
Unwind_Substr_Tseng _Rogenski for T7 transcription	ATTTAGGTGACACTATAGAATACACGGA ATTCGAGCTCGCCCATGGTGGATTGTAA ATTGTAATGTTGTTGCGCGCGCTATA GTGAGTCGTATTAGGGGATCCTCTAGAG TCG	(Tseng- Rogenski & Chang, 2004)
R5_DNA	AACGACGGCCAGTGAATTCGAGCTCGGT ACCCAGTCTTAAGCCTTGACTAGTCAGCT TGAATAAGCGATTGACT	(Thakur et al., 2013)
R4_DNA	AGTCTTAAGCCTTGACTAGTCAGCTTGAC TAAGCGATTGACTAACGACGGCCAGTGAA TTCGAGCTCGGTACCC	(Thakur et al., 2013)
R3_DNA	AACGACGGCCAGTGAATTCGAGCTCGGT ACCC	(Thakur et al., 2013)
T1_DNA	TGTGGAATGCTACAGGCGTTGTAGTTT GTAAGGTTGACGAACTCAGTGTAACG GTACATGGGTTTCTATTGGGCTTGCTATCCCT GAAAATGAGGGTGG	(Thakur et al., 2013)
B11_DNA	CCACCCTCATTTCAGGGATAGCAAGCCCAAT AGGGGTACCGAGCTCGAATTCAGTGGCCGTC GTTCCAGTACAACTACAACGCCTGTAGCATT CCACA	(Thakur et al., 2013)
R5_RNA	AACGACGGCCAGUGAAUUCGAGCUCGGUAC CCAGUCUUAAGCCUU	(Thakur et al., 2013)
R4_RNA	UAAGCGAUUGACUAACGACGGCCAGUGAAU UCGAGCUCGGUACCC	(Thakur et al., 2013)
R3_RNA	AACGACGGCCAGUGAAUUCGAGCUCGGUAC CC	(Thakur et al., 2013)

6.2 Methods

6.2.1 Molecular Methods

6.2.1.1 Polymerase chain reaction

The polymerase chain reaction allows the amplification of DNA fragments of interest *in vitro*. For the reaction, the Phusion High Fidelity PCR Master Mix (Thermo Fisher Scientific) and DNA oligonucleotides (see 4.1.7) were used. The reaction mix used is stated below:

DNA template	<50 ng
2x Master mix	1x
Forward primer	1 μ M
Reverse primer	1 μ M

The PCR was performed in a thermocycler using the following program.

Program	Temp	Time	Cycles
Initiation	95° C	5'	1
Denaturing	95°C	1'	30 -35
Annealing	50-60°C	30''	
Elongation	72°C	30'' per KB	
Final elongation	72°C	2 x Elongation	1

The melting temperature of the primers were calculated by SnapGene (Version 1.1.3) and a T_m difference of 4°C was always chosen.

6.2.1.2 Agarose Gel electrophoreses

For the separation of nucleotides by size, agarose gel was used. Depending on the size of the DNA, a 0.5-2% agarose was dissolved in 1x TBE buffer and boiled till the solution was clear. To visualize the nucleic acids, Ethidium Bromide to a final concentration of 5µg/ml was added. The electrophoresis was carried out at 120 Volt for 30-60 min.

6.2.1.3 Purification of DNA from gels or reactions

For the purification of DNA-fragments from agarose gels or PCRs, the NucleoSpin Gel and PCR Clean-up (Macherey-Nagel) kit was used as per manufacturer's instruction.

6.2.1.4 Restriction digestion and dephosphorylation of DNA

The DNA fragments and plasmid vectors were hydrolyzed by restriction endonucleases (Thermo Fisher Scientific). This reaction was carried out in a preparation containing the DNA, the recommended buffer suitable for the enzyme and 1-5 U of the enzyme for 1 to 16 h depending on the enzyme activity and the amount of DNA.

For the dephosphorylation of digested plasmids the Thermosensitive Alkaline Phosphatase (FastAP – Thermo Fisher Scientific) was used. This was achieved by adding 1 µl of FastAP to the restriction digestion reaction and incubating the reaction for 1h at 37°C. The digested DNA was then purified as described above.

6.2.1.5 Ligation of DNA fragments

To generate vectors containing a desired DNA fragment, digested fragments and linearized vectors were ligated by T4 Ligase (Thermo Fisher Scientific). For 20 µl of ligation reaction, a 5-fold excess of insert was mixed with a linearized plasmid, 1 U of T4 DNA ligase (Thermo Fisher Scientific) and 1x reaction buffer. The reaction was incubated either overnight at 16°C or for 2h at room temperature. For calculation of the vector:insert ratio, the NEB online tool was used (<http://nebiocalculator.neb.com/#!/main>). After ligation, the entire reaction was used for transformation in chemically competent DH5α *E. coli* cells.

6.2.1.6 Preparation of competent *E. coli* cells

The *E. coli* cells were made chemical competent by growing them in 50 ml LB media at 180 rpm and 37 °C overnight. 4 ml of this culture was transferred to fresh 400 ml of LB and incubated at 37°C until an OD₆₀₀ of 0.375 was reached. The cells were incubated on ice for 10 min and pelleted via centrifugation at 4°C, 1,600 xg for 7 minutes. This cell pellet was resuspended in 80 ml of buffer containing 60 mM CaCl₂, 15% glycerol, 10 mM PIPES pH 7.0. After the resuspension, the cells were again centrifuged and resuspended in 16 ml of the CaCl₂-Buffer as described before. The cells were then aliquoted, snap frozen and stored at -80°C.

6.2.1.7 Transformation of chemically competent *E. coli* strains

Chemically competent *E. coli* cells were transformed with the desired vector by heat shock method. For this, the cells were thawed on ice for 20 min and 5-10 µl of ligation reaction or 50 to 100 ng of plasmid-DNA was added. After gently mixing, the sample was incubated on ice for 30 min and heat shock was given at 42°C or 90 seconds. After this the cells were incubated for 2 minutes on ice and 700 µl of pre-warmed LB media was added. The cells were then incubated at 37°C for 1h shaking (1,000 rpm). 90% of the cells were plated on agar plates, containing antibiotics corresponding to the vector-encoded resistance gene.

6.2.1.8 Colony screening of transformed bacteria

For testing potentially positive clones, bacterial colonies were picked from the agar plates with the vector specific antibiotics and transferred in a 4 ml LB media for overnight incubation at 37°C with shaking at 200 rpm. The purified plasmids were digested by restriction enzymes and the resulting DNA fragments were analyzed on an agarose gel. The plasmid sequence was verified by sequencing (Eurofins, Germany).

6.2.1.9 Purification plasmids-vectors derived from bacteria

Plasmid DNA derived from bacteria were purified by using the NucleoSpin Plasmid QuickPure Kit (Macherey-Nagel) as per manufacturer's instructions.

6.2.1.10 Bacterial cryo-stock preparation

For generation of long-time storage of bacterial cryo-stocks, 500 µl of overnight bacterial culture was mixed with 500 µl of 50% sterile glycerol. They were then snap frozen and stored at -80°C.

6.2.1.11 Site-directed mutagenesis

To generate mutations on vector-plasmids, a site-directed mutagenesis approach by PCR was used. In the first step two mutagenic primers are phosphorylated at the 5' end using the T4 Polynucleotide Kinase (Thermo Fisher Scientific):

oligonucleotide	250 pmol
10X reaction buffer A for T4 Polynucleotide Kinase	1x
ATP	2 mM
T4 Polynucleotide Kinase	2 U

The phosphorylated primers were used for the PCR amplification of the target plasmid:

DNA template	50-200 ng
Primer (for or rev)	10 pMol
Phusion DNA Polymerase Mastermix 2x	1x

Program	Temp	Time	Cycles
Initiation	95° C	5'	1
Denaturing	95°C	1'	30 -35
Annealing	50-60°C	30''	
Elongation	72°C	30'' per KB	
Final elongation	72°C	2 x Elongation	1

Subsequently the maternal DNA was digested with 1 U of DpnI (Thermo Fisher Scientific) at 37°C for 1h. 10-20% of the reaction mixture was afterwards transformed into *E. coli*. Positive colonies were tested for desired mutations by sequencing.

6.2.1.12 DNA sequencing

DNA sequencing was performed by Eurofins Germany.

6.2.2 Eukaryotic Cell Culture

6.2.2.1 Culture and maintenance of adherent cells

The cell lines were grown at 5% CO₂, 37 °C and 100% humidity in the appropriate medium. After reaching a 95% confluency the cells were split 1:10 or according to the experimental confluency. For passaging, the cells were washed with PBS and detached by Trypsin-EDTA (life technologies). The cells were washed and resuspended in fresh media. According to the required dilution, the cell pellet was resuspended and plated to a fresh plate.

6.2.2.2 Preparation of cryo stocks of the eukaryotic cell lines

Cells were washed with PBS, detached from the plate by Trypsin-EDTA and pelleted by centrifugation (5 min at 400 xg). The cell pellet was resuspended in cryo medium. Cells were kept at -20 °C for 4h and then at -80 °C. To start a new culture, the cryo vial was thawed and diluted in a pre-warmed fresh medium. Cells were pelleted, the supernatant was removed and resuspended in fresh media.

6.2.2.3 Generation of stable Flp-In T-Rex 293 cell lines

Tetracycline inducible stable Flp-In T-Rex 293 cell lines expressing the ORF of the protein of interest were generated by co-transfection of POG44 and the pFRT-vector into 30-40% confluent cells in an antibiotic-free medium using Lipofectamine (Thermo Fisher Scientific). Medium was changed after 24h. For selection of clones, 48h post plating the cells were switched to a selection medium containing 10 µg/ml Blasticidin and 100 µg/ml Hygromycin B. After every 2 – 4 days, the media was changed until single colonies were clearly visible on the surface of the plate. Colonies were picked with Trypsin-EDTA and transferred to a 6-well plate and further growth. To confirm the expression of the protein of interest, cells were induced with tetracycline (1:2000) and checked by Western blotting.

6.2.3 Biochemical Methods

6.2.3.1 Bradford assay

The protein concentrations of solutions were determined using the Bradford assay. 1 to 10 µl of the protein sample 1X Bradford reagent (BioRad) (5X Bradford reagent was diluted with water). The protein concentration of the sample was measured against the blank and calculated based on a BSA standard curve in a spectrometer (Eppendorf) at 595 nm. The standard curve was made using BSA (Sigma-Aldrich) of known concentration 0,5 µg, 1 µg, 2 µg, 4 µg and 5 µg.

6.2.3.2 SDS-Page

Protein separation on the basis of molecular weight was achieved by denaturing (SDS) polyacrylamide gel electrophoresis (SDS-Page). The SDS-Page was run in 1x Lämmli-buffer at a constant current of 65-75 mA.

Composition of a typical 10% Gel:

Separation Gel	
Rotiphere Gel 30 (Acrylamide:Bisacrylamid 37:1)	10 ml
1,5 mM Tris-HCl, pH 8.8	5.5 ml
ddH ₂ O	14.5 ml
APS	67 µl
TEMED	67 µl

Stacking Gel	
Rotiphere Gel 30 (Acrylamide:Bisacrylamid 37:1)	1.65 ml
1,5 mM Tris-HCl, pH 8.8	2.45 ml
ddH ₂ O	5.9 ml
APS	67 µl
TEMED	67 µl

6.2.3.3 Coomassie-staining of SDS-gels

Proteins separated by SDS-PAGE were non-specifically stained with Coomassie blue staining solution (20% (v/v) Isopropanol, 10% Acetic acid, 0,15% Serva blue R) for 20 min. Afterwards the gel was rinsed with water and destained with 20% ethanol to visualize the protein bands.

6.2.3.4 Silver-staining of SDS-gels

A more sensitive way to stain proteins separated by SDS-PAGE is the silver-staining method. Here the proteins separated by SDS-PAGE were fixed by 50% (v/v) methanol, 12% (v/v) acetic acid and 0.5 ml/l formaldehyde (37%) for 1h. The gel then is washed 50% (v/v) ethanol for 10 min and incubated in 0.2 g/l sodium thiosulfate for 1 min. After 3 times washing with ddH₂O for 30 seconds the gel is incubated for 20 min with 2g/l AgNO₃ and 0.75 ml/l formaldehyde (37%). The gel is washed 3 times with ddH₂O for 30 seconds and developed with 60g/l Na₂CO₃ and 0.5 ml/l formaldehyde (37%) until protein bands are clearly visible. The reaction is stopped by adding 50% (v/v) methanol and 12% (v/v) acetic acid.

6.2.3.5 Expression and Purification of recombinant full-length DHX30

To analyze the biochemical behavior of full-length DHX30 wild-type and mutant forms, the proteins were expressed and purified from *E. coli*. For this 6xHis-SUMO-DHX30 wild-type and mutant constructs were transformed into *E. coli* BL21 (DE3) pLysS pRARE competent cells. After 24h, colonies were inoculated into 100 mL of super broth (SB) medium supplemented with 2% glucose, 0.1% kanamycin and 0.1% chloramphenicol and incubated overnight at 37°C under shaking at 200 rpm. 20 ml of this bacterial pre-culture was transferred into 2L of SB medium with required antibiotics and incubated at 37°C under shaking at 180 rpm until an OD₆₀₀=1 was reached. Protein expression was then induced by adding 1 mM of IPTG, temperature was lowered to 14°C and cells were cultured overnight under shaking at 180 rpm. The bacterial cells expressing 6xHis-SUMO-fusion proteins were collected by centrifugation (8000 xg, 20 min) and pellets were stored at -20 °C. For the protein purification cell pellets were resuspended in 50 mL of lysis buffer (20 mM HEPES pH 7.5, 500 mM NaCl, 5 mM MgCl₂, 0.01% NP-40, 10% glycerol, 5 mM β-mercaptoethanol, 0.1 mM AEBSF, 0.5 mg/L leupeptin/pepstatin A, 2 mg/L aprotinin). Solubilized samples were additionally sonified with the Brandson 250 sonifier. Insoluble cell debris was removed by ultracentrifugation with 45Ti Beckman rotor at 25,000 rpm for 1h at 4°C. Cell lysates were incubated for 2h at 4°C on Ni-NTA beads (Qiagen, #30210)

which were equilibrated with lysis buffer. Beads were washed three times with an equivalent of 10 times bed volume of beads with wash buffer (20 mM HEPES pH 7.5, 500 mM NaCl, 5 mM MgCl₂, 0.01% NP-40, 10% glycerol, 40 mM Imidazole, 5 mM β-mercaptoethanol, 0.1 mM AEBSF, 0.5 mg/L leupeptin/pepstatin A, 2 mg/L aprotinin). Bound proteins were eluted with an equivalent of 8 times bed volume of beads with elution buffer (20 mM HEPES pH 7.5, 500 mM NaCl, 5 mM MgCl₂, 10% glycerol, 300 mM imidazole, 5 mM β-mercaptoethanol). The elution fractions were analyzed by SDS-PAGE and followed by a Coomassie blue staining. Afterwards the fractions containing the target protein were pooled and the sample was concentrated using concentrators (Vivaspin™ 500, MWCO 10,000). For further purification via size exclusion chromatography, up to 5 mg of the concentrated protein sample was applied onto the Superdex 75/100 column and separated by size in an Äkta™ purifier system (GE Healthcare) at a flow rate of 0.3 mL/min. The elution fractions were analyzed for the presence of the target protein by SDS-PAGE and Coomassie staining. Target protein was quantified from the Coomassie stained gel using the ImageJ software.

6.2.3.6 Polysomal gradient centrifugation

Before lysis, the cells were treated with 25 µg/ml cycloheximide for 10 min and washed with cold PBS. Cells were lysed in 100 mM KCl, 20 mM HEPES pH 7.5, 5 mM MgCl₂, 1 mM DTT, 1:1000 protease inhibitors, 4 U/ml RNase inhibitor murine (New England Biolabs). After incubation for 10 min on ice, the lysate was cleared from the cell debris by centrifugation at 11,000 rpm for 15 min at 4°C on a tabletop centrifuge (Eppendorf). The cleared lysate was loaded on a 5-45% (w/v) sucrose gradient made in the respective buffer and was centrifuged for 2h at 34,500 rpm in a SW40Ti rotor. The gradient was fractionated using a gradient fractionator, which measures the UV-profile (Biocomp, Piston Gradient Fractionator and BioRad, UV-lamp and Fraction Collector). The fractions of the gradient were then analyzed either via SDS-PAGE followed by a Western blot or were used for RNA isolation.

6.2.4 Immunobiological Methods

6.2.4.1 Western blot (WB)

To probe for the required protein of interest, the bands separated by SDS-PAGE were transferred to a PVDF membrane for immunoblotting by using a semi dry western blotting apparatus. For this, three layers of Whatman paper were soaked with a 1x Towbin blot buffer (1x Laemmli in 10 % methanol) and placed in the blotting chamber. The PVDF membrane was activated for one minute in methanol and then laid on top of the Whatmann sheets. The SDS gel was soaked in the transfer buffer and placed on the top of the membrane. Finally, three additional layers of Whatman paper was placed on top of the gel and air bubbles were removed. The blotting takes place at 1 mA/cm² for 2h. To check for the success of the transfer, the membrane was stained with amido black solution for 1 min and destained with a destaining solution (90% methanol) till the background was washed away. The membrane was then washed with 1xPBS-Tween and blocked for 1h with 5% milk-powder in 1xPBS-Tween solution. After blocking, the membrane was washed 3 times in 1x PBS-tween for 10 minutes and then incubated with the primary antibody overnight at 4°C. Next day the membrane was washed again 3 times with 1x PBS-Tween and incubated 90 minutes with the secondary antibody. After three additional washes, the membrane was developed using enhanced chemical luminescence (ECL). For this 10 ml of 0.222 g/l luminol in Tris-HCL pH 8.5 were mixed with 100 µl of 6.8 mM coumaric acid in DMSO and 8 µl H₂O₂ (30%). After 1 minute of incubation the signal was detected by Gel Doc Gel Documentation System (Biorad).

6.2.4.2 Antibody based immune precipitation (IP)

DHX30 protein complexes were purified from stable Flp-In T-Rex 293 cells (6.1.3.2). Cells were grown to a confluency of 70% and the protein overexpression was induced with 1:2,000 tetracycline overnight. Next day, cells were washed with cold PBS and scraped in IP buffer (50 mM HEPES pH 7.5, 150 mM NaCl, 3 mM MgCl₂, 0.5 % NP-40, 0.5 mM DTT, 1:1000 protease inhibitors and 4 U/ml RNase inhibitor murine). The lysate was cleared by centrifugation for 20 min, 11 000 xg at 4 °C on a tabletop centrifuge. The protein concentration was determined via Bradford assay and equal amounts of each lysate was incubated for 2h with anti-FLAG M2 agarose beads (Sigma-Aldrich) on a head-over-tail rotor at 4 °C. The beads were collected by centrifugation (1000 xg, 5 min. at 4°C) and washed five times with the IP buffer. The elution was carried out with 200 µg/ml 3x FLAG peptide and 4°C overnight on the head-over-tail rotor. The eluate was either analyzed via mass spectrometry or on a SDS-PAGE was done followed by either silver-staining or a Western blot. For the investigation of immunoprecipitated DHX30 protein complexes on sucrose gradients the eluate was loaded on a 5-45% (w/v) sucrose gradient in 50 mM HEPES pH 7.5, 150 mM NaCl, 3 mM MgCl₂ and 0.5 mM DTT. The gradients were centrifuged in a SW60Ti rotor (Beckman Coulter) at 34,500 rpm at 4°C for 2h.

6.2.4.3 Indirect immunofluorescence

U2OS cells were seeded to a confluency of 70 % on coverslips. After 24h the coverslips were washed with cold PBS for 5 min. The cells were then fixed using 3.7% formaldehyde in 1x PBS for 10 min at RT. After washing the cells with cold 1x PBS for 5 min, permeabilization with 0.2% Triton X-100 and 1% BSA in 1x PBS for 30 min at 4 °C was done. The cells were incubated with primary antibody overnight at 4 °C. Next day the cells were washed two times with cold 1x PBS for 5 min, and then incubated with the secondary antibody for 2h at RT. After washing the cells with cold 1x PBS for 5 min the coverslips were mounted for microscopy with a mounting medium containing DAPI (Vectashield®) and sealed with nail polish.

6.2.4.4 Fluorescence microscopy and image processing

Immunofluorescence microscopy of U2OS cells was performed on the Leica TCS SP2 confocal microscope. The following laser sources for excitation were used: Ar laser (488 nm); and Diode UV laser (405 nm). Images were processed using ImageJ (<https://imagej.nih.gov/ij/>), Fiji software (<http://fiji.sc>).

6.2.5 RNA Methods

6.2.5.1 Total RNA isolation and RNA isolation from sucrose gradient fractions

Crude lysates, purified protein complexes or sucrose gradient fractions were mixed with an equivalent amount of TRIzol and incubated at room temperature for 5 min. To promote the phase separation, 0.4 mL of chloroform per mL of TRIzol was added to each sample and vortexed for 15 sec. Samples were incubated 2-3 min at room temperature and centrifuged for 15 min at 12,000 xg at 4°C. The aqueous phase was transferred into a new reaction tube and mixed with isopropanol in a ratio of 1:1 and with 1 µl of GlycoBlue (final amount ~25 ug, working stock 15 µg/µl). The sample was incubated at -80°C for 1h and centrifuged at 15,000 xg for 1h. The RNA pellet was washed with 70% EtOH, air dried and resuspended in ddH₂O. The samples were stored at -20°C for short term storage or at -80°C for long term storage.

6.2.5.2 RNA sequencing (RNA-Seq)

For transcriptome analysis RNA sequencing (RNA-seq) was performed. For this purpose, isolated RNAs (6.2.5.1) were sent in triplicates (≥ 500 ng each) to the company Novogene Inc (Oxford, UK). The company performed quality and concentration controls, with a subsequent synthesis of cDNA and a directional mRNA library preparation (poly A enrichment). The library was sequenced by *next-generation-sequencing* (NGS) by the NovaSeq PE150 System. The reads were filtered and mapped against the *Homo Sapiens* genome (GRCh38/hg38). Subsequently a quantitative gene analysis was performed.

6.2.5.3 5' end labeling of DNA and RNA oligonucleotides

For the 5' end labeling of DNA and RNA, 20 μ M of the oligonucleotide was incubated in a 20 μ l reaction with 2 μ l T4 polynucleotide kinase (PNK, Thermo Fisher Scientific) and 3 μ l γ -[32 P]-ATP (10 mCi/ml, 6,000 Ci/mmol) in the reaction buffer A for 1h at 37 °C. The sample was mixed with an equal volume of 2x denaturing RNA sample buffer and the labeled product was purified by denaturing gel electrophoresis (6.2.5.4), followed by elution of band of interest and precipitation.

6.2.5.4 Denaturing RNA polyacrylamide gels

Denaturing (~ 8 M Urea) polyacrylamide (PAA) gels were used for separating RNA by size. For this a 12% acrylamide gel was prepared by dissolving 24 g urea in 10 ml 5x TBE buffer, 15 ml Rotiphorese Gel 40 (19:1 Acrylamide/bisacrylamide) and 7.7 ml water and adding 300 μ l APS and 30 μ l TEMED. The electrophoresis was then performed in 1x TBE at 15 to 30 mA for 60-90 min. Before loading the samples, they were mixed with a 2x denaturing RNA sample buffer and boiled for 3 min. Later, the gel was wrapped in saran wrap and was exposed to a film (Amersham) for autoradiography. Non-radioactive RNA was visualized by UV (260 nm) shadowing against a F-254 DC kieselgel plate.

6.2.5.5 Non-denaturing polyacrylamide gels

For separating RNAs or DNAs under non-denaturing conditions native polyacrylamide (PAA) gels were used. For preparing a 6% native PAA gel 3.75 ml of 5x TBE buffer, 2 ml 80% Glycerol, 7.5 ml Rotiphorese Gel A (30% Acrylamide), 1.5 ml Rotiphorese Gel B (2% Bisacrylamide) and 22.85 ml ddH₂O were mixed and 375 µl APS and 37.5 µl TEMED was added. The electrophoresis was performed in 0.5x TBE at 15 to 30 mA for 60-90 min. Samples were mixed with a non-denaturing sample buffer and loaded on the gel. After the electrophoresis, the gel was wrapped in saran wrap and exposed to a film (Amersham) for autoradiography.

6.2.5.6 cDNA synthesis and quantitative PCR (qPCR)

Target mRNAs of DHX30 were quantified by quantitative PCR (qPCR) using cDNA as a template. For cDNA synthesis 1 µg of RNA was used. The synthesis was performed with the RNA Superscript II first strand synthesis kit (Invitrogen) as per manufacturer's instruction. Synthesized cDNA was stored at -20°C. For qPCR, the cDNA was diluted 1:10 in water. For each reaction the following preparation was used:

cDNA dilution	3 µl
SYBR Green mastermix	6 µl
qPCR primer pair (1µM each)	3 µl
Total	12 µl

The preparation was pipetted in a MicroAmp™ EnduraPlate™ 96 well plate (Thermo Fisher Scientific) and sealed with a transparent cover. The qPCR was performed with the QuantStudio™ 5 Real-Time PCR system (Thermo Fisher Scientific). Each determined C_t value was normalized to a housekeeping gene (β-actin). The following formula was used to calculate the expression changes of each target gene:

$$\text{relative fold gene expression level} = 2^{-\Delta\Delta C_t}$$

6.2.5.7 *In vitro* synthesis of RNA molecules

To test the RNA unwinding activity of DHX30, a ^{32}P -labeled RNA duplex was synthesized using the T7 RNA polymerase from a linearized DNA template which was designed by Tseng-Rogenski and Chang (Tseng-Rogenski & Chang, 2004). The *in vitro* transcription reaction comprised of 1x transcription buffer (40 mM Tris-HCl pH 7.9, 1 mM Spermidine, 26 mM MgCl_2 , 0,01% Triton X, 5mM DTT), NTPs (GTP 8 mM, ATP 5 mM, CTP 5 mM, UTP 2 mM, 50 μCi of ^{32}P -UTP), 3 μM DNA template, 3 μM top strand primer (5'-TAATACGACTCACTATAG-3'), 7U of T7 RNA polymerase. Transcription reactions were incubated for 3h at 37°C.

The RNA transcript was precipitated by adding 0.1 volumes of 3M NaoAc pH 5.5 and 3 volumes of ethanol p.a. for 30 min at -20°C and centrifugation (13,000 xg, 30 min at 4°C). RNA pellets were rinsed with 70 % ethanol p.a., dried and resuspended in DEPC H_2O . RNA samples were mixed with 2x denaturing RNA loading dye boiled and analyzed on 8% UREA-PAGE in 1X TBE. Radioactive signals were detected by autoradiography and the RNA band was excised from the gel. The RNA product was extracted from the gel in the RNA extraction buffer (200 mM Tris-HCL pH 7.0, 0.1% SDS, 1 mM EDTA). Subsequently, RNA was precipitated as described above and the RNA pellets were resuspended in 100 mM KCl. To promote the formation of the RNA duplex, the RNA sample was boiled at 95°C for 5 min and let it cool down for 2h. The sample was mixed with 2X non-denaturing loading dye (1X TBE, 20% glycerol, 0.1% Bromophenol Blue, 0.1% Xylene Cyanol FF), separated on 8% native PAGE and the RNA duplex was excised from the gel and purified as described before. RNA concentration was determined at 260 nm using a spectrophotometer (Eppendorf).

6.2.5.8 Preparation of R-loop and D-loop substrates

50 pM of DNA or RNA oligonucleotides were radio labeled at the 5' end with γ -[³²P] ATP using T4 polynucleotide kinase according to manufacturer's instructions in a 20 μ l reaction (Thermo Fisher Scientific). Depending on the desired overhang either the R3, R4 or R5 oligo was used (4.1.7). After incubating for 1h at 37°C the preparation was loaded onto a G25 column and centrifuged for 5 minutes at 1,000 xg. To the radiolabeled RNA or DNA oligo a complementary DNA B11 oligo in a ratio of 1:2 was added in the presence of 1X SSC buffer (3.0 M sodium chloride and 0.3 M sodium citrate) and 10 mM MgCl₂. This preparation was boiled at 95°C for 5 minutes in a heating block, which was then turned off to reach room temperature. Annealed RNA:DNA or DNA:DNA duplexes were loaded on a 8% polyacrylamide native gel in 0.5X TBE buffer and the gel was run till the Bromophenol dye was half to the gel.

The duplex was carefully cut out of the gel and extracted by RNA extraction buffer (200 mM Tris-HCL pH 7.0, 0.1% SDS, 1 mM EDTA) overnight on an end-to-end rocker. The duplex was precipitated with 1 volume of isopropanol and 1 μ l of glycogen at -20 °C for 1h. The sample was centrifuged for 45 minutes at 12,000 xg, the pellet was washed with 70 % ethanol and air dried. The pellet was resuspended in 1x SSC buffer and 10 mM MgCl₂ and 50 picomole of the partial DNA complementary strand (oligo T1) to the annealed substrates was added. This sample was gradually heated to a temperature of 65°C and kept constant for 15 min. The heat block was switched off to cool down gradually. The annealed structures were loaded on a 8% native polyacrylamide gel in 0.5X TBE, the desired bands cut out and extracted from the gel as described above. The annealed products were stored in 1x SSC buffer and 10 mM MgCl₂.

6.2.5.9 RNA unwinding assay

Unwinding reactions were prepared in a 20 μ l reaction mixture containing up to 40 nm of purified protein, 25 fmol of radioactively labeled nucleic acid substrate, 17 mM HEPES-KOH pH 7.5, 150 mM NaCl, 1 mM MgCl₂, 2 mM DTT, 1 mM spermidine, 0.3% PEG8000, 5% glycerol, 150 mM KCl, 20 units of RNasin™ Plus (Promega), 1 mM ATP. The mixture was then incubated for 30 min at 37°C and subsequently mixed with 2X non-denaturing loading dye and subjected to gel electrophoresis non-denaturing 8% PAGE (19:1) in 0.5X TBE at 4°C. Unwinded products were visualized by autoradiography.

6.2.5.10 ATPase assay

For the ATPase assay of DHX30 protein variants a 20 μ l reaction mixture containing 20 nm of purified protein, 25 fmol unlabeled RNA duplex, 17 mM HEPES-KOH pH 7.5, 150 mM NaCl, 1 mM MgCl₂, 2 mM DTT, 1 mM spermidine, 0.3% PEG8000, 5% glycerol, 150 mM KCl, 5 μ Ci α -[³²P]-ATP (Hartmann analytics) was prepared. In the samples without RNA substrate, the RNA duplex was left out. The preparations were incubated for 30 min at 37°C and 2 μ l of the sample was applied to a PEI Cellulose F thin layer chromatography plate (20x20 cm, Merck) to separate ATP, ADP, AMP and inorganic phosphate. The plate was dried, run in a glass container containing 0.75 M KH₂PO₄ for 50 min and dried again. The hydrolyzed products were visualized by autoradiography.

6.2.5.11 Purification of 80S ribosomes from HeLa S3 pellets

HeLa S3 cells were cultivated in a bioreactor and harvested until a cell density of at $6-9 \times 10^5$ cells/ml was reached. The cells were collected via centrifugation at 800 xg for 20 min. at 4°C. The pellets were washed with ice cold 1x PBS, snap frozen and stored at -80°C. The purification was carried out on ice at 4°C. First the pellet was thawed on ice and incubated with 3x volume of hypotonic buffer (20 mM HEPES pH 7.5, 10 mM KOAc, 5 mM MgOAc, 2 mM DTT and 1:1000 protease inhibitors) for 20 min. The resuspended cells were lysed with the help of a 40 ml B-tight douncer. After clearing the lysate via centrifugation (22,000 xg for 30 min) it was loaded on a sucrose cushion (1 M sucrose, 100 mM KOAc, 20 mM HEPES pH 7.5, 5 mM MgOAc, 2 mM DTT). After centrifugation in a 45Ti rotor at 40,000 rpm for 4 h, the crude ribosomal pellet was washed with 7 ml resuspension buffer 1 (500 mM KOAc, 20 mM HEPES pH 7.5, 5 mM MgOAc, 2 mM DTT and 1:1000 protease inhibitors) followed by resuspension in 2 ml of resuspension buffer 1 overnight. The ribosomes were loaded on a second cushion (composition as described before but 500 mM KOAc was used instead) followed by centrifugation.

After resuspension, the ribosomes were loaded on a 10-30% (w/v) sucrose gradient in resuspension buffer 1 and was centrifuged for 12h at 22,000 rpm in an SW32Ti rotor (Beckman Coulter). After harvesting the gradient, the absorption peak at 260 nm of each fraction was measured and the fractions containing the 80S peak were pooled and pelleted in a 70Ti rotor (Beckman Coulter) at 35,500 rpm for 4 h. The ribosomal pellet was then resuspended in resuspension buffer 2 (100 mM KOAc, 50 mM HEPES pH 7.5, 15 mM MgOAc, 2 mM DTT), snap frozen and stored at -80°C.

6.2.5.12 Purification of the 40S and 60S ribosomal subunits from HeLa S3 cells

For the purification of ribosomal subunits HeLa S3 pellets were resuspended in hypotonic lysis buffer (10 mM KCl, 20 mM HEPES pH 7.5, 5 mM MgCl₂, 2 mM DTT and 1:1000 protease inhibitors) and lysed as described above. The lysate was cleared at 22,000 xg for 30 min and loaded on a sucrose cushion (1 M sucrose, 20 mM HEPES pH 7.5, 100 mM KCl 5 mM MgCl₂, 2 mM DTT) and centrifuged in a 45Ti rotor at 40,000 rpm for 4 h. After resuspension in resuspension buffer 1 (20 mM HEPES pH 7.5, 50 mM KCl, 4 mM MgCl₂ and 2 mM DTT) the RNA concentration (A260) was measured and the crude 80S was diluted to a A260 value of 0.150 in a total volume of 13 ml. To split up the 80S ribosome to its 60S and 40S subunits, 131.3 µl of puromycin-HCl (0.1 M) was added and incubated for 10 min on ice followed by an additional incubation of 10 min at 30 °C. Next, 1.69 ml of 4 M KCl in resuspension buffer 1 was added dropwise under constant shaking. The ribosomes were loaded on a 10-30% (w/v) sucrose gradient in 20 mM HEPES, 500 mM KCl, 4 mM MgCl₂ and 2 mM DTT followed and centrifugation with a SW32Ti rotor at 22,000 rpm for 17 h at 4°C.

After harvesting and determination of the RNA profile the peak fractions of the 40S ribosomal subunit were pooled and diluted with the 3-fold volume of 100 mM KCl, 20 mM Tris-HCl pH 7.5, 2 mM MgCl₂ and 2 mM DTT. The 60S subunits were pooled and diluted with the 2-fold volume of the same buffer. The 60S and 40S ribosomal subunits were pelleted in a 45Ti rotor for 15 h at 38,600 rpm at 4°C, resuspended in resuspension buffer 2 (20 mM HEPES pH 7.5, 100 mM KCl, 2 mM MgCl₂, 0.25 M sucrose, 2 mM DTT). While the 40S subunits were snap frozen and stored at -80°C the 60S subunits were diluted to 50 mM KCl and loaded on a second 10-30% (w/v) sucrose gradient in, 20 mM HEPES pH 7.5, 50 mM KCl, 2 mM MgCl₂ and 2 mM DTT. The gradient is centrifuged in a SW32Ti rotor at 22,000 xg for 17 h at 4°C. After fractionation, the RNA concentration of each fraction was determined, and the peak fractions were pooled and diluted as described above. The diluted 60S subunits were pelleted by centrifugation in a 70Ti rotor at 35,500 rpm for 15.5 h at 4°C and resuspended in resuspension buffer 2. After snap freezing, the 60S subunits were stored at -80 °C.

6.2.5.13 Test for direct interaction of DHX30 with ribosomal particles

To investigate direct interaction of recombinant DHX30 with ribosomal particles, purified ribosomes (80S, 60S or 40S) were incubated with the equimolar amount (typically 700 pmol were used) of the recombinant protein for 20 min at 30°C, followed by 5 min incubation on ice. The formed complex was loaded on a 5-30% (w/v) sucrose gradient in 20 mM HEPES pH 7,5, 150 mM KCl, 10 mM MgCl₂ and 2 mM DTT. The gradients were centrifuged in a SW60Ti rotor (Beckman Coulter) at 34,500 rpm at 4°C for 2h. After centrifugation, the gradients were fractionated, and the fractions were analyzed via SDS-PAGE followed by WB.

6.2.6 Bioinformatics Methods

6.2.6.1 Enriched gene ontology term analysis

Analysis of enriched GO-terms was performed using the online interface of the ShinyGO gene ontology consortium based on a large annotation database derived from Ensembl and STRING-db version 0.741 (Ge et al., 2020).

7. Abbreviations

A	Adenosine	mA	Milliampere
APS	ammonium persulfate	min	minute
ATP	Adenosine 5'-triphosphate	ml	Milliliter
C	Cytosine	mRNA	messenger RNA
cDNA	Copy DNA	MS	Mass spectrometry
C-terminus	Carboxyl-terminus	ng	Nano gram
dATP	2',3'deoxyadenosine 5' triphosphate	nmol	Nano mole
ddH ₂ O	double distilled water	N-terminus	Amino-terminus
Da	Dalton	NTP	Nucleoside-5'-triphosphate
DMSO	Dimethyl sulfoxide	pH	A measure of the acidity or alkalinity of a solution
DNA	Deoxyribonucleic acid	RNA	Ribonucleic acid
DNase	Deoxyribonuclease	RNase	Ribonuclease
DTT	dithiothreitol	RNP	Ribonucleoprotein
dNTP	2',3'deoxy nucleoside 5' triphosphate	Rpm	Rotation per minute
<i>E. coli</i>	<i>Escherichia coli</i>	RT	Room temperature
<i>et al.</i>	And others (Lat.: <i>Et alterae</i>)	S	Svedberg
HEPES	4-(2-hydroxyethyl)-1- piperazineethanesulfonic acid	SDS	sodium dodecyl sulfate
<i>In vitro</i>	within the reagent glass	Sec	Second
<i>In vivo</i>	in living organism	TEMED	n,n',n',n'-tetramethylethane- 1,2-diamine
L	Liter	UTR	Untranslated region
kDa	Kilo Dalton	v/v	volume per volume
M	Molar (mol/L)	w/v	weight per volume

The single letter amino acid code

G	Glycine	P	Proline
A	Alanine	V	Valine
L	Leucine	I	Isoleucine
M	Methionine	C	Cysteine
F	Phenylalanine	Y	Tyrosine
W	Tryptophan	H	Histidine
K	Lysine	R	Arginine
Q	Glutamine	N	Asparagine
E	Glutamic Acid	D	Aspartic Acid
S	Serine	T	Threonine

8. Appendix



Figure S1: Details of the SWISS-MODEL of the DHX30 helicase core.

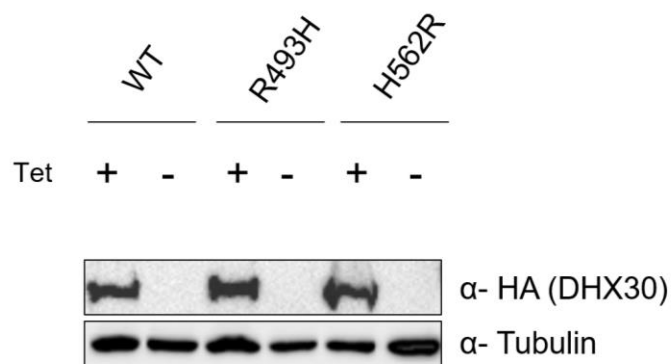


Figure S2: Induction test of the generated DHX30-FLAG/HA Flp-In T-REx 293 cells with tetracycline. Western blot against the C-terminal FLAG/HA-tagged DHX30-WT and mutants.

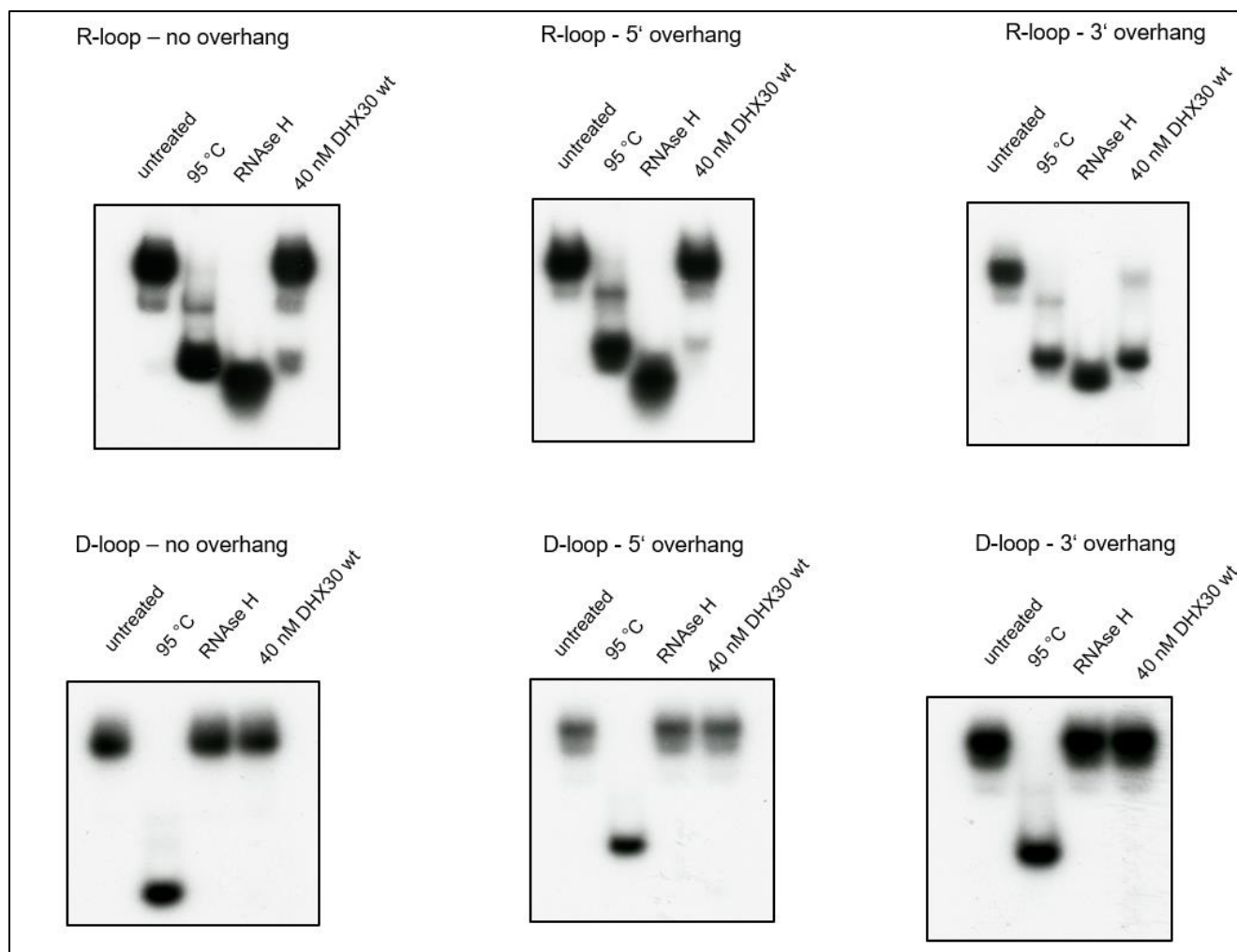


Figure S3: R-loop and D-loops structures incubated with RNase H. To show that the substrates are properly formed R-loop and D-loop structures were incubated with 1U of RNase H and incubated for 1h at 37°C. Samples were loaded on a 6% native gel. RNase H hydrolyzes RNA:DNA hybrids specifically (upper panel). DNA only substrates (lower panel) are not hydrolyzed.

Table S1: Identified peptides in the DHX30-FLAG/HA WT IP against the control IP by mass spectrometry

Protein names	Gene names	Molecular weight in kDa
182 kDa tankyrase-1-binding protein	TNKS1BP1	181.79
26S proteasome non-ATPase regulatory subunit 6	PSMD6	45.531
28S ribosomal protein S18b, mitochondrial	MRPS18B	29.395
28S ribosomal protein S22, mitochondrial	MRPS22	41.28
28S ribosomal protein S27, mitochondrial	MRPS27	41.329
28S ribosomal protein S29, mitochondrial	DAP3	41.044
28S ribosomal protein S31, mitochondrial	MRPS31	45.318
28S ribosomal protein S5, mitochondrial	MRPS5	48.006
28S ribosomal protein S9, mitochondrial	MRPS9	45.834
39S ribosomal protein L37, mitochondrial	MRPL37	48.117
39S ribosomal protein L38, mitochondrial	MRPL38	44.596
39S ribosomal protein L39, mitochondrial	MRPL39	38.711
40S ribosomal protein S10	RPS10;RPS10-NUDT3	18.898
40S ribosomal protein S11	RPS11	18.431
40S ribosomal protein S12	RPS12	14.515
40S ribosomal protein S13	RPS13	17.222
40S ribosomal protein S14	RPS14	16.159
40S ribosomal protein S15	RPS15	17.04
40S ribosomal protein S15a	RPS15A	14.839
40S ribosomal protein S16	RPS16	16.445
40S ribosomal protein S17	RPS17	64.532
40S ribosomal protein S18	RPS18	17.718
40S ribosomal protein S2	RPS2	31.324
40S ribosomal protein S21	RPS21	8.85
40S ribosomal protein S23	RPS23	15.807
40S ribosomal protein S24	RPS24	15.423
40S ribosomal protein S25	RPS25	13.742
40S ribosomal protein S26; Putative 40S ribosomal protein S26-like 1	RPS26;RPS26P11	13.015
40S ribosomal protein S27	RPS27	9.461
40S ribosomal protein S27; 40S ribosomal protein S27-like	RPS27L	11.345
40S ribosomal protein S28	RPS28	7.8409
40S ribosomal protein S29	RPS29	10.256
40S ribosomal protein S3	RPS3	26.688

40S ribosomal protein S30	FAU	6.6478
40S ribosomal protein S3a	RPS3A	29.945
40S ribosomal protein S4, X isoform	RPS4X	29.597
40S ribosomal protein S5; 40S ribosomal protein S5, N-terminally processed	RPS5	22.391
40S ribosomal protein S6	RPS6	28.68
40S ribosomal protein S7	RPS7	22.127
40S ribosomal protein S8	RPS8	24.205
40S ribosomal protein S9	RPS9	22.591
40S ribosomal protein SA	RPSA	29.404
5-3 exoribonuclease 1	XRN1	192.84
5-3 exoribonuclease 2	XRN2	108.58
60S acidic ribosomal protein P0; 60S acidic ribosomal protein P0-like	RPLP0;RPLP0P6	34.273
60S acidic ribosomal protein P1	RPLP1	11.514
60S acidic ribosomal protein P2	RPLP2	11.665
60S ribosomal export protein NMD3	NMD3	60.125
60S ribosomal protein L10	RPL10	24.604
60S ribosomal protein L10a	RPL10A	24.831
60S ribosomal protein L11	RPL11	20.252
60S ribosomal protein L12	RPL12	17.818
60S ribosomal protein L13	RPL13	24.261
60S ribosomal protein L13a	RPL13A;RPL13a	23.577
60S ribosomal protein L14	RPL14	23.432
60S ribosomal protein L15; Ribosomal protein L15	RPL15	24.146
60S ribosomal protein L17	RPL17;RPL17-C18orf32	19.586
60S ribosomal protein L18	RPL18	21.728
60S ribosomal protein L18a	RPL18A	18.079
60S ribosomal protein L21	RPL21	18.565
60S ribosomal protein L23	RPL23	14.865
60S ribosomal protein L23a	RPL23A	17.695
60S ribosomal protein L24	RPL24	14.369
60S ribosomal protein L26	RPL26	17.258
60S ribosomal protein L27	RPL27	15.798
60S ribosomal protein L27a	RPL27A	12.201
60S ribosomal protein L28	RPL28	15.747
60S ribosomal protein L29	RPL29	18.512
60S ribosomal protein L3	RPL3	46.108

60S ribosomal protein L30	RPL30	12.784
60S ribosomal protein L31	RPL31	14.463
60S ribosomal protein L32	RPL32	15.616
60S ribosomal protein L34	RPL34	13.293
60S ribosomal protein L35	RPL35	14.551
60S ribosomal protein L35a	RPL35A	12.538
60S ribosomal protein L36	RPL36	12.254
60S ribosomal protein L36a	RPL36A;RPL36A-HNRNPH2	13.228
60S ribosomal protein L37; Ribosomal protein L37	RPL37	11.078
60S ribosomal protein L37a	RPL37A	10.275
60S ribosomal protein L4	RPL4	47.697
60S ribosomal protein L5	RPL5	34.362
60S ribosomal protein L6	RPL6	32.728
60S ribosomal protein L7	RPL7	29.225
60S ribosomal protein L7a	RPL7A	29.995
60S ribosomal protein L8	RPL8	28.024
60S ribosomal protein L9	RPL9	21.863
Activating signal cointegrator 1 complex subunit 1	ASCC1	36.876
A-kinase anchor protein 8	AKAP8	76.107
A-kinase anchor protein 8-like	AKAP8L	71.639
Aminoacyl tRNA synthase complex-interacting multifunctional protein 1;Endothelial monocyte- activating polypeptide 2	AIMP1	34.352
Ankyrin repeat and KH domain-containing protein 1	ANKHD1	269.45
Ankyrin repeat domain-containing protein 17	ANKRD17	263.25
Antigen KI-67	MKI67	358.69
Apoptotic chromatin condensation inducer in the nucleus	ACIN1	145.44
Ataxin-2	ATXN2	105.13
Ataxin-2-like protein	ATXN2L	113.37
ATP-binding cassette sub-family F member 2	ABCF2	71.289
ATP-dependent RNA helicase A	DHX9	140.96
ATP-dependent RNA helicase DDX1	DDX1	82.431
ATP-dependent RNA helicase DDX24	DDX24	91.48
ATP-dependent RNA helicase DDX50	DDX50	82.564
ATP-dependent RNA helicase DDX54	DDX54	98.665
ATP-dependent RNA helicase DDX55	DDX55	65.19
ATP-dependent RNA helicase DHX29	DHX29	155.23

ATP-dependent RNA helicase DHX36	DHX36	111.48
Bcl-2-associated transcription factor 1	BCLAF1	83.134
Bloom syndrome protein	BLM	144.47
cAMP-dependent protein kinase catalytic subunit alpha	PRKACA;KIN27	40.589
Caprin-1	CAPRIN1	78.365
Casein kinase II subunit alpha; Casein kinase II subunit alpha 3	CSNK2A1;CSNK2A3	40.717
CCR4-NOT transcription complex subunit 1	CNOT1	266.94
CCR4-NOT transcription complex subunit 10	CNOT10	82.309
CCR4-NOT transcription complex subunit 11	CNOT11	55.215
CCR4-NOT transcription complex subunit 2	CNOT2	59.191
CCR4-NOT transcription complex subunit 3	CNOT3	81.871
CDK5 regulatory subunit-associated protein 3	CDK5RAP3	56.92
CDKN2A-interacting protein	CDKN2AIP	61.124
Cell death regulator Aven	AVEN	38.506
Cell differentiation protein RCD1 homolog	RQCD1	33.631
Cell growth-regulating nucleolar protein	LYAR	43.614
Chromodomain-helicase-DNA-binding protein 1	CHD1	196.59
Chromodomain-helicase-DNA-binding protein 4	CHD4	215.49
Coiled-coil domain-containing protein 124	CCDC124	25.835
Coiled-coil domain-containing protein 137	CCDC137	33.231
Coiled-coil domain-containing protein 47	CCDC47	55.873
Coiled-coil domain-containing protein 86	CCDC86	40.235
Constitutive coactivator of PPAR-gamma-like protein 1	FAM120A	121.89
Cyclin-dependent kinase 9	CDK9	42.777
Cytoplasmic polyadenylation element-binding protein 4	CPEB4	77.296
DBIRD complex subunit ZNF326	ZNF326	65.653
DDRKG domain-containing protein 1	DDRKG1	33.939
Developmentally-regulated GTP-binding protein 1	DRG1	40.542
DIS3-like exonuclease 2	DIS3L2	99.278
DNA dC->dU-editing enzyme APOBEC-3F	APOBEC3F	45.02
DNA mismatch repair protein Msh6	MSH6	152.78
DNA topoisomerase 1	TOP1	90.725
DNA topoisomerase 2-alpha	TOP2A	174.38
DNA topoisomerase 2-beta;DNA topoisomerase 2	TOP2B	182.66
DNA topoisomerase 3-beta-1;DNA topoisomerase	TOP3B	96.661
DNA-binding protein SMUBP-2	IGHMBP2	109.15

DNA-directed RNA polymerase, mitochondrial	POLRMT	138.62
DNA-directed RNA polymerases I and III subunit RPAC1	POLR1C	39.249
DnaJ homolog subfamily A member 3, mitochondrial	DNAJA3	52.488
DnaJ homolog subfamily B member 11	DNAJB11	40.513
DnaJ homolog subfamily B member 6	DNAJB6	36.087
DnaJ homolog subfamily C member 21	DNAJC21	62.027
Dolichyl-diphosphooligosaccharide—protein glycosyltransferase 48 kDa subunit	DDOST	48.799
Double-stranded RNA-binding protein Staufen homolog 1	STAU1	63.182
Double-stranded RNA-binding protein Staufen homolog 2	STAU2	58.97
Double-stranded RNA-specific adenosine deaminase	ADAR	136.06
Dual specificity protein phosphatase 12	DUSP12	37.687
E3 ISG15--protein ligase HERC5	HERC5	116.85
E3 ubiquitin-protein ligase HERC2	HERC2	527.22
E3 ubiquitin-protein ligase listerin	LTN1	200.55
E3 ubiquitin-protein ligase makorin-1	MKRN1	47.639
E3 ubiquitin-protein ligase RBBP6	RBBP6	197.29
E3 ubiquitin-protein ligase TRIM56	TRIM56	81.487
E3 ubiquitin-protein ligase TTC3	TTC3	194.06
E3 UFM1-protein ligase 1	UFL1	89.594
ELAV-like protein 1	ELAVL1	36.091
ELAV-like protein;ELAV-like protein 2;ELAV-like protein 4	ELAVL2;ELAVL4	42.632
Elongation factor 1-delta	EEF1D	28.821
Endoribonuclease Dicer	DICER1	218.68
Enhancer of mRNA-decapping protein 4	EDC4	151.66
Enhancer of rudimentary homolog	ERH	12.259
Eukaryotic initiation factor 4A-III;Eukaryotic initiation factor 4A-III, N-terminally processed	EIF4A3	46.871
Eukaryotic translation initiation factor 3 subunit A	EIF3A	166.57
Eukaryotic translation initiation factor 3 subunit H	EIF3H	41.581
Eukaryotic translation initiation factor 3 subunit M	EIF3M	42.502
Eukaryotic translation initiation factor 4 gamma 1	EIF4G1	171.64
Eukaryotic translation initiation factor 4 gamma 3	EIF4G3	195.27
Eukaryotic translation initiation factor 5B	EIF5B	138.68
Eukaryotic translation initiation factor 6	EIF6	26.599
Exosome complex component RRP4	EXOSC2	32.789
Exosome complex component RRP40	EXOSC3	29.572

Exosome complex component RRP42	EXOSC7	31.821
Exosome complex component RRP45	EXOSC9	48.948
Exosome component 10	EXOSC10	100.83
FACT complex subunit SSRP1	SSRP1	81.074
F-actin-capping protein subunit alpha-1	CAPZA1	32.922
Far upstream element-binding protein 3	FUBP3	61.64
Focadhesin	FOCAD	200.07
Fragile X mental retardation protein 1	FMR1	68.454
Fragile X mental retardation syndrome-related protein 1	FXR1	69.72
Fragile X mental retardation syndrome-related protein 2	FXR2	74.222
GDNF-inducible zinc finger protein 1	GZF1	80.491
GDP-mannose 4,6 dehydratase	GMDS	39.053
General transcription factor 3C polypeptide 1	GTF3C1	236.28
Glioma tumor suppressor candidate region gene 2 protein	GLTSCR2	54.389
Glycylpeptide N-tetradecanoyltransferase 1	NMT1	56.806
GTPase Era, mitochondrial	ERAL1	48.349
Guanine nucleotide-binding protein subunit beta-2-like 1; Guanine nucleotide-binding protein subunit beta-2-like 1, N-terminally processed	GNB2L1	35.076
Guanine nucleotide-binding protein-like 1	GNL1	68.66
Guanine nucleotide-binding protein-like 3	GNL3	60.54
Guanine nucleotide-binding protein-like 3-like protein	GNL3L	65.572
H/ACA ribonucleoprotein complex subunit 4	DKC1	57.673
HBS1-like protein	HBS1L	70.624
HEAT repeat-containing protein 1; HEAT repeat-containing protein 1, N-terminally processed	HEATR1	233.27
Helicase SKI2W	SKIV2L	137.75
Heterochromatin protein 1-binding protein 3	HP1BP3	61.206
Heterogeneous nuclear ribonucleoprotein A/B	HNRNPAB	30.588
Heterogeneous nuclear ribonucleoprotein A3	HNRNPA3	39.594
Heterogeneous nuclear ribonucleoprotein D0	HNRNPD	32.834
Heterogeneous nuclear ribonucleoprotein D-like	HNRNPDL	40.04
Heterogeneous nuclear ribonucleoprotein H2	HNRNPH2	49.263
Heterogeneous nuclear ribonucleoprotein L	HNRNPL	64.132
Heterogeneous nuclear ribonucleoprotein M	HNRNPM	73.62
Heterogeneous nuclear ribonucleoprotein Q	SYNCRIP	69.602

Heterogeneous nuclear ribonucleoprotein R	HNRNPR	70.942
Heterogeneous nuclear ribonucleoprotein U-like protein 1	HNRNPUL1	90.291
Heterogeneous nuclear ribonucleoprotein U-like protein 2	HNRNPUL2;HNRNPUL2-BSCL2	85.104
Heterogeneous nuclear ribonucleoproteins C1/C2	HNRNPC	28.916
Histone H1.4;Histone H1.3	HIST1H1E;HIST1H1D	21.865
Histone H1x	H1FX	22.487
Histone H2B type 1-L;Histone H2B;Histone H2B type 1-M; Histone H2B type 1-N;Histone H2B type 1-H; Histone H2B type 2-F;Histone H2B type 1-C/E/F/G/I; Histone H2B type 1-D;Histone H2B type 1-K; Histone H2B type F-S	HIST1H2BL;HIST1H2BN;HIST1H2BM;HIST1H2BH;HIST2H2BF;HIST1H2BC;HIST1H2BD;HIST1H2BK;H2BFS	13.952
Histone RNA hairpin-binding protein	SLBP	32.094
Hsp70-binding protein 1	HSPBP1	39.302
Importin-4	IPO4	118.71
Inhibitor of Bruton tyrosine kinase	IBTK	150.53
Inorganic pyrophosphatase	PPA1	32.66
Insulin-like growth factor 2 mRNA-binding protein 1	IGF2BP1	63.48
Insulin-like growth factor 2 mRNA-binding protein 2	IGF2BP2	66.785
Insulin-like growth factor 2 mRNA-binding protein 3	IGF2BP3	63.704
Interferon-inducible double-stranded RNA-dependent protein kinase activator A	PRKRA	34.404
Interferon-related developmental regulator 1	IFRD1	50.268
Interferon-related developmental regulator 2	IFRD2	48.047
Interferon-stimulated 20 kDa exonuclease-like 2	ISG20L2	39.153
Interleukin enhancer-binding factor 2	ILF2	38.91
Interleukin enhancer-binding factor 3	ILF3	95.807
Intracellular hyaluronan-binding protein 4	HABP4	45.785
Keratin, type II cytoskeletal 6B	KRT6B	60.066
KH domain-containing, RNA-binding, signal transduction-associated protein 1	KHDRBS1	48.227
Krueppel-related zinc finger protein 1	HKR1	73.208
La-related protein 1	LARP1	123.51
La-related protein 1B	LARP1B	126.21
La-related protein 4	LARP4	80.595
La-related protein 4B	LARP4B	80.551
La-related protein 7	LARP7	66.898
Large subunit GTPase 1 homolog	LSG1	75.225

LINE-1 retrotransposable element ORF1 protein	L1RE1	40.055
Lupus La protein	SSB	46.836
Malate dehydrogenase, mitochondrial;Malate dehydrogenase	MDH2	35.503
Malonyl-CoA-acyl carrier protein transacylase, mitochondrial	MCAT	42.961
MAP7 domain-containing protein 1	MAP7D1	92.819
Matrin-3	MATR3	99.966
Metastasis-associated protein MTA2	MTA2	75.022
Mitochondrial ribonuclease P protein 1	TRMT10C	47.346
MKI67 FHA domain-interacting nucleolar phosphoprotein	NIFK	34.222
mRNA export factor	RAE1	40.968
mRNA turnover protein 4 homolog	MRT04	27.56
Multiple myeloma tumor-associated protein 2	MMTAG2	20.536
Muscleblind-like protein 1;Muscleblind-like protein 2	MBNL1;MBLL;MBNL2	37.898
Myb-binding protein 1A	MYBBP1A	148.85
Myelin expression factor 2	MYEF2	64.149
Nascent polypeptide-associated complex subunit alpha; Nascent polypeptide-associated complex subunit alpha, muscle-specific form	NACA	15.016
Neuralized-like protein 4	NEURL4	153.06
NF-kappa-B-repressing factor	NKRF	77.672
Nicalin	NCLN	62.846
Nipped-B-like protein	NIPBL	298.88
Nodal modulator 2;Nodal modulator 3	NOMO3;NOMO2	139.38
Non-canonical poly(A) RNA polymerase PAPD5	PAPD5	69.597
Non-specific serine/threonine protein kinase;Serine/threonine-protein kinase MRCK alpha	CDC42BPA	193.63
Nuclear cap-binding protein subunit 1	NCBP1	91.838
Nuclear export mediator factor NEMF	NEMF	118.02
Nuclear fragile X mental retardation-interacting protein 1	NUFIP1	56.299
Nuclear fragile X mental retardation-interacting protein 2	NUFIP2	76.12
Nuclear mitotic apparatus protein 1	NUMA1	236.51
Nuclear valosin-containing protein-like	NVL	95.05
Nuclease-sensitive element-binding protein 1	YBX1	35.924
Nucleolar GTP-binding protein 1	GTPBP4	73.964
Nucleolar GTP-binding protein 2	GNL2	83.654
Nucleolar protein 56	NOP56	66.049
Nucleolar protein 58	NOP58	59.578

Nucleolar RNA helicase 2	DDX21	87.343
Nucleolin	NCL	76.613
Nucleophosmin	NPM1	32.575
p21-activated protein kinase-interacting protein 1	PAK1IP1	43.963
PCI domain-containing protein 2	PCID2	43.374
Periodic tryptophan protein 1 homolog	PWP1	55.827
Periodic tryptophan protein 2 homolog	PWP2	102.45
PERQ amino acid-rich with GYF domain-containing protein 2	GIGYF2	148.63
Pescadillo homolog	PES1	66.077
Phosphorylated adapter RNA export protein	PHAX	44.402
Plakophilin-2	PKP2	92.755
Plasminogen activator inhibitor 1 RNA-binding protein	SERBP1	44.965
Pleiotropic regulator 1	PLRG1	56.289
Polyadenylate-binding protein 1;Polyadenylate-binding protein; Polyadenylate-binding protein 3	PABPC1;PABPC3	70.67
Polyadenylate-binding protein 2	PABPN1	31.496
Polyadenylate-binding protein 4;Polyadenylate-binding protein	PABPC4	72.39
Polyadenylate-binding protein-interacting protein 1	PAIP1	53.524
Polynucleotide 5-hydroxyl-kinase NOL9	NOL9	79.322
pre-rRNA processing protein FTSJ3	FTSJ3	96.557
Pre-rRNA-processing protein TSR1 homolog	TSR1	91.809
Probable 28S rRNA (cytosine(4447)-C(5))-methyltransferase	NOP2	89.301
Probable ATP-dependent RNA helicase DDX27	DDX27	86.604
Probable ATP-dependent RNA helicase DDX28	DDX28	59.58
Probable ATP-dependent RNA helicase DDX31	DDX31	83.515
Probable ATP-dependent RNA helicase DDX5	DDX5	69.147
Probable ATP-dependent RNA helicase DDX56	DDX56	61.589
Probable ATP-dependent RNA helicase DDX6	DDX6	54.416
Probable ATP-dependent RNA helicase YTHDC2	YTHDC2	160.25
Probable dimethyladenosine transferase	DIMT1	35.236
Probable helicase senataxin	SETX	302.88
Probable helicase with zinc finger domain	HELZ	218.97
Probable rRNA-processing protein EBP2	EBNA1BP2	40.684
Procollagen-lysine,2-oxoglutarate 5-dioxygenase 1	PLOD1	83.549
Proliferation-associated protein 2G4	PA2G4	43.786
Proline-, glutamic acid- and leucine-rich protein 1	PELP1	119.7
Protein arginine N-methyltransferase 3	PRMT3	52.901

Protein argonaute-1;Protein argonaute	AGO1	101.07
Protein argonaute-2	AGO2	97.207
Protein CASC3	CASC3	76.277
Protein FAM193A	FAM193A	166.37
Protein FAM98A	FAM98A	55.272
Protein lin-28 homolog B	LIN28B	27.957
Protein LTV1 homolog	LTV1	54.854
Protein pelota homolog	PELO	43.359
Protein PRRC2A	PRRC2A	228.86
Protein PRRC2B	PRRC2B	242.96
Protein PRRC2C	PRRC2C	308.77
Protein RRP5 homolog	PDCD11	208.83
Protein SDA1 homolog	SDAD1	75.44
Protein Smaug homolog 2	SAMD4B	75.292
Protein SON	SON	259.59
Protein transport protein Sec61 subunit alpha isoform 1	SEC61A1	52.949
Protein transport protein Sec61 subunit beta	SEC61B	9.9743
Pumilio domain-containing protein KIAA0020	KIAA0020	73.584
Pumilio homolog 1	PUM1	126.47
Putative ATP-dependent RNA helicase DHX30	DHX30	133.94
Putative ATP-dependent RNA helicase DHX57	DHX57	155.6
Putative helicase MOV-10	MOV10	113.67
Putative methyltransferase C9orf114	C9orf114	42.008
Putative RNA-binding protein Luc7-like 2	LUC7L2	46.513
Ras GTPase-activating protein-binding protein 1	G3BP1	52.164
Ras GTPase-activating protein-binding protein 2	G3BP2	54.12
Regulator of nonsense transcripts 1	UPF1	124.34
Regulator of nonsense transcripts 3B	UPF3B	56.213
Replication factor C subunit 1	RFC1	128.18
Replication factor C subunit 2	RFC2	39.157
Replication factor C subunit 3	RFC3	40.556
Replication factor C subunit 4	RFC4	39.681
Replication factor C subunit 5	RFC5	38.496
Retrotransposon-derived protein PEG10	PEG10	88.209
Ribonuclease 3	DROSHA	151.29
Ribonuclease P protein subunit p40	RPP40	39.327
Ribonucleases P/MRP protein subunit POP1	POP1	114.71

Ribonucleoprotein PTB-binding 1	RAVER1	77.843
Ribose-phosphate pyrophosphokinase 2	PRPS2	34.769
Ribosomal biogenesis protein LAS1L	LAS1L	81.242
Ribosomal L1 domain-containing protein 1	RSL1D1	54.972
Ribosomal protein L19;60S ribosomal protein L19	RPL19	23.134
Ribosomal RNA processing protein 1 homolog B	RRP1B	84.427
Ribosome biogenesis protein BMS1 homolog	BMS1	145.81
Ribosome biogenesis protein BOP1	BOP1	83.629
Ribosome biogenesis protein BRX1 homolog	BRX1	41.401
Ribosome biogenesis regulatory protein homolog	RRS1	41.193
Ribosome production factor 2 homolog	RPF2	35.582
Ribosome-binding protein 1	RRBP1	152.45
RISC-loading complex subunit TARBP2	TARBP2	36.916
RNA 3-terminal phosphate cyclase-like protein	RCL1	40.842
RNA-binding motif protein, X chromosome;RNA-binding motif protein, X chromosome, N-terminally processed	RBMX	42.331
RNA-binding motif, single-stranded-interacting protein 1	RBMS1	44.136
RNA-binding protein 14	RBM14	69.491
RNA-binding protein 28	RBM28	85.737
RNA-binding protein 34	RBM34	48.564
RNA-binding protein 4	RBM4	40.313
RNA-binding protein 7	RBM7	30.59
RNA-binding protein FUS	FUS	53.496
RNA-binding protein Musashi homolog 2	MSI2	34.812
RNA-binding protein NOB1	NOB1	46.674
RNA-binding protein Raly	RALY	30.364
rRNA 2-O-methyltransferase fibrillarin	FBL	33.784
RRP12-like protein	RRP12	143.7
RRP15-like protein	RRP15	31.484
S phase cyclin A-associated protein in the endoplasmic reticulum	SCAPER	158.29
SAFB-like transcription modulator	SLTM	117.15
Sentrin-specific protease 3	SEN3;SEN3-EIF4A1	65.009
Serine beta-lactamase-like protein LACTB, mitochondrial	LACTB	60.693
Serine/arginine-rich splicing factor 1	SRSF1	28.329
Serine/arginine-rich splicing factor 11	SRSF11	53.413
Serine/arginine-rich splicing factor 2	SRSF2	15.371
Serine/arginine-rich splicing factor 3	SRSF3	14.203

Serine/arginine-rich splicing factor 4	SRSF4	56.678
Serine/arginine-rich splicing factor 5	SRSF5	31.263
Serine/arginine-rich splicing factor 6	SRSF6	26.306
Serine/arginine-rich splicing factor 7	SRSF7	15.763
Serine/threonine-protein kinase RIO3	RIOK3	57.474
Serpin B6	SERPINB6	43.024
Serrate RNA effector molecule homolog	SRRT	100.15
Sideroflexin-4	SFXN4	37.998
Signal recognition particle 54 kDa protein	SRP54	55.704
Signal recognition particle subunit SRP68	SRP68	70.729
Signal recognition particle subunit SRP72	SRP72	74.605
Slit homolog 2 protein;Slit homolog 2 protein N-product;Slit homolog 2 protein C-product	SLIT2	171.34
SPATS2-like protein	SPATS2L	54.178
Spermatid perinuclear RNA-binding protein	STRBP	71.966
Squamous cell carcinoma antigen recognized by T-cells 3	SART3	111.96
SRSF protein kinase 1	SRPK1	74.324
SRSF protein kinase 2;SRSF protein kinase 2 N-terminal;SRSF protein kinase 2 C-terminal	SRPK2	77.526
Superkiller viralicidic activity 2-like 2	SKIV2L2	117.8
Suppressor of SWI4 1 homolog	PPAN-P2RY11;PPAN	58.199
Surfeit locus protein 6	SURF6	41.45
Survival motor neuron protein	SMN1;SMN2	30.415
TAR DNA-binding protein 43	TARDBP;TDP43	44.739
Target of EGR1 protein 1	TOE1	56.547
Telomerase-binding protein EST1A	SMG6	160.46
Terminal uridylyltransferase 7	ZCCHC6	171.23
Testis-expressed sequence 10 protein	TEX10	103.91
Testis-specific Y-encoded-like protein 1	TSPYL1	49.192
Tetratricopeptide repeat protein 37	TTC37	175.48
THAP domain-containing protein 11	THAP11	34.455
Thioredoxin	TXN	11.737
THO complex subunit 2	THOC2	182.77
Thyroid hormone receptor-associated protein 3	THRAP3	103.52
tr A0A2R8Y4Z8 A0A2R8Y4Z8_HUMAN Coiled- coil domain-containing protein 9	CCDC9	65.306
Transcription factor 25	TCF25	76.666
Transcriptional activator protein Pur-alpha	PURA	34.91

Transcriptional activator protein Pur-beta	PURB	33.24
Transducin beta-like protein 2	TBL2	45.935
Transducin beta-like protein 3	TBL3	89.034
Transformer-2 protein homolog alpha	TRA2A	32.688
Transformer-2 protein homolog beta	TRA2B	33.665
Trinucleotide repeat-containing gene 6A protein	TNRC6A	205.15
TRMT1-like protein	TRMT1L	81.746
tRNA (guanine(26)-N(2))-dimethyltransferase	TRMT1	69.305
tRNA-splicing ligase RtcB homolog	RTCB	55.21
Tudor domain-containing protein 3	TDRD3	83.102
Twinkle protein, mitochondrial	PEO1	77.153
U1 small nuclear ribonucleoprotein A	SNRPA	31.279
U2 snRNP-associated SURP motif-containing protein	U2SURP	118.23
U3 small nucleolar RNA-associated protein 18 homolog	UTP18	62.003
U4/U6 small nuclear ribonucleoprotein Prp3	PRPF3	77.528
U4/U6.U5 tri-snRNP-associated protein 1	SART1	90.254
U5 small nuclear ribonucleoprotein 40 kDa protein	SNRNP40;DKFZp434D199	39.31
Ubiquitin carboxyl-terminal hydrolase 10	USP10	87.133
Ubiquitin-40S ribosomal protein S27a; Ubiquitin;40S ribosomal protein S27a	RPS27A	17.965
Ubiquitin-60S ribosomal protein L40;Ubiquitin; 60S ribosomal protein L40;Polyubiquitin-B; Ubiquitin;Polyubiquitin-C;Ubiquitin	UBA52;UBB;RPS27A;UBC	14.728
Ubiquitin-associated protein 2-like	UBAP2L	116.64
Uncharacterized protein C17orf85	C17orf85	70.592
Uncharacterized protein C7orf50	C7orf50	22.083
Unconventional myosin-Va	MYO5A	212.2
Vesicle-associated membrane protein-associated protein A	VAPA	27.893
von Willebrand factor A domain-containing protein 8	VWA8	210.92
WD repeat-containing protein 18	WDR18	43.237
WD repeat-containing protein 36	WDR36	99.365
WD repeat-containing protein 43	WDR43	74.89
WD repeat-containing protein 5	WDR5	36.588
WD repeat-containing protein 61; WD repeat-containing protein 61, N-terminally processed	WDR61	33.58
WD repeat-containing protein 74	WDR74	40.207
Y-box-binding protein 3	YBX3	40.089

YTH domain-containing family protein 1	YTHDF1	60.873
YTH domain-containing family protein 2	YTHDF2	62.333
YTH domain-containing protein 1	YTHDC1	84.699
Zinc finger and BTB domain-containing protein 11	ZBTB11	119.38
Zinc finger C3H1 domain-containing protein	ZFC3H1	217.49
Zinc finger CCCH domain-containing protein 15	ZC3H15	48.602
Zinc finger CCCH domain-containing protein 18	ZC3H18	108.94
Zinc finger CCCH domain-containing protein 8	ZC3H8	34.315
Zinc finger CCCH-type antiviral protein 1	ZC3HAV1	114.08
Zinc finger CCHC domain-containing protein 3	ZCCHC3	43.547
Zinc finger CCHC domain-containing protein 7	ZCCHC7	63.052
Zinc finger CCHC domain-containing protein 8	ZCCHC8	78.576
Zinc finger protein 16	ZNF16	76.471
Zinc finger protein 189	ZNF189	62.061
Zinc finger protein 224	ZNF224	82.279
Zinc finger protein 225	ZNF225	82.471
Zinc finger protein 226	ZNF226	91.92
Zinc finger protein 227	ZNF227	92.032
Zinc finger protein 30 homolog	ZFP30	61.557
Zinc finger protein 324A	ZNF324	61.103
Zinc finger protein 346	ZNF346	32.932
Zinc finger protein 354A	ZNF354A	69.236
Zinc finger protein 385A	ZNF385A	40.453
Zinc finger protein 417	ZNF417	65.604
Zinc finger protein 420	ZNF420	80.246
Zinc finger protein 45	ZNF45	78.241
Zinc finger protein 48	ZNF48	67.819
Zinc finger protein 483	ZNF483	85.097
Zinc finger protein 551	ZNF551	69.332
Zinc finger protein 567	ZNF567	71.556
Zinc finger protein 616	ZNF616	90.272
Zinc finger protein 62 homolog	ZFP62	98.779
Zinc finger protein 622	ZNF622	54.271
Zinc finger protein 629	ZNF629	96.619
Zinc finger protein 668	ZNF668	67.889
Zinc finger protein 768	ZNF768	60.228
Zinc finger protein 771	ZNF771	35.702
Zinc finger protein 792	ZNF792	64.042

Zinc finger protein 850	ZNF850	121.88
Zinc finger protein with KRAB and SCAN domains 8	ZKSCAN8	65.815
Zinc finger RNA-binding protein	ZFR	117.01

9. References

- Abaeva, I. S., Marintchev, A., Pisareva, V. P., Hellen, C. U. & Pestova, T. V. 2011. Bypassing of stems versus linear base-by-base inspection of mammalian mRNAs during ribosomal scanning. *EMBO J*, 30, 115-29.
- Agrawal, M. & Welshhans, K. 2021. Local Translation Across Neural Development: A Focus on Radial Glial Cells, Axons, and Synaptogenesis. *Front Mol Neurosci*, 14, 717170.
- Aguilera, A. & Garcia-Muse, T. 2012. R loops: from transcription byproducts to threats to genome stability. *Mol Cell*, 46, 115-24.
- Anantharaman, V., Koonin, E. V. & Aravind, L. 2002. Comparative genomics and evolution of proteins involved in RNA metabolism. *Nucleic Acids Res*, 30, 1427-64.
- Antonicka, H. & Shoubridge, E. A. 2015. Mitochondrial RNA Granules Are Centers for Posttranscriptional RNA Processing and Ribosome Biogenesis. *Cell Rep*, 10, 920-932.
- Bai, B., Wang, X., Li, Y., Chen, P. C., Yu, K., Dey, K. K., Yarbrow, J. M., Han, X., Lutz, B. M., Rao, S., Jiao, Y., Sifford, J. M., Han, J., Wang, M., Tan, H., Shaw, T. I., Cho, J. H., Zhou, S., Wang, H., Niu, M., Mancieri, A., Messler, K. A., Sun, X., Wu, Z., Pagala, V., High, A. A., Bi, W., Zhang, H., Chi, H., Haroutunian, V., Zhang, B., Beach, T. G., Yu, G. & Peng, J. 2020. Deep Multilayer Brain Proteomics Identifies Molecular Networks in Alzheimer's Disease Progression. *Neuron*, 106, 700.
- Ballut, L., Marchadier, B., Baguet, A., Tomasetto, C., Seraphin, B. & Le Hir, H. 2005. The exon junction core complex is locked onto RNA by inhibition of eIF4AIII ATPase activity. *Nat Struct Mol Biol*, 12, 861-9.
- Baltz, A. G., Munschauer, M., Schwanhauser, B., Vasile, A., Murakawa, Y., Schueler, M., Youngs, N., Penfold-Brown, D., Drew, K., Milek, M., Wyler, E., Bonneau, R., Selbach, M., Dieterich, C. & Landthaler, M. 2012. The mRNA-bound proteome and its global occupancy profile on protein-coding transcripts. *Mol Cell*, 46, 674-90.
- Bebee, T. W., Park, J. W., Sheridan, K. I., Warzecha, C. C., Cieply, B. W., Rohacek, A. M., Xing, Y. & Carstens, R. P. 2015. The splicing regulators *Esrp1* and *Esrp2* direct an epithelial splicing program essential for mammalian development. *Elife*, 4.
- Bessonov, S., Anokhina, M., Will, C. L., Urlaub, H. & Luhrmann, R. 2008. Isolation of an active step I spliceosome and composition of its RNP core. *Nature*, 452, 846-50.
- Bleichert, F. & Baserga, S. J. 2007. The long unwinding road of RNA helicases. *Mol Cell*, 27, 339-52.
- Bolinger, C., Sharma, A., Singh, D., Yu, L. & Boris-Lawrie, K. 2010. RNA helicase A modulates translation of HIV-1 and infectivity of progeny virions. *Nucleic Acids Res*, 38, 1686-96.
- Bosco, B., Rossi, A., Rizzotto, D., Hamadou, M. H., Bisio, A., Giorgetta, S., Perzoli, A., Bonollo, F., Gaucherot, A., Catez, F., Diaz, J. J., Dassi, E. & Inga, A. 2021. DHX30 Coordinates Cytoplasmic Translation and Mitochondrial Function Contributing to Cancer Cell Survival. *Cancers (Basel)*, 13.
- Brady, S., Singh, G., Bolinger, C., Song, Z., Boeras, I., Weng, K., Trent, B., Brown, W. C., Singh, K., Boris-Lawrie, K. & Heng, X. 2019. Virion-associated, host-derived DHX9/RNA helicase A enhances the processivity of HIV-1 reverse transcriptase on genomic RNA. *J Biol Chem*, 294, 11473-11485.
- Brambati, A., Zardoni, L., Nardini, E., Pelliccioli, A. & Liberi, G. 2020. The dark side of RNA:DNA hybrids. *Mutat Res Rev Mutat Res*, 784, 108300.
- Castello, A., Fischer, B., Eichelbaum, K., Horos, R., Beckmann, B. M., Strein, C., Davey, N. E., Humphreys, D. T., Preiss, T., Steinmetz, L. M., Krijgsveld, J. & Hentze, M. W. 2012. Insights into RNA biology from an atlas of mammalian mRNA-binding proteins. *Cell*, 149, 1393-406.

- Cheng, Z., Muhrad, D., Lim, M. K., Parker, R. & Song, H. 2007. Structural and functional insights into the human Upf1 helicase core. *EMBO J*, 26, 253-64.
- Cockman, E., Anderson, P. & Ivanov, P. 2020. TOP mRNPs: Molecular Mechanisms and Principles of Regulation. *Biomolecules*, 10.
- Coller, J. & Parker, R. 2005. General translational repression by activators of mRNA decapping. *Cell*, 122, 875-86.
- Cordin, O. & Beggs, J. D. 2013. RNA helicases in splicing. *RNA Biol*, 10, 83-95.
- Corley, M., Burns, M. C. & Yeo, G. W. 2020. How RNA-Binding Proteins Interact with RNA: Molecules and Mechanisms. *Mol Cell*, 78, 9-29.
- Cristini, A., Groh, M., Kristiansen, M. S. & Gromak, N. 2018. RNA/DNA Hybrid Interactome Identifies DXH9 as a Molecular Player in Transcriptional Termination and R-Loop-Associated DNA Damage. *Cell Rep*, 23, 1891-1905.
- Crossley, M. P., Bocek, M. & Cimprich, K. A. 2019. R-Loops as Cellular Regulators and Genomic Threats. *Mol Cell*, 73, 398-411.
- Deribe, Y. L., Pawson, T. & Dikic, I. 2010. Post-translational modifications in signal integration. *Nat Struct Mol Biol*, 17, 666-72.
- Eldomery, M. K., Coban-Akdemir, Z., Harel, T., Rosenfeld, J. A., Gambin, T., Stray-Pedersen, A., Kury, S., Mercier, S., Lessel, D., Denecke, J., Wiszniewski, W., Penney, S., Liu, P., Bi, W., Lalani, S. R., Schaaf, C. P., Wangler, M. F., Bacino, C. A., Lewis, R. A., Potocki, L., Graham, B. H., Belmont, J. W., Scaglia, F., Orange, J. S., Jhangiani, S. N., Chiang, T., Doddapaneni, H., Hu, J., Muzny, D. M., Xia, F., Beaudet, A. L., Boerwinkle, E., Eng, C. M., Plon, S. E., Sutton, V. R., Gibbs, R. A., Posey, J. E., Yang, Y. & Lupski, J. R. 2017. Lessons learned from additional research analyses of unsolved clinical exome cases. *Genome Med*, 9, 26.
- Esteve, P., Rueda-Carrasco, J., Ines Mateo, M., Martin-Bermejo, M. J., Draffin, J., Pereyra, G., Sandonis, A., Crespo, I., Moreno, I., Aso, E., Garcia-Esparcia, P., Gomez-Tortosa, E., Rabano, A., Fortea, J., Alcolea, D., Lleo, A., Heneka, M. T., Valpuesta, J. M., Esteban, J. A., Ferrer, I., Dominguez, M. & Bovolenta, P. 2019. Elevated levels of Secreted-Frizzled-Related-Protein 1 contribute to Alzheimer's disease pathogenesis. *Nat Neurosci*, 22, 1258-1268.
- Fairman-Williams, M. E., Guenther, U. P. & Jankowsky, E. 2010. SF1 and SF2 helicases: family matters. *Curr Opin Struct Biol*, 20, 313-24.
- Fairman, M. E., Maroney, P. A., Wang, W., Bowers, H. A., Gollnick, P., Nilsen, T. W. & Jankowsky, E. 2004. Protein displacement by DExH/D "RNA helicases" without duplex unwinding. *Science*, 304, 730-4.
- Fernandez, E., Rajan, N. & Bagni, C. 2013. The FMRP regulon: from targets to disease convergence. *Front Neurosci*, 7, 191.
- Filvaroff, E. H., Guillet, S., Zlot, C., Bao, M., Ingle, G., Steinmetz, H., Hoeffel, J., Bunting, S., Ross, J., Carano, R. A., Powell-Braxton, L., Wagner, G. F., Eckert, R., Gerritsen, M. E. & French, D. M. 2002. Stanniocalcin 1 alters muscle and bone structure and function in transgenic mice. *Endocrinology*, 143, 3681-90.
- Fischer, N. & Weis, K. 2002. The DEAD box protein Dhh1 stimulates the decapping enzyme Dcp1. *EMBO J*, 21, 2788-97.
- Flucher, B. E. & Campiglio, M. 2019. STAC proteins: The missing link in skeletal muscle EC coupling and new regulators of calcium channel function. *Biochim Biophys Acta Mol Cell Res*, 1866, 1101-1110.
- Fonseca, B. D., Zakaria, C., Jia, J. J., Graber, T. E., Svitkin, Y., Tahmasebi, S., Healy, D., Hoang, H. D., Jensen, J. M., Diao, I. T., Lussier, A., Dajadian, C., Padmanabhan, N., Wang, W., Matta-Camacho, E., Hearnden, J., Smith, E. M., Tsukumo, Y., Yanagiya, A., Morita, M., Petroulakis, E., Gonzalez, J. L., Hernandez, G., Alain, T. & Damgaard, C. K. 2015. La-

- related Protein 1 (LARP1) Represses Terminal Oligopyrimidine (TOP) mRNA Translation Downstream of mTOR Complex 1 (mTORC1). *J Biol Chem*, 290, 15996-6020.
- Gandin, V., Masvidal, L., Hulea, L., Gravel, S. P., Cargnello, M., Mclaughlan, S., Cai, Y., Balanathan, P., Morita, M., Rajakumar, A., Furic, L., Pollak, M., Porco, J. A., Jr., St-Pierre, J., Pelletier, J., Larsson, O. & Topisirovic, I. 2016. nanoCAGE reveals 5' UTR features that define specific modes of translation of functionally related MTOR-sensitive mRNAs. *Genome Res*, 26, 636-48.
- Ge, S. X., Jung, D. & Yao, R. 2020. ShinyGO: a graphical gene-set enrichment tool for animals and plants. *Bioinformatics*, 36, 2628-2629.
- Gehring, N. H., Wahle, E. & Fischer, U. 2017. Deciphering the mRNP Code: RNA-Bound Determinants of Post-Transcriptional Gene Regulation. *Trends Biochem Sci*, 42, 369-382.
- Grohmann, K., Schuelke, M., Diers, A., Hoffmann, K., Lucke, B., Adams, C., Bertini, E., Leonhardt-Horti, H., Muntoni, F., Ouvrier, R., Pfeufer, A., Rossi, R., Van Maldergem, L., Wilmshurst, J. M., Wienker, T. F., Sendtner, M., Rudnik-Schoneborn, S., Zerres, K. & Hubner, C. 2001. Mutations in the gene encoding immunoglobulin mu-binding protein 2 cause spinal muscular atrophy with respiratory distress type 1. *Nat Genet*, 29, 75-7.
- Grunseich, C., Wang, I. X., Watts, J. A., Burdick, J. T., Guber, R. D., Zhu, Z., Bruzel, A., Lanman, T., Chen, K., Schindler, A. B., Edwards, N., Ray-Chaudhury, A., Yao, J., Lehky, T., Piszczek, G., Crain, B., Fischbeck, K. H. & Cheung, V. G. 2018. Senataxin Mutation Reveals How R-Loops Promote Transcription by Blocking DNA Methylation at Gene Promoters. *Mol Cell*, 69, 426-437 e7.
- Guenther, U. P., Handoko, L., Lagerbauer, B., Jablonka, S., Chari, A., Alzheimer, M., Ohmer, J., Plottner, O., Gehring, N., Sickmann, A., Von Au, K., Schuelke, M. & Fischer, U. 2009. IGHMBP2 is a ribosome-associated helicase inactive in the neuromuscular disorder distal SMA type 1 (DSMA1). *Hum Mol Genet*, 18, 1288-300.
- Hagerman, R. J., Berry-Kravis, E., Hazlett, H. C., Bailey, D. B., Jr., Moine, H., Kooy, R. F., Tassone, F., Gantois, I., Sonenberg, N., Mandel, J. L. & Hagerman, P. J. 2017. Fragile X syndrome. *Nat Rev Dis Primers*, 3, 17065.
- Hara, K., Maruki, Y., Long, X., Yoshino, K., Oshiro, N., Hidayat, S., Tokunaga, C., Avruch, J. & Yonezawa, K. 2002. Raptor, a binding partner of target of rapamycin (TOR), mediates TOR action. *Cell*, 110, 177-89.
- Hartman, T. R., Qian, S., Bolinger, C., Fernandez, S., Schoenberg, D. R. & Boris-Lawrie, K. 2006. RNA helicase A is necessary for translation of selected messenger RNAs. *Nat Struct Mol Biol*, 13, 509-16.
- Holt, C. E., Martin, K. C. & Schuman, E. M. 2019. Local translation in neurons: visualization and function. *Nat Struct Mol Biol*, 26, 557-566.
- Holt, I. J. 2019. The mitochondrial R-loop. *Nucleic Acids Res*, 47, 5480-5489.
- Iadevaia, V., Caldarola, S., Tino, E., Amaldi, F. & Loreni, F. 2008. All translation elongation factors and the e, f, and h subunits of translation initiation factor 3 are encoded by 5'-terminal oligopyrimidine (TOP) mRNAs. *RNA*, 14, 1730-6.
- Jankowsky, E. 2011. RNA helicases at work: binding and rearranging. *Trends Biochem Sci*, 36, 19-29.
- Jankowsky, E. & Fairman, M. E. 2007. RNA helicases--one fold for many functions. *Curr Opin Struct Biol*, 17, 316-24.
- Jankowsky, E., Gross, C. H., Shuman, S. & Pyle, A. M. 2001. Active disruption of an RNA-protein interaction by a DExH/D RNA helicase. *Science*, 291, 121-5.
- Jaramillo, M., Browning, K., Dever, T. E., Blum, S., Trachsel, H., Merrick, W. C., Ravel, J. M. & Sonenberg, N. 1990. Translation initiation factors that function as RNA helicases from mammals, plants and yeast. *Biochim Biophys Acta*, 1050, 134-9.
- Jarmoskaite, I. & Russell, R. 2011. DEAD-box proteins as RNA helicases and chaperones. *Wiley Interdiscip Rev RNA*, 2, 135-52.

- Jiang, W. Q., Chang, A. C., Satoh, M., Furuichi, Y., Tam, P. P. & Reddel, R. R. 2000. The distribution of stanniocalcin 1 protein in fetal mouse tissues suggests a role in bone and muscle development. *J Endocrinol*, 165, 457-66.
- Jung, H., Gkogkas, C. G., Sonenberg, N. & Holt, C. E. 2014. Remote control of gene function by local translation. *Cell*, 157, 26-40.
- Kalashnikova, E., Lorca, R. A., Kaur, I., Barisone, G. A., Li, B., Ishimaru, T., Trimmer, J. S., Mohapatra, D. P. & Diaz, E. 2010. SynDIG1: an activity-regulated, AMPA- receptor-interacting transmembrane protein that regulates excitatory synapse development. *Neuron*, 65, 80-93.
- Kashima, I., Yamashita, A., Izumi, N., Kataoka, N., Morishita, R., Hoshino, S., Ohno, M., Dreyfuss, G. & Ohno, S. 2006. Binding of a novel SMG-1-Upf1-eRF1-eRF3 complex (SURF) to the exon junction complex triggers Upf1 phosphorylation and nonsense-mediated mRNA decay. *Genes Dev*, 20, 355-67.
- Kawaoka, J., Jankowsky, E. & Pyle, A. M. 2004. Backbone tracking by the SF2 helicase NPH-II. *Nat Struct Mol Biol*, 11, 526-30.
- Kawaoka, J. & Pyle, A. M. 2005. Choosing between DNA and RNA: the polymer specificity of RNA helicase NPH-II. *Nucleic Acids Res*, 33, 644-9.
- Kazi, J. U., Kabir, N. N. & Ronnstrand, L. 2015. Brain-Expressed X-linked (BEX) proteins in human cancers. *Biochim Biophys Acta*, 1856, 226-33.
- Khemici, V. & Linder, P. 2018. RNA helicases in RNA decay. *Biochem Soc Trans*, 46, 163-172.
- Kim, D. H., Sarbassov, D. D., Ali, S. M., King, J. E., Latek, R. R., Erdjument-Bromage, H., Tempst, P. & Sabatini, D. M. 2002. mTOR interacts with raptor to form a nutrient-sensitive complex that signals to the cell growth machinery. *Cell*, 110, 163-75.
- Lahr, R. M., Fonseca, B. D., Ciotti, G. E., Al-Ashtal, H. A., Jia, J. J., Niklaus, M. R., Blagden, S. P., Alain, T. & Berman, A. J. 2017. La-related protein 1 (LARP1) binds the mRNA cap, blocking eIF4F assembly on TOP mRNAs. *Elife*, 6.
- Lang, K. S., Hall, A. N., Merrikh, C. N., Ragheb, M., Tabakh, H., Pollock, A. J., Woodward, J. J., Dreifus, J. E. & Merrikh, H. 2017. Replication-Transcription Conflicts Generate R-Loops that Orchestrate Bacterial Stress Survival and Pathogenesis. *Cell*, 170, 787-799 e18.
- Laplante, M. & Sabatini, D. M. 2012. mTOR signaling in growth control and disease. *Cell*, 149, 274-93.
- Lee, H. K., Lee, H. S. & Moody, S. A. 2014. Neural transcription factors: from embryos to neural stem cells. *Mol Cells*, 37, 705-12.
- Lessel, D., Schob, C., Kury, S., Reijnders, M. R. F., Harel, T., Eldomery, M. K., Coban-Akdemir, Z., Denecke, J., Edvardson, S., Colin, E., Stegmann, A. P. A., Gerkes, E. H., Tessarech, M., Bonneau, D., Barth, M., Besnard, T., Cogne, B., Revah-Politi, A., Strom, T. M., Rosenfeld, J. A., Yang, Y., Posey, J. E., Immken, L., Oundjian, N., Helbig, K. L., Meeks, N., Zegar, K., Morton, J., Study, D. D. D., Schieving, J. H., Claasen, A., Huentelman, M., Narayanan, V., Ramsey, K., Group, C. R. R., Brunner, H. G., Elpeleg, O., Mercier, S., Bezieau, S., Kubisch, C., Kleefstra, T., Kindler, S., Lupski, J. R. & Kreienkamp, H. J. 2017. De Novo Missense Mutations in DHX30 Impair Global Translation and Cause a Neurodevelopmental Disorder. *Am J Hum Genet*, 101, 716-724.
- Linder, P. & Jankowsky, E. 2011. From unwinding to clamping - the DEAD box RNA helicase family. *Nat Rev Mol Cell Biol*, 12, 505-16.
- Lunde, B. M., Moore, C. & Varani, G. 2007. RNA-binding proteins: modular design for efficient function. *Nat Rev Mol Cell Biol*, 8, 479-90.
- Mannucci, I., Dang, N. D. P., Huber, H., Murry, J. B., Abramson, J., Althoff, T., Banka, S., Baynam, G., Bearden, D., Beleza-Meireles, A., Benke, P. J., Berland, S., Bierhals, T., Bilan, F., Bindoff, L. A., Braathen, G. J., Busk, O. L., Chenbhanich, J., Denecke, J., Escobar, L. F., Estes, C., Fleischer, J., Groepper, D., Haaxma, C. A., Hempel, M., Holler-Managan, Y., Houge, G., Jackson, A., Kellogg, L., Keren, B., Kiraly-Borri, C., Kraus, C., Kubisch, C., Le

- Guyader, G., Ljungblad, U. W., Brenman, L. M., Martinez-Agosto, J. A., Might, M., Miller, D. T., Minks, K. Q., Moghaddam, B., Nava, C., Nelson, S. F., Parant, J. M., Prescott, T., Rajabi, F., Randrianaivo, H., Reiter, S. F., Schuurs-Hoeijmakers, J., Shieh, P. B., Slavotinek, A., Smithson, S., Stegmann, A. P. A., Tomczak, K., Tveten, K., Wang, J., Whitlock, J. H., Zweier, C., Mcwaller, K., Juusola, J., Quintero-Rivera, F., Fischer, U., Yeo, N. C., Kreienkamp, H. J. & Lessel, D. 2021. Genotype-phenotype correlations and novel molecular insights into the DHX30-associated neurodevelopmental disorders. *Genome Med*, 13, 90.
- Merrick, W. C. 2010. Eukaryotic protein synthesis: still a mystery. *J Biol Chem*, 285, 21197-201.
- Meyuhas, O. & Kahan, T. 2015. The race to decipher the top secrets of TOP mRNAs. *Biochim Biophys Acta*, 1849, 801-11.
- Mitchell, S. F. & Parker, R. 2014. Principles and properties of eukaryotic mRNPs. *Mol Cell*, 54, 547-58.
- Nagano, S., Jinno, J., Abdelhamid, R. F., Jin, Y., Shibata, M., Watanabe, S., Hirokawa, S., Nishizawa, M., Sakimura, K., Onodera, O., Okada, H., Okada, T., Saito, Y., Takahashi-Fujigasaki, J., Murayama, S., Wakatsuki, S., Mochizuki, H. & Araki, T. 2020. TDP-43 transports ribosomal protein mRNA to regulate axonal local translation in neuronal axons. *Acta Neuropathol*, 140, 695-713.
- Nicholls, T. J. & Minczuk, M. 2014. In D-loop: 40 years of mitochondrial 7S DNA. *Exp Gerontol*, 56, 175-81.
- Nittoli, V., Fortunato, A. E., Fasano, G., Coppola, U., Gentile, A., Maiella, S., Langellotto, F., Porreca, I., De Paolo, R., Marino, R., Fiengo, M., Donizetti, A., Aniello, F., Kondo, T., Ristoratore, F., Canzoniero, L. M. T., Duboule, D., Wilson, S. W. & Sordino, P. 2019. Characterization of paralogous uncx transcription factor encoding genes in zebrafish. *Gene X*, 2, 100011.
- Pan, X., Jiang, N., Chen, X., Zhou, X., Ding, L. & Duan, F. 2014. R-loop structure: the formation and the effects on genomic stability. *Yi Chuan*, 36, 1185-94.
- Pang, P. S., Jankowsky, E., Planet, P. J. & Pyle, A. M. 2002. The hepatitis C viral NS3 protein is a processive DNA helicase with cofactor enhanced RNA unwinding. *EMBO J*, 21, 1168-76.
- Parsyan, A., Svitkin, Y., Shahbazian, D., Gkogkas, C., Lasko, P., Merrick, W. C. & Sonenberg, N. 2011. mRNA helicases: the tacticians of translational control. *Nat Rev Mol Cell Biol*, 12, 235-45.
- Pisareva, V. P., Pisarev, A. V., Komar, A. A., Hellen, C. U. & Pestova, T. V. 2008. Translation initiation on mammalian mRNAs with structured 5'UTRs requires DExH-box protein DHX29. *Cell*, 135, 1237-50.
- Pyle, A. M. 2008. Translocation and unwinding mechanisms of RNA and DNA helicases. *Annu Rev Biophys*, 37, 317-36.
- Ranji, A., Shkriabai, N., Kvaratskhelia, M., Musier-Forsyth, K. & Boris-Lawrie, K. 2011. Features of double-stranded RNA-binding domains of RNA helicase A are necessary for selective recognition and translation of complex mRNAs. *J Biol Chem*, 286, 5328-37.
- Rizzotto, D., Zaccara, S., Rossi, A., Galbraith, M. D., Andrysik, Z., Pandey, A., Sullivan, K. D., Quattrone, A., Espinosa, J. M., Dassi, E. & Inga, A. 2020. Nutlin-Induced Apoptosis Is Specified by a Translation Program Regulated by PCBP2 and DHX30. *Cell Rep*, 30, 4355-4369 e6.
- Rocak, S. & Linder, P. 2004. DEAD-box proteins: the driving forces behind RNA metabolism. *Nat Rev Mol Cell Biol*, 5, 232-41.
- Rufenach, B. & Van Petegem, F. 2021. Structure and function of STAC proteins: Calcium channel modulators and critical components of muscle excitation-contraction coupling. *J Biol Chem*, 297, 100874.

- Saito, T., Lo, L., Anderson, D. J. & Mikoshiba, K. 1996. Identification of novel paired homeodomain protein related to *C. elegans* unc-4 as a potential downstream target of MASH1. *Dev Biol*, 180, 143-55.
- Sanchez, R. S. & Sanchez, S. S. 2013. Characterization of pax1, pax9, and uncx sclerotomal genes during *Xenopus laevis* embryogenesis. *Dev Dyn*, 242, 572-9.
- Sarbassov, D. D., Guertin, D. A., Ali, S. M. & Sabatini, D. M. 2005. Phosphorylation and regulation of Akt/PKB by the rictor-mTOR complex. *Science*, 307, 1098-101.
- Saxton, R. A. & Sabatini, D. M. 2017. mTOR Signaling in Growth, Metabolism, and Disease. *Cell*, 168, 960-976.
- Sengoku, T., Nureki, O., Nakamura, A., Kobayashi, S. & Yokoyama, S. 2006. Structural basis for RNA unwinding by the DEAD-box protein *Drosophila* Vasa. *Cell*, 125, 287-300.
- Shen, L. & Pelletier, J. 2020. General and Target-Specific DExD/H RNA Helicases in Eukaryotic Translation Initiation. *Int J Mol Sci*, 21.
- Shigeoka, T., Koppers, M., Wong, H. H., Lin, J. Q., Cagnetta, R., Dwivedy, A., De Freitas Nascimento, J., Van Tartwijk, F. W., Strohl, F., Cioni, J. M., Schaeffer, J., Carrington, M., Kaminski, C. F., Jung, H., Harris, W. A. & Holt, C. E. 2019. On-Site Ribosome Remodeling by Locally Synthesized Ribosomal Proteins in Axons. *Cell Rep*, 29, 3605-3619 e10.
- Short, J. D. & Pfarr, C. M. 2002. Translational regulation of the JunD messenger RNA. *J Biol Chem*, 277, 32697-705.
- Shorts-Cary, L., Xu, M., Ertel, J., Kleinschmidt-Demasters, B. K., Lillehei, K., Matsuoka, I., Nielsen-Preiss, S. & Wierman, M. E. 2007. Bone morphogenetic protein and retinoic acid-inducible neural specific protein-3 is expressed in gonadotrope cell pituitary adenomas and induces proliferation, migration, and invasion. *Endocrinology*, 148, 967-75.
- Simsek, D., Tiu, G. C., Flynn, R. A., Byeon, G. W., Leppek, K., Xu, A. F., Chang, H. Y. & Barna, M. 2017. The Mammalian Ribo-interactome Reveals Ribosome Functional Diversity and Heterogeneity. *Cell*, 169, 1051-1065 e18.
- Studer, M. K., Ivanovic, L., Weber, M. E., Marti, S. & Jonas, S. 2020. Structural basis for DEAH-helicase activation by G-patch proteins. *Proc Natl Acad Sci U S A*, 117, 7159-7170.
- Surguchov, A., Palazzo, R. E. & Surgucheva, I. 2001. Gamma synuclein: subcellular localization in neuronal and non-neuronal cells and effect on signal transduction. *Cell Motil Cytoskeleton*, 49, 218-28.
- Suzuki, H., Kawai, J., Taga, C., Yaoi, T., Hara, A., Hirose, K., Hayashizaki, Y. & Watanabe, S. 1996. Stac, a novel neuron-specific protein with cysteine-rich and SH3 domains. *Biochem Biophys Res Commun*, 229, 902-9.
- Swanger, S. A. & Bassell, G. J. 2011. Making and breaking synapses through local mRNA regulation. *Curr Opin Genet Dev*, 21, 414-21.
- Tauchert, M. J., Fourmann, J.-B., Lührmann, R. & Ficner, R. 2017. Structural insights into the mechanism of the DEAH-box RNA helicase Prp43. *Elife*, 6, e21510.
- Tcherkezian, J., Cargnello, M., Romeo, Y., Huttlin, E. L., Lavoie, G., Gygi, S. P. & Roux, P. P. 2014. Proteomic analysis of cap-dependent translation identifies LARP1 as a key regulator of 5'TOP mRNA translation. *Genes Dev*, 28, 357-71.
- Tettweiler, G. & Lasko, P. 2006. A new model for translational regulation of specific mRNAs. *Trends Biochem Sci*, 31, 607-10.
- Thakur, R. S., Basavaraju, S., Somyajit, K., Jain, A., Subramanya, S., Muniyappa, K. & Nagaraju, G. 2013. Evidence for the role of *Mycobacterium tuberculosis* RecG helicase in DNA repair and recombination. *FEBS J*, 280, 1841-60.
- Thandapani, P., O'connor, T. R., Bailey, T. L. & Richard, S. 2013. Defining the RGG/RG motif. *Mol Cell*, 50, 613-23.
- Theobald, D. L., Mitton-Fry, R. M. & Wuttke, D. S. 2003. Nucleic acid recognition by OB-fold proteins. *Annu Rev Biophys Biomol Struct*, 32, 115-33.

- Tseng-Rogenski, S. S. & Chang, T. H. 2004. RNA unwinding assay for DExD/H-box RNA helicases. *Methods Mol Biol*, 257, 93-102.
- Tsokas, P., Grace, E. A., Chan, P., Ma, T., Sealfon, S. C., Iyengar, R., Landau, E. M. & Blitzer, R. D. 2005. Local protein synthesis mediates a rapid increase in dendritic elongation factor 1A after induction of late long-term potentiation. *J Neurosci*, 25, 5833-43.
- Tsokas, P., Ma, T., Iyengar, R., Landau, E. M. & Blitzer, R. D. 2007. Mitogen-activated protein kinase upregulates the dendritic translation machinery in long-term potentiation by controlling the mammalian target of rapamycin pathway. *J Neurosci*, 27, 5885-94.
- Umate, P., Tuteja, N. & Tuteja, R. 2011. Genome-wide comprehensive analysis of human helicases. *Commun Integr Biol*, 4, 118-37.
- Wahl, M. C., Will, C. L. & Luhrmann, R. 2009. The spliceosome: design principles of a dynamic RNP machine. *Cell*, 136, 701-18.
- Wang, K., Wang, H., Li, C., Yin, Z., Xiao, R., Li, Q., Xiang, Y., Wang, W., Huang, J., Chen, L., Fang, P. & Liang, K. 2021. Genomic profiling of native R loops with a DNA-RNA hybrid recognition sensor. *Sci Adv*, 7.
- Yangyuru, P. M., Bradburn, D. A., Liu, Z., Xiao, T. S. & Russell, R. 2018. The G-quadruplex (G4) resolvase DHX36 efficiently and specifically disrupts DNA G4s via a translocation-based helicase mechanism. *J Biol Chem*, 293, 1924-1932.
- Ye, P., Liu, S., Zhu, Y., Chen, G. & Gao, G. 2010. DEXH-Box protein DHX30 is required for optimal function of the zinc-finger antiviral protein. *Protein Cell*, 1, 956-64.
- Young, D. J. & Guydosh, N. R. 2022. Rebirth of the translational machinery: The importance of recycling ribosomes. *Bioessays*, 44, e2100269.
- Zheng, H. J., Tsukahara, M., Liu, E., Ye, L., Xiong, H., Noguchi, S., Suzuki, K. & Ji, Z. S. 2015. The novel helicase helG (DHX30) is expressed during gastrulation in mice and has a structure similar to a human DEXH box helicase. *Stem Cells Dev*, 24, 372-83.

10. Publications

Parts of this Work is/will be published in the following papers:

Mannucci, I., Dang, N. D. P., **Huber, H.**, Murry, J. B., Abramson, J., Althoff, T., Banka, S., Baynam, G., Bearden, D., Beleza-Meireles, A., Benke, P. J., Berland, S., Bierhals, T., Bilan, F., Bindoff, L. A., Braathen, G. J., Busk, O. L., Chenbhanich, J., Denecke, J., Escobar, L. F., Estes, C., Fleischer, J., Groepper, D., Haaxma, C. A., Hempel, M., Holler-Managan, Y., Houge, G., Jackson, A., Kellogg, L., Keren, B., Kiraly-Borri, C., Kraus, C., Kubisch, C., Le Guyader, G., Ljungblad, U. W., Brenman, L. M., Martinez-Agosto, J. A., Might, M., Miller, D. T., Minks, K. Q., Moghaddam, B., Nava, C., Nelson, S. F., Parant, J. M., Prescott, T., Rajabi, F., Randrianaivo, H., Reiter, S. F., Schuurs-Hoeijmakers, J., Shieh, P. B., Slavotinek, A., Smithson, S., Stegmann, A. P. A., Tomczak, K., Tveten, K., Wang, J., Whitlock, J. H., Zweier, C., Mcwalter, K., Juusola, J., Quintero-Rivera, F., Fischer, U., Yeo, N. C., Kreienkamp, H. J. & Lessel, D. 2021. Genotype-phenotype correlations and novel molecular insights into the DHX30-associated neurodevelopmental disorders. *Genome Med*, 13, 90.

Huber, H., Schneider, C., Schlosser, A., Urlaub, H., Fischer, U., The RNA helicase DHX30 regulates the translation of 5'-TOP mRNAs via direct interaction with the ribosome (to be submitted).

11. Acknowledgments

I would like to express my thanks to all the people who helped and supported me and thus contributed to this thesis. I especially thank Prof. Dr. Utz Fischer for the supervision, support and funding throughout this work.

I thank PD Dr. Sibylle Jablonka for being the second supervisor of this thesis.

I want to thank Prof. Dr. Alexander Buchberger for helpful suggestions and discussions and for examination of this dissertation as the third evaluator.

Also, I want to thank Dr. Cornelius Schneider for all the lively discussions and the input for the experimental work for this project.

I thank all collaborators I was working with during my time in Würzburg: Prof. Hans-Jürgen Kreienkamp & Illaria Mannucci from UKE Hamburg and Prof. Ying Liu & Szymon Barwacz from the University of Copenhagen.

Also, I want to thank Stephanie Lamer and Prof. Andreas Schlosser for the mass spectrometry measurements and the bioinformatical analysis of the data. I want to thank Prof. Henning Urlaub & Juliane Schwartz from Max Planck Institute for biophysical chemistry in Göttingen for performing and analysis of the crosslink mass spectrometry experiment.

Special thanks to Isotta, Julia, Sam, Manisha and Archana for supervision, discussion, support (technically and mentally) and teamwork and for being great lab members. Also many thanks to Lissy and Jürgen who had always helped and supported me. I thank all members of the AG Buchberger for collaboration, discussion, and help: Mona, Maria, Sven, Beyenech, Nazife. Also a warm thanks to Susanne, Emilia, Cihan, Michael and Georg who were always there for a nice chat. Also thanks to Andrea for their constant help in the background.

I thank also the Graduate School of Life Sciences of the University of Würzburg (especially Dr. Blum-Oehler) for their tremendous help and support throughout my PhD.

Finally, I thank my mom and dad and my two sisters, who always encouraging me and for wanting all the best for me. You are the best people I could ever have in my life!

12. Curriculum vitae

Education

Since 02/2017 **Ph.D. Student (Biochemistry)**

University of Würzburg

» Dissertation at the Chair of Biochemistry, Theodor-Boveri-Institute at the Biocentre: "Biochemical and functional characterization of DHX30, an RNA helicase linked to neurodevelopmental disorder"
Advisor: Prof. Dr. Utz Fischer

10/2014 -
12/2016

Master of Science (Molecular & Cellular Biology)

Philipps-University Marburg

» Master's thesis at the Department of Pharmaceutical Chemistry, Marburg: "Analysis of the interaction between the *long non-coding RNA* Inc02 and the 14-3-3 β protein & Role of RNA secondary structures within the transcription start regions of the Ebola virus (EBOV)"
Advisor: Prof. Dr. Arnold Grünweller

10/2010 -
10/2014

Bachelor of Science (Biology)

University of Bayreuth

» Bachelor's thesis at the Research Centre of Food Quality of the University of Bayreuth in Kulmbach: "Influence of moisture on the microbiology of poppy seeds"
Advisor: Prof. Dr. Franz Meußdoerffer

Professional experience

- 04/2014 - Internship at Axolabs GmbH in Kulmbach
10/2014
- » Establishing an *in vitro* reporter system to monitor de-repression of miRNA target genes after transfection of cells with anti-miRNA derivatives.
 - » Emphases: miRNAs, RNA interference, Nucleic Acid Medicines, Oligonucleotide Therapeutics, RNA Biology
- 09/2013 - Internship at Robert Koch Institute in Wernigerode,
10/2013 Junior Research Group 3: „Virulent Factors of Salmonella“
- » Analysis of protein-protein interactions of components of Salmonella pathogenicity island 4.
 - » Emphases: Molecular & Medical Microbiology, Molecular Cloning, Bacterial Two-Hybrid (Protein-Protein Interactions)

Publications

Mannucci, I., Dang, N.D.P., **Huber, H.** *et al.*

Genotype–phenotype correlations and novel molecular insights into the *DHX30*-associated neurodevelopmental disorders.

Genome Medicine **13**, 90 (2021). <https://doi.org/10.1186/s13073-021-00900-3>

Conferences

- Oral presentations
- » FASEB Science Research Conference
 - Helicase and Nucleic Acid-based Machine Conference in Steamboat Springs, Colorado, USA
 - July 21-26, 2019
- Poster presentations
- » International Symposium organized by the Students of the Graduate School of Life Sciences: EUREKA, in Würzburg, Germany
 - October 8-10, 2021

» International Symposium organized by the Students of the Graduate School of Life Sciences: EUREKA, in Würzburg, Germany
October 8-10, 2019

Scientific Initiatives

2019 Member of the organizing committee of the International Symposium organized by the Doctoral Researchers of the Graduate School of Life Sciences “EUREKA”
Würzburg, Germany

Place, Date

Signature